Simulation of the Laptev Sea shelf dynamics with focus on the Lena Delta region

by
Vera Fofonova

A Thesis submitted in partial fulfillment
of the requirements for the degree of

Doctor of Philosophy in Geosciences

Approved Dissertation Committee

Prof. Dr. Karen Helen Wiltshire
Jacobs University Bremen;
Alfred Wegener Institute, Helmholtz Centre for Polar and
Marine Research
Dr. Sergey Danilov
Alfred Wegener Institute, Helmholtz Centre for Polar and
Marine Research
Prof. Dr. Vikram Unnithan
Jacobs University Bremen
Dr. Jens Schröter
Alfred Wegener Institute, Helmholtz Centre for Polar and
Marine Research

Date of Defense: 26th of June, 2014

School of Engineering and Science

Abstract

The polar shelf zones are highly dynamic and diverse systems. They form a border between warm and fresh water of continental drain and the cold currents of the northern seas. The Lena River is one of the largest rivers in the Arctic, with the largest delta. The south-eastern part of the Laptev Sea, which includes the Lena Delta region, is the place where substantial changes in ocean circulation and ecosystem may happen in changing climate. Exploring processes there, which may serve as an indicator of climate change, acquire a special importance.

The Lena freshwater plume propagation dominates many aspects of dynamics in the Laptev Sea shelf. However, the direct measurements are by far insufficient, calling for a modeling approach which would enable one to estimate the impact of different factors on the circulation dynamics and would lay the foundation for further ecosystem modeling. The complexity of the region's geometry and insufficient data make modeling of ocean circulation in the Lena Delta vicinity a challenging technical task not solved in the necessary detail previously. The quantitative effect of various factors (tides, winds, hear exchange with the atmosphere) on the freshwater plume propagation also has not been fully explored.

The main goal of this thesis is the analysis of the Lena River freshwater plume dynamics in the summer season on the basis of a full baroclinic numerical model of the Laptev Sea shelf with focus on the Lena Delta region. The setup is based on FVCOM (The Unstructured Grid Finite Volume Coastal/Community Ocean Model; Chen et al. 2006).

The thesis contains a detailed description of the model setup, including the generation of an unstructured mesh, analysis of barotropic and baroclinic dynamics in the region of interest, the description of new approaches for the model elaboration and visualization of simulation results and a comparison of the impact of different atmospheric forcing products on the simulated dynamics. Special attention is paid to the Lena River hydrology regime in the basin outlet, which is taken into account in simulations.

Since tides are responsible for a considerable fraction of mixing over the shallow shelf of the Laptev Sea, the first step consisted in accurate modeling of barotropic tides in the Lena Delta region of the Laptev Sea. This demanded using accurate topography data and the design of optimized open boundary conditions that would provide the best agreement with observations. The simulated tidal maps for principal semidiurnal constituents, which are the most important in the considered area, showed an improved agreement with observations as compared to other modeling efforts. Important

information about barotropic currents, evolution of energy fluxes in the region and residual circulation, which affects sediment and nutrients transport, was obtained in this work.

The next important step toward more realistic simulations was taking into account the Lena River hydrology. This step required substantial preliminary work on compiling and analyzing respective Lena River characteristics in the basin outlet area. The anomaly in surface water temperature was found to exist at the most downstream location in the summer season. Its description and basic analysis is presented. To sort the problem of anomaly out, the observational data in the scope of hydrology and morphology for the Lena River delta and main channel area, including data on permafrost conditions under the river channel, were considered.

The third step was full baroclinic simulations with focus on the Lena River freshwater plume dynamics in the summer season. The role of tides, winds and thermohaline forcing in shaping the plume dynamics was explored by applying different sources of atmospheric forcing and switching on/off tidal dynamics. In addition, the roles of local bathymetry and techniques of freshwater distribution were assessed. A detailed comparison with the available observational data was also performed showing a good agreement. It was found that the surface salinity distribution is most sensitive to winds, with the implication that the ability of model to predict it relies on the availability of high-quality wind forcing data. Tidal mixing and residual transport are important, but only locally, whereas heat exchange with the atmosphere influences the water mass properties, but has only a weak impact on dynamics.

This understanding together with the proof that the model simulations agree well with the observational data are the main results of this thesis. They demonstrate that the model can serve as a platform for future ecosystem modeling in the Lena Delta region.

List of acronyms

AARI – Arctic and Antarctic Research Institute

AMSR-E – Advanced Microwave Scanning Radiometer - Earth Observing System Sensor on the NASA Aqua Satellite

AO – Arctic Ocean

AWI – Alfred Wegener Institute, Helmholtz Centre for Polar and Marine Research

AOTIM5 – Arctic Ocean Tidal Inverse Model

COSMO – Consortium for Small-Scale Modeling

CTD – Conductivity, Temperature, and Depth

DOE – Department of Energy

ECMWF – European Centre for Medium-Range Weather Forecasts

EP – Erofeeva and Padman (Padman and Erofeeva, 2004)

FVCOM – Unstructured Grid Finite Volume Coastal/Community Ocean Model

GEBCO – General Bathymetric Chart of the Oceans

GS – Gauging Station

IBCAO – International Bathymetric Chart of the Arctic Ocean

KP – Kowalik and Proshutinsky (Kowalik and Proshutinsky, 1993, 1994)

MDS – Multidimensional Scaling Projection

NAOSIM – North Atlantic/Arctic Sea Ice - Ocean Model

NOAA – National Oceanic and Atmospheric Administration

NCEP – National Centers for Environmental Prediction

NCAR – National Center for Atmospheric Research

OOBC – Optimized Open Boundary Conditions

PSMSL – Permanent Service for Mean Sea Level

SIC – Sea Ice Concentration

TPXO6.2 (7.1) – Global Inverse Tide Model

UMASSD-WHOI – University of Massachusetts - Woods Hole Oceanographic Institution

Table of contents

List of figures

Chapter 1

1. The Laptev Sea map. The additional bottom picture shows detailed seabed topography based on a Soviet digitized map. This map visualizes the locations of main channels where local extrema of freshwater discharge are located.

2. Mean surface air temperature from 1936 to 2009, Tiksi Bay, for different time periods.

Chapter 2

1. Mean monthly discharge for the period from 1935 to 2011.

2. Time of the year when the daily flow of the Lena River reaches a maximum from 1936 to 2013.

3. Total annual discharge from 1936 to 2013.

Chapter 3

1. Schematic of the no-flux boundary condition on the bottom slope .

Chapter 4

1. Linkages between the main directions of the work presented in this thesis.

2. Substeps of the main work directions.

Chapter 5

1. Bathymetry of the selected domain. The dots indicate the positions of tide gauges and moorings, which provide the information about elevation and parameters of barotropic ellipses accordantly.

2. Coastline of the computational domain. The red line corresponds to the NOAA data, the green one is GEBCO based and the blue one is the used coastline. It is constructed using both data sets, but drawn so as to have bounded curvature (using cubic b-splines).

3. Amplitude of the M_2 constituent in the Lena Delta region of the Laptev Sea from different inverse tidal solutions.

4. Error of different models against coastal tide gauges for the M_2 and S_2 constituents.

5. Tidal map for the M_2 and S_2 constituents. Simulations use optimal boundary conditions for tidal elevation.

6. Ellipses of barotropic velocities for the M_2 constituent. Simulations use OOBC.

7. Residual circulation for the M_2 constituent superimposed on bathymetry map for the western part of the considered domain. Simulations use OOBC.

8. Comparison of major axes in simulations based on the open boundary conditions from different inverse models and predicted directly by these models with observational data.

9. a) Difference between GEBCO bathymetry and additional bathymetric data from digitized Soviet map. b) Difference between amplitudes of the M_2 in simulations based on GEBCO and modified bathymetry.

10. Total energy for the M_2 and S_2 waves. Simulations use OOBC.

11. The amplitudes of the M_2, M_4, M_6, M_8 harmonics and Z_0 at all coastal stations. Simulations use OOBC.

12. Energetic budget for the M_2 and S_2 waves. Simulations use OOBC.

13. Fluxes of tidal energy for the M_2 and S_2 waves. Simulations use OOBC.

Chapter 6

1. Selected domain and constructed coastline.

2. Results of simulation with OOBC for amplitude and phase for M_2 constituent.

3. Surface temperature fields at the end of May in cases with different types of thermodynamic forcing.

4. Surface salinity distribution in the middle of May, 2008 in cases with different types of forcing and different techniques of freshwater distribution.

Chapter 7

1. Model computational domain with shown cross sections used for the analysis, mooring positions, open boundary segments and structure of freshwater distribution.

2. Initial of salinity fields (surface and bottom layers).

3. Surface salinity distribution in cases with different wind products (short run simulations).

4. The Brunt–Väisälä frequency and isohaline lines in cross-sections in cases with different forcing (short run simulations).

5. Mean vertical shear induced by M_2 wave at the moment of maximum kinetic energy.

6. Observed and simulated near-bottom temperature and salinity at Khatanga and Anabar mooring positions.

7. Simulated surface salinity patterns at different time points driven by ECMWF atmospheric forcing. The dots indicate the positions of CTD measurements available to us.

8. The simulated versus observed temperature and salinity for September, 2008.

Chapter 8

1. Scheme of gauging station locations.

2. Transverse profile of the riverbed in the area of GS Kusur based on observations in 2012, first decade of June.

3. Transverse profile of the riverbed in the area of GS Habarova based on observations in 1991, last decade of November.

4. Mean monthly surface water temperature measured at GS Kusur, Habarova and Tit-Ary from 1936 to 2011 for different summer months.

5. Mean summer (June-September) water temperature at GS Kusur and Habarova.

6. Mean monthly surface air and water temperatures at GS Kusur and Habarova for the summer season for each year from 2002 to 2011.

7. Stream temperature profiles and mean surface air temperatures on a corresponding date.

8. Mean daily surface air and water temperatures measured at GS Kusur, Habarova and Eremeyka for the summer season (2002-2011).

9. a) Correlation between mean monthly surface temperatures measured at GS Kusur and Eremeyka.

   b) Correlation between surface temperatures measured at GS Habarova and Eremeyka. The histograms show the variation of the correlation coefficient across all the bootstrap samples.

10. Correlation between times at GS Kusur and Habarova when the surface water temperature reaches maximum. The histograms show the variation of the correlation coefficient across all the bootstrap samples.

11. Correlation between the normalized surface water temperature at GS Eremeyka and amplitude of anomaly. The histograms show the variation of the correlation coefficient across all the bootstrap samples.

12. The Lena River bed profile, area of GS Stolb, main channel. The picture is taken from Bolshiyanov et al., 2013.

Chapter 9

1. MDS projections and the considered domain. Selected points on the projections and corresponding points on the domain are highlighted. Two test cases are presented: without tides and without wind forcing.

2. The upper picture shows the positions of CTD measurements in August, 2010 in the Lena Delta. The bottom picture presents the difference between measured maximum and minimum temperatures marked on the upper picture.

3. The daily surface air temperature at Samoylovskay Island based on observations and ECMWF modeling results.

List of tables

Chapter 4

1. Manuscripts presented in the current work.

Chapter 5

1. Comparison of amplitudes and phases from different models and observational data for the M_2 constituent.
2. Comparison of ellipse parameters from different models and observational data in open water season for M_2 (S_2).

Chapter 6

1. Error of different models against coastal tide gauges for the M_2 constituent.

Chapter 8

1. Available data used in this work.
2. Mean surface water temperature measured at different gauging stations.
3. Date of the first ice appearance in the autumn.
4. Mean discharge rate for the Lena River for the period from 1935 to 2011, measured at mainstream Kusur Station and mean water level for the period from 2002 to 2011.

Introduction

Coastal seas at high latitudes are affected by the changing climate, which explains the increasing interest in them, as evidenced by recent observational and modeling studies (Nicholls et al., 2007; http://www.ipcc.ch/ipccreports/tar/wg2/index.php?idp=283). This thesis focuses on modeling the circulation in the Lena Delta region of the Laptev Sea and analyzes the factors influencing the propagation of the Lena freshwater plume.

The particular focus on the Lena Delta is motivated by the fact that the Lena River is one of the largest contributors of freshwater to the Arctic Basin. The spread of the Lena freshwater plume governs the stability of the water column and, accordingly, vertical mixing and vertical exchanges over a wide portion of the Laptev Sea shelf. Additionally, the Lena water transports considerable amounts of organic and inorganic material containing carbon in diverse molecular forms into the Laptev Sea (Kattner et al., 1999). The thawing of the Siberian permafrost may increase this input (Örek et al., 2013). A large number of observations available for the Lena Delta region suggest significant changes in climatology and as a consequence in the ecosystem over the past fifty years (Bauch et al., 2009; Costard et al., 2007; Dmitrenko et al., 2008a; Hölemann et al., 2011). Due to global warming, the Northeast Passage becomes more in demand, and the large Tiksi harbour in the south-eastern part of the Laptev Sea becomes more important. This is one more reason why the circulation dynamics and environmental conditions in the Laptev Sea must be examined.

Despite the considerable amount of accumulated observational data and the existing analyses of plume dynamics, which are based on these observations, there is a need for more detailed understanding of the dynamics, which can be provided by a modeling of the circulation in the shelf zone of the Laptev Sea. The main question is whether or not it is possible to predict, with the available forcing data, how the Lena freshwater plume spreads over the Laptev Sea. Apparently, it is partly governed by the circulation arising due to the huge density contrast between the plume and ambient saline water. However, winds will modify the circulation, and together with tides mix the plume water and the residual circulation due to tides may contribute too, modifying locally the path of freshwater. Finally, heat exchange with the atmosphere can be another factor. A question naturally arises about the relative roles of these factors.

The south-eastern part of the Laptev Sea, which includes the Lena Delta region, represents a large, shallow, estuarine area with dominant depths of about 10–30 m and a complex shape of the coastline. Modeling the Lena Delta region should be able to deal with sufficiently small scales associated with particular channels, complex coastline and bottom topography. It should incorporate

tides, because they are responsible for a part of the water column mixing and transport. It should also resolve baroclinic dynamics of the freshwater plume with sufficient degree of certainty. This calls for setting up a regional model relying on a large-scale model as a source of information for temperature and salinity at the open boundary, driven by atmospheric forcing, prescribed tidal elevation at the open boundary and prescribed the Lena River discharge along the Delta boundary. Available modeling studies with some focus on the region are either performed on too coarse meshes, or exclude tidal dynamics, and/or fail in prescribing the freshwater discharge accurately (Johnson and Polyakov, 2001; Ernsdorf et al., 2011; Rozman et al., 2011). Even tidal solutions available for the Arctic, including data-based solutions, do not properly resolve the Laptev Sea shelf and predict rather different tidal maps for the area (see discussion in Section 5.3.3). For this reason, modeling of the freshwater plume propagation to answer the indicated questions requires, in the first turn, setting up a model that would make it possible.

The main goal of this thesis is therefore two-fold. First, is the setup of a full numerical model of the circulation in the Laptev Sea shelf zone with focus on the Lena Delta region and its verification against available observational data. Second, is the analysis of freshwater plume dynamics in this region in the summer season based on this model. The setup is based on FVCOM (The Unstructured Grid Finite Volume Coastal/Community Ocean Model, Chen et al., 2006). The capability of the model to work on unstructured meshes is essential, and the necessity of it dictated by the geometrical complexity of the domain. Achieving this goal required two preliminary steps, which are the subjects of separate papers.

First, accurate modeling of the tides is a prerequisite to modeling full dynamics. The main challenge here is the absence of sufficiently accurate, data-based solutions for tidal sea surface elevation that can be used at the model's open boundaries. To alleviate this difficulty, optimized open boundary conditions (OOBC) are proposed (Section 5 of this thesis, Manuscript 1 in the list in Section 4), which improve the model accuracy in simulating the main semidiurnal components dominating in the region. These conditions are obtained by combining the data-based solutions with the tide-gauge measurements at locations nearest to the open boundary, and selecting the combination that minimizes the error at the remaining gauging stations. It is shown that using OOBC reduces the error between model simulations and available tide gauge data, and that model simulation of tidal ellipses has a good agreement with observations. This work contains analysis of tidal dynamics obtained in simulations with OOBC, in particular of tidally driven residual

circulation. These OOBC are further used in simulations with the full baroclinic model (see Sections 6 and 7, Manuscripts 2 and 3 listed in Section 4).

Second, one needs to specify properties of input water. It motivated analysis of available observational data for the Lena water characteristics (Section 8, Manuscript 4). The collected and analyzed data are used as an input for the full model (partly described in Section 9.2). The analysis revealed correlations between the temperatures of water and air, and between the water temperatures along stream locations. It simultaneously indicated the presence of water temperature anomaly at the northernmost station where the temperature is systematically higher than at locations upstream. Possible causes of temperature anomaly are discussed. This study incorporates virtually all available water temperature measurement data and presents interesting topic on its own as the most comprehensive data compilation. It also shows that the Lena River temperature in the basin outlet area is highly variable.

These two preliminary steps serve as the basis for the model setup. The first of them also includes the mesh design (see Sections 5-7, Manuscripts 1-3). There are other components of the setup, which include initial conditions and forcing, which are described in detail in Manuscripts 2 and 3 (Sections 6 and 7) dealing with full baroclinic dynamics. In modeling full baroclinic plume dynamics, a special focus is placed on exploring the impact of tides and atmospheric forcing. Simulations were performed for the 2008 summer season, a period for which forcing, initialization and observational data were available. They included series of the short-term simulations (May, 2008) with different atmospheric forcing and with or without tides, performed to assess the relative impact of various factors on plume propagation. The long-term simulations (May-September, 2008) included a full dynamics and were compared to the available measurements in the area.

In addition to the mentioned work directions, the work on different techniques of result visualization and statistical approach to model Lena water temperature at the mouth area was carried out. Since it is not yet completed, it is presented as the materials in preparation for submission.

The papers containing the main results obtained in the course of a PhD studentship also review the relevant literature, which is not repeated here. To facilitate reading, Sections 1 and 2 present a general description of the region and the Lena River hydrological regime. Section 3 briefly describes the model implementation. Section 4 lists the manuscripts and steps needed to perform the work. Sections 5-8 reproduce articles and manuscripts. The overview of the materials in preparation for submission is in Section 9. Section 10 recapitulates the main results obtained in this thesis and discusses the research needs.

1. General description of the Laptev Sea region

The Laptev Sea is east of the Taymyr Peninsula and Severnaya Zemlya and extends to the New Siberian Islands (Fig. 1). Among the seas of the Arctic Ocean into the Laptev Sea the largest number of rivers flows: Lena (provides approximately 70% of total runoff to the Laptev Sea), Olenyok, Khatanga, Anabar, Yana, Omoloy, Gusiha and other small others. The total amount of annual flow into the sea is more than 700 km.[3] The Sea shores are winding and form gulfs and bays of various sizes. The coastal landscape is also diverse, with small mountains near the sea in some places (Sofina, 2008).

The main gulfs of the Laptev Sea coast are the Khatanga Gulf, Olenyok Gulf, Buor-Khaya Gulf and Yana Bay (Fig. 1). The Laptev Sea shelf area contains a lot of small islands mostly in the western part of the Sea and in the river deltas with the total area of 3,784 km.[2] The area of the Sea is 650,000 km[2]; its volume is 338,000 km[3] (http://bse.sci-lib.com/article068747.html).

As in the Kara Sea, a deep gully enters the western part of the Laptev Sea from the north; saline and somewhat warmer waters flow into the Laptev Sea through it. The average depth of the Laptev Sea is 519 m and its greatest depth is 2,980 m. However, there dominant depth is about 50-100 m (Fig. 1).

The sea floor of the southern Laptev Sea is a sloping plain, lowering to the north, cut by canyon-like troughs, which are now only weakly pronounced. These troughs are all located at the mouths of the rivers, entering the sea from the south. The underwater troughs appear to be the traces of the river valleys which crossed the low plain many millennia ago (Kotyukh et al., 1990).

The wind speed over the Laptev Sea is an average of only 5 m/s in the summer season; storms occur three to four times monthly. Cloudiness remains slight and precipitation is also less than in other neighbouring regions. Relative humidity reaches 95-98 %, which is why fog is quite frequent, especially in the regions with considerable ice accumulation (Timokhov, 1994).
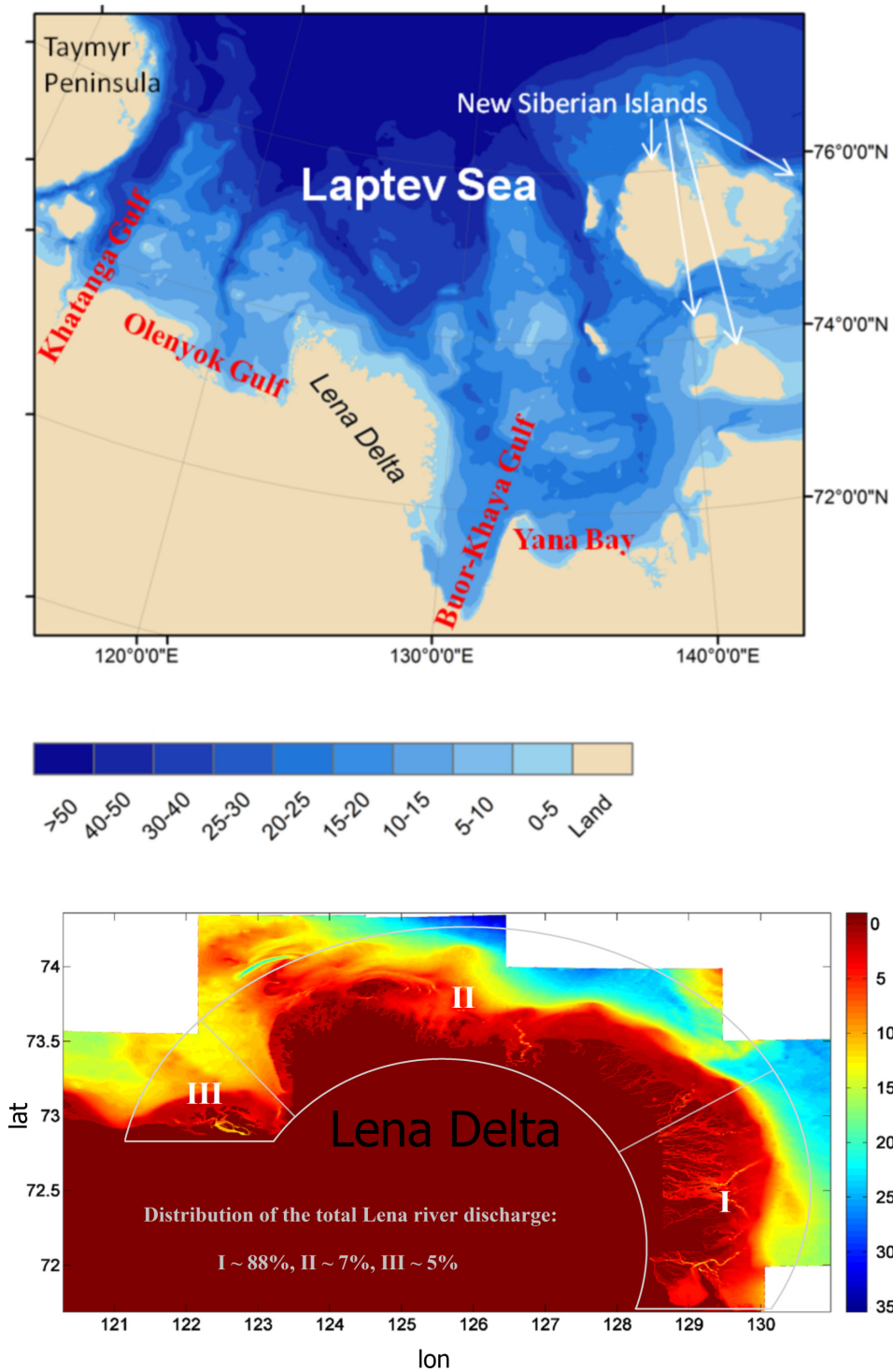
Fig. 1. The Laptev Sea map. Colour shows the IBCAO (The International Bathymetric Chart of the Arctic Ocean; Jakobsson et al., 2012*)* topography, [m]. The additional bottom picture shows detailed seabed topography based on a Soviet digitized map, [m] (0m – terrestrial area). This map visualizes the locations of main channels where local extrema of freshwater discharge are located. The transparent figures visualize the mean summer (May-September) freshwater discharge distribution according to Magritsky (2001) and Bolshiyanov et al. (2013).

9

The atmospheric observations are sparse in the region. However, based on observational data at Tiksi hydrometeorological Station we have obtained some important information about climate data changes in the Laptev Sea region. Figure 2 shows the mean surface air temperature dynamics from 1936 to 2009 for different periods. For the annual scale, we do not have significant trends for the air temperature. However, Figure 2 clearly shows the anomaly high annual air temperature in 2007. Also for mean air temperature in May there is no significant trend, but there is an emerging trend and two clear-cut maximums in 1990 and 2007 from the beginning of the observations. For the summer mean air temperature, a significant trend exists, which shows the increasing of air temperature by 1°C form the beginning of the observations. But there is no guarantee that this trend is reliable, due to the high variance of the temperature values.
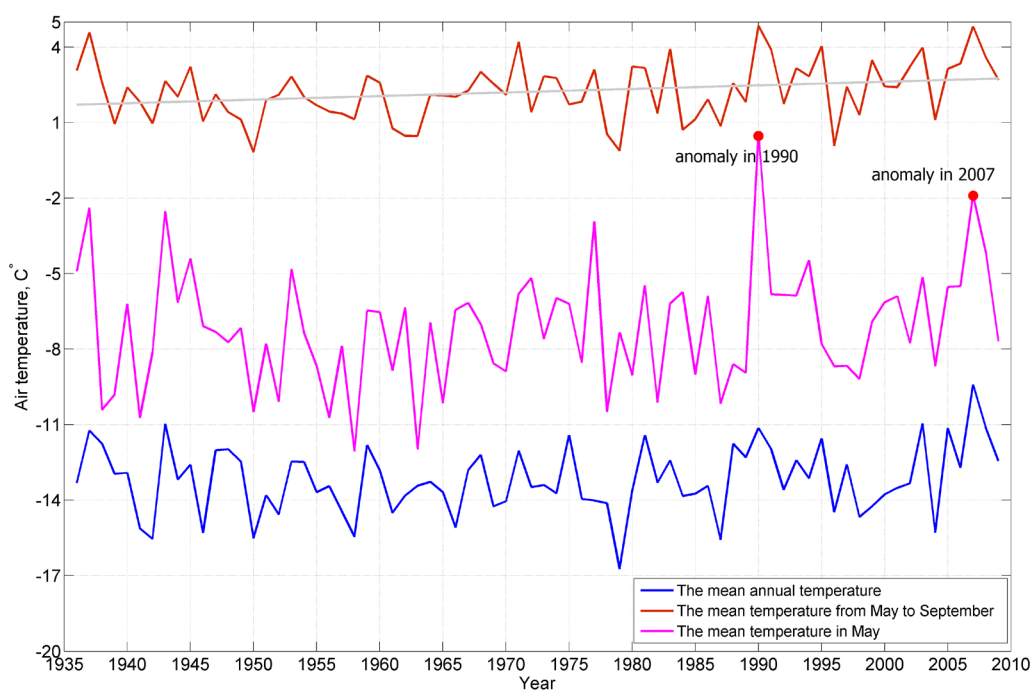
Fig. 2. The mean surface air temperature from 1936 to 2009, Tiksi Bay. The regression line is shown in grey. The theoretical slope of the line is significantly different from 0 with 98% probability.

The Laptev Sea is one of the most significant regions of net ice production and export among the Siberian Shelf Seas (Krumpen et al., 2012). The Laptev Sea is ice covered from October to June. In August and September the Laptev Sea is more often ice free. The ice formation starts in September in the north and in October in the southern part of the Laptev Sea. In the winter season there is a large sheet of ice with the thickness up to 2 meters exist in the south-eastern part of the sea as well as near the coast. The ice cover can be divided into three types: the fast ice, the pack ice, and flaw polynyas (Alexandrov et al., 2000; Krumpen et al., 2012).

2. Lena River hydrology regime

The Lena River catchment area is about 2,430,000 km^2, the mean annual runoff volume of the River from 1935 to 2012 is at about 539 km^3 (these estimates are provided by centers of the Hydrometeorology and Environmental Monitoring in Tiksi). The winter discharge from November to April is minor compared to summer discharge. Figure 1 shows the dynamics of mean monthly discharge rate in a year for the period from 1935 to 2011 at the basin outlet area.
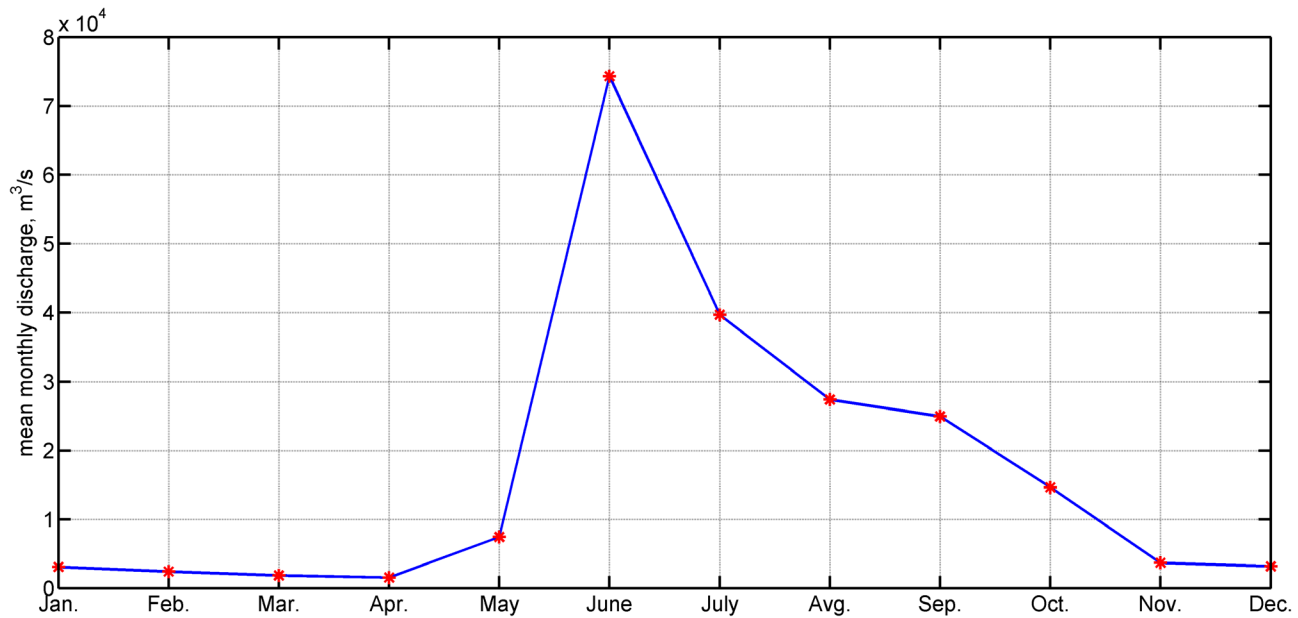
Fig. 1. The mean monthly discharge for the period from 1935 to 2011 (Kusur Station).

The maximum daily discharge rate can reach 200,000 m^3/s. There is evidence that the daily discharge maximum has tendency to an earlier onset based on the data from twentieth century (Yang et al., 2002). The available modern data confirm this (Fig. 2). Also the tendency to increase the total volume of runoff exists (Fig. 3).
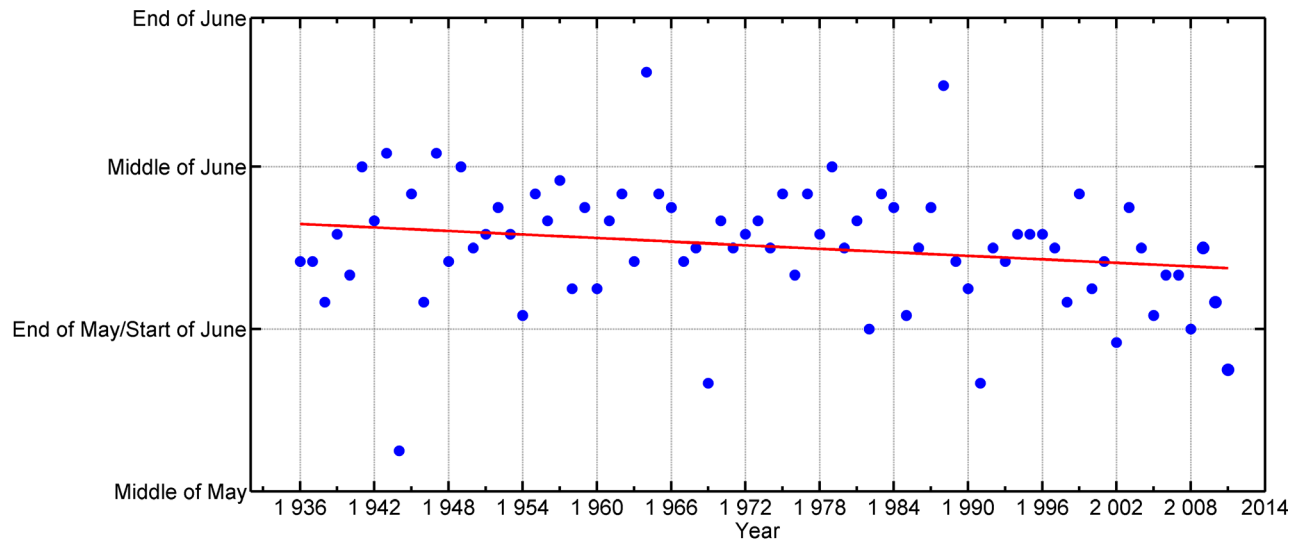
Fig. 2. The time of the year when the daily flow of the Lena River reached a maximum from 1936 to 2013 (Kusur Station). The regression line is shown in red. The theoretical slope of the line is significantly different from 0 with 94.1% probability.
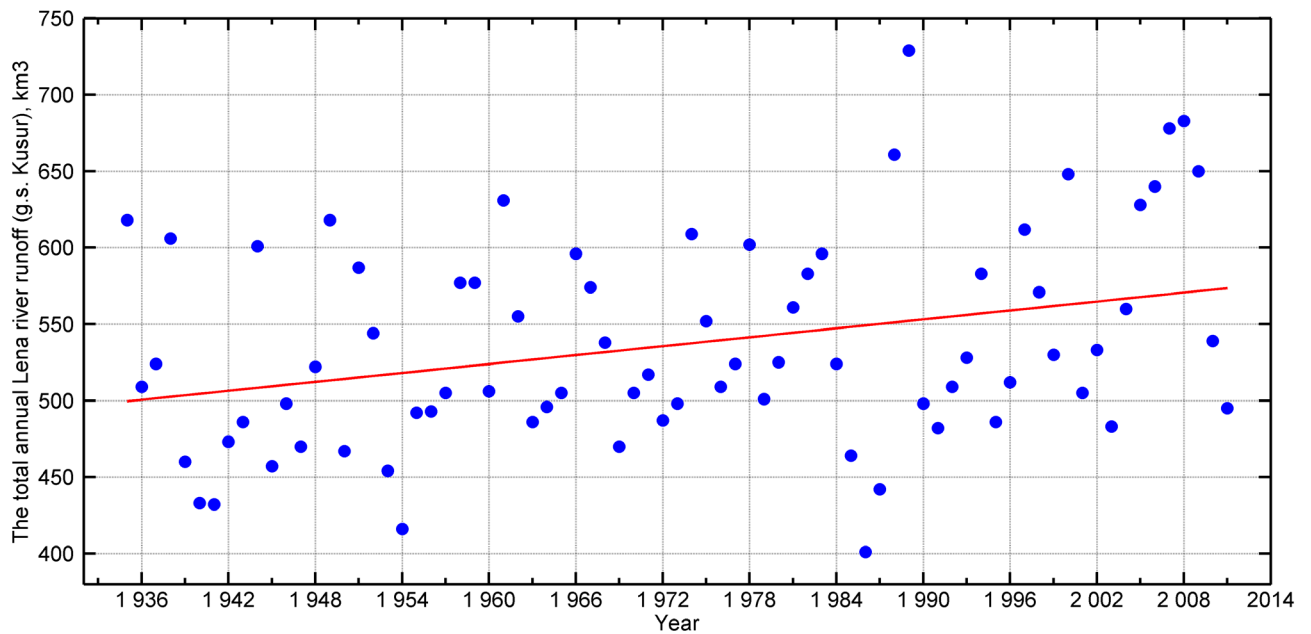
Fig. 3. The total annual discharge from 1936 to 2013 (Kusur Station). The regression line is shown in red. The theoretical slope of the line is significantly different from 0 with 99.6% probability.

The mean summer Lena River temperature at the basin outlet area does not have a clear trend. However, when different summer months are considered separately, some tendencies are detected. We should mention here that the Lena River hydrology behaviour at the basin outlet area is rather complex. The detailed analysis of the Lena River discharge characteristics should include information from the available stations at the basin outlet. This topic will be discussed further in Section 8.

As a result the coastal region under the influence of the discharge from the Lena Delta channels has become a new focus of attention investigating the phytoplankton communities and the influence of physic-chemical parameters and stratification on their abundance.

3. Short model description

The Finite Volume Coastal/Community Ocean Model (called FVCOM) is used as a tool for the current study. FVCOM was originally developed by UMASSD-WHOI for the estuarine processes and the tidal-, buoyancy- and wind-driven circulation in the coastal region characterized by complex irregular geometry and steep bottom topography. FVCOM is a prognostic, finite-volume, free-surface, unstructured-grid, 3-D primitive equation coastal ocean circulation model (Chen et al., 2006; Chen et al., 2003).

FVCOM solves the following set of equations (written here in Cartesian coordinates and z-coordinate in vertical for simplicity) for momentum, continuity, temperature and salinity, completed by the equation of state:

$$\frac{\partial u}{\partial t} + u\frac{\partial u}{\partial x} + v\frac{\partial u}{\partial y} + w\frac{\partial u}{\partial z} - fv = -\frac{1}{\rho_0}\frac{\partial P}{\partial x} + \frac{\partial}{\partial z}\left(K_m\frac{\partial u}{\partial z}\right) + F_u$$

$$\frac{\partial v}{\partial t} + u\frac{\partial v}{\partial x} + v\frac{\partial v}{\partial y} + w\frac{\partial v}{\partial z} + fu = -\frac{1}{\rho_0}\frac{\partial P}{\partial y} + \frac{\partial}{\partial z}\left(K_m\frac{\partial v}{\partial z}\right) + F_v$$

$$\frac{\partial P}{\partial z} = -\rho g$$

$$\frac{\partial u}{\partial x} + \frac{\partial v}{\partial y} + \frac{\partial w}{\partial z} = 0$$

$$\frac{\partial T}{\partial t} + u\frac{\partial T}{\partial x} + v\frac{\partial T}{\partial y} + w\frac{\partial T}{\partial z} = \frac{\partial}{\partial z}\left(K_h\frac{\partial T}{\partial z}\right) + F_T$$

$$\frac{\partial S}{\partial t} + u\frac{\partial S}{\partial x} + v\frac{\partial S}{\partial y} + w\frac{\partial S}{\partial z} = \frac{\partial}{\partial z}\left(K_h\frac{\partial S}{\partial z}\right) + F_S$$

$$\rho = \rho(T, S, P),$$

where x, y, z are the east, north, and vertical axes in the Cartesian coordinate system; $u, v,$ and w are the x, y, z velocity components; ρ is the density; P is the pressure; f is the Coriolis parameter; g is the gravitational acceleration; T is the temperature; S is the salinity; K_m is the vertical eddy viscosity coefficient and K_h is the thermal vertical eddy diffusion coefficient. F_u, F_v, F_T and F_S represent the horizontal momentum, thermal, and salt diffusion terms. The total water column depth

is $D = H + \zeta$, where H is the bottom depth (relative to $z = 0$) and ζ is the height of the free surface (relative to $z = 0$) (Chen et al., 2006).

The surface and bottom boundary conditions for temperature are:

$$\frac{\partial T}{\partial z} = \frac{1}{\rho c_P K_h}[Q_n(x,y,t) - SW(x,y,\zeta,t)], \text{ at } z = \zeta(x,y,t)$$

$$\frac{\partial T}{\partial z} = \frac{A_H \tan \alpha}{K_h}\frac{\partial T}{\partial n}, \text{ at } z = -H(x,y),$$

where $Q_n(x,y,t)$ is the surface net heat flux, which consists of four components: downward shortwave, longwave radiation, sensible, and latent fluxes, $SW(x,y,0,t)$ is the shortwave flux incident at the sea surface, and c_P is the specific heat of seawater. A_H is the horizontal thermal diffusion coefficient, α is the slope of the bottom bathymetry, and n is the horizontal coordinate shown in Fig. 1 (Pedlosky, 1974; Chen et al., 2006).

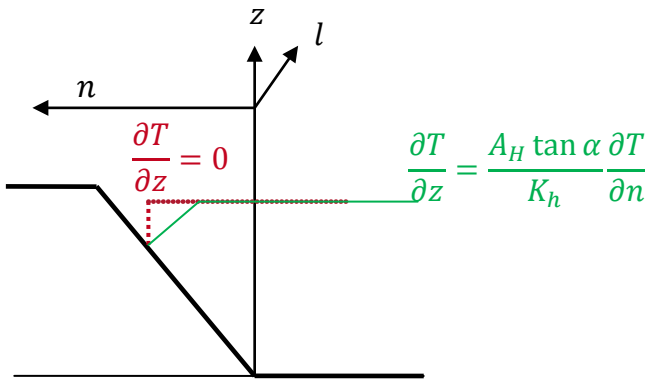**Fig. 1.** Schematic of the no-flux boundary condition on the bottom slope.

The surface and bottom boundary conditions for salinity are:

$$\frac{\partial S}{\partial z} = -\frac{S(\hat{P}-\hat{E})}{K_h \rho}\cos \gamma, \text{ at } z = \zeta(x,y,t),$$

where $\gamma = \dfrac{1}{\sqrt{1+|\nabla\zeta|^2}}$

$$\frac{\partial S}{\partial z} = \frac{A_H \tan \alpha}{K_h}\frac{\partial S}{\partial n}, \text{ at } z = -H(x,y),$$

15

where $\hat{P}$ is precipitation and $\hat{E}$ is evaporation rates. The groundwater flux can be added into the model by modifying the bottom boundary conditions for vertical velocity and salinity (Chen et al., 2006).

The surface and bottom boundary conditions for $u, v,$ and w are:

$$K_m\left(\frac{\partial u}{\partial z}, \frac{\partial v}{\partial z}\right) = \frac{1}{\rho_0}\left(\tau_{sx}, \tau_{sy}\right), w = \frac{\partial \zeta}{\partial t} + u\frac{\partial \zeta}{\partial x} + v\frac{\partial \zeta}{\partial y} + \frac{E-P}{\rho}, \text{ at } z = \zeta(x, y, t)$$

$$K_m\left(\frac{\partial u}{\partial z}, \frac{\partial v}{\partial z}\right) = \frac{1}{\rho_0}\left(\tau_{bx}, \tau_{by}\right), w = -u\frac{\partial H}{\partial x} - v\frac{\partial H}{\partial y} + \frac{Q_b}{\Omega}, \text{ at } z = -H(x, y),$$

where $\left(\tau_{sx}, \tau_{sy}\right)$ and $\left(\tau_{bx}, \tau_{by}\right) = C_d(u^2 + v^2)(u, v)$ are the x and y components of surface wind and bottom stresses, Q_b is the groundwater volume flux at the bottom and Ω is the area of the groundwater source. The drag coefficient C_d is determined by matching a logarithmic bottom layer to the model at a height z_{ab} above the bottom (Chen et al., 2006):

$$C_d = \max\left(\frac{k^2}{\ln\left(\frac{z_{ab}}{z_0}\right)^2}, 0.0025\right),$$

where $k = 0.4$ is the Von Kármán constant and z_0 is the bottom roughness parameter.

The kinematic, salt and heat fluxes conditions on the solid boundary are set as:

$$v_n = 0; \frac{\partial T}{\partial n} = 0; \frac{\partial S}{\partial n} = 0,$$

where n is the coordinate normal to the boundary and v_n is the velocity component normal to the boundary.

4. Overview of the manuscripts and main steps

4.1. List of manuscripts

The versions of papers presented below are those submitted to the journals. Table 1 contains a list of manuscripts and the corresponding section number. In Manuscripts 1 and 2 (Table 1), the published versions underwent some editing and slightly deviate from the text below.

Table 1. The manuscripts presented in the current work.

Manuscripts	Workflow	№ of Section
1. V. Fofonova, A. Androsov, S. Danilov, M. Janout, E. Sofina and K.H. Wiltshire (2014): **Semidiurnal tides in the Laptev Sea Shelf zone in the summer season**. Continental Shelf Research, 73, pp. 119-132. doi: 10.1016/j.csr.2013.11.010 **(published).**	**1, 2**	**5**
2. V. Fofonova, S. Danilov, A. Androsov, M. Zhukov, O. Semenova, P. Overduin, K. H. Wiltshire (2013): **Simulation of shelf circulation dynamics in the Laptev Sea.** Geo-Siberia-2013, Remote sensing and photogrammetry methods, environmental monitoring, geoecology, Novosibirsk 2013, Siberian State Geodesic Academy, v. 2, pp. 8-18 **(published).**	**1, 4.5, 4.6**	**6**
3. V. Fofonova, S. Danilov, A. Androsov, M. Bauer, P. Overduin, P. Itkin, K.H. Wiltshire (2014): **Impact of wind and tides on the Lena River freshwater plume dynamics (submitted to the Ocean Dynamics, after revision).**	**3.1, 3.2**	**7**
4. V. Fofonova, M. Kraineva, D. Yakshina, N. Tananaev, N. Volkova, and K.H. Wiltshire (2014): **The stream temperature characteristics of the Lena River at basin outlet in summer period (full version, short version is ready for submission to the Geophysical Research Letters).**	**1, 4.1, 4.3, 4.4**	**8**
5. Materials in preparation for submission	**3.3, 3.4, 4.2**	**9**

The papers based on this work, either published or submitted, have been written in collaboration with the author's colleagues. In all cases, however, the author's contribution is dominant and includes simulations, data analysis and writing. The contributions of the colleagues either through shared data or discussions or both are greatly appreciated.

4.2. Workflow

The linkage between main directions listed in the Introduction and Section 4.1 is shown in Figure 1. However, the work reported in this thesis included many substeps, which were essential for achieving the final goal: the setup of the model and analysis of the dynamics in the Lena Delta region. In order to better characterize the work done Figure 2 demonstrates the most important substeps. The detailed information about every substep is presented in Sections 5-9. Table 1 (Section 4.1) shows the interconnection between chapters and substeps.
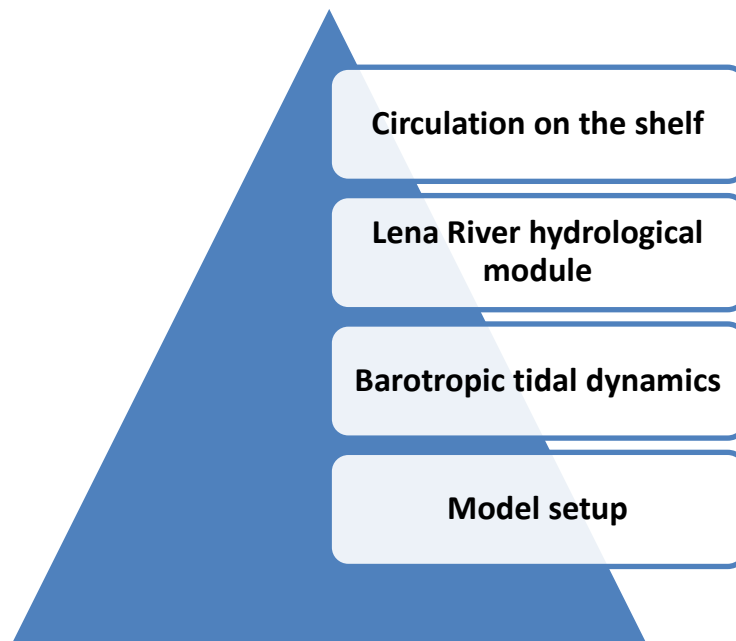

Fig.1. The linkages between the main directions of the work presented in this thesis.

Model setup

1. Selection of computational domain (a part of the Laptev Sea which is large enough to contain the main portion of the plume and the open boundary of which does not pass in the close vicinity of amphidromes)
2. Compilation of bathymetry (merging GEBCO and data from the Soviet digitized map)
3. Derivation of coastline by combining of available data with the aid of cubic b-splines
4. Triangulation of the selected area based on the algorithm by Persson and Strang (2004) based on constructed functions that specify local resolution and the distance to the boundary. The local resolution function depends on the depth and the gradients of topography
5. Porting of FVCOM
6. Setup of atmospheric forcing, initial fields and the temperature and salinity 'climatology' at the open boundary

Barotropic tidal dynamics

1. Comparison of simulations driven by different available data for the elevation at the open boundary
2. Construction of optimized open boundary conditions (OOBC) for the elevation (to reach better agreement with observations)
3. Construction of tidal maps for main tidal components with OOBC
4. Sensitivity study to additional bathymetric data
5. Analysis of tidal ellipses and comparison with observations
6. Analysis of residual circulation, energy fluxes and energy budget

Circulation on the shelf

1. Study of the impact of different factors (tides, winds) on the Lena freshwater plume propagation in the region
2. Applying multidimensional scaling procedure for the visualization of the results
3. Comparison of different atmospheric forcing products
4. Comparison of simulations against observations
5. Applying different techniques of the Lena River freshwater input in to the model
6. Study of the effects of forcing modified with the presence of polynyas

Lena River hydrological module

1. Analysis of hydrologic trends in the Lena River lower reaches (stream temperature, runoff volume and timing of hydrological events)
2. Description and analysis of water temperature anomaly found in the Lena Delta head area
3. Modeling of the Lena River stream temperature using nonlinear regression
4. Creating the Lena River hydrological module and incorporating it into the circulation model
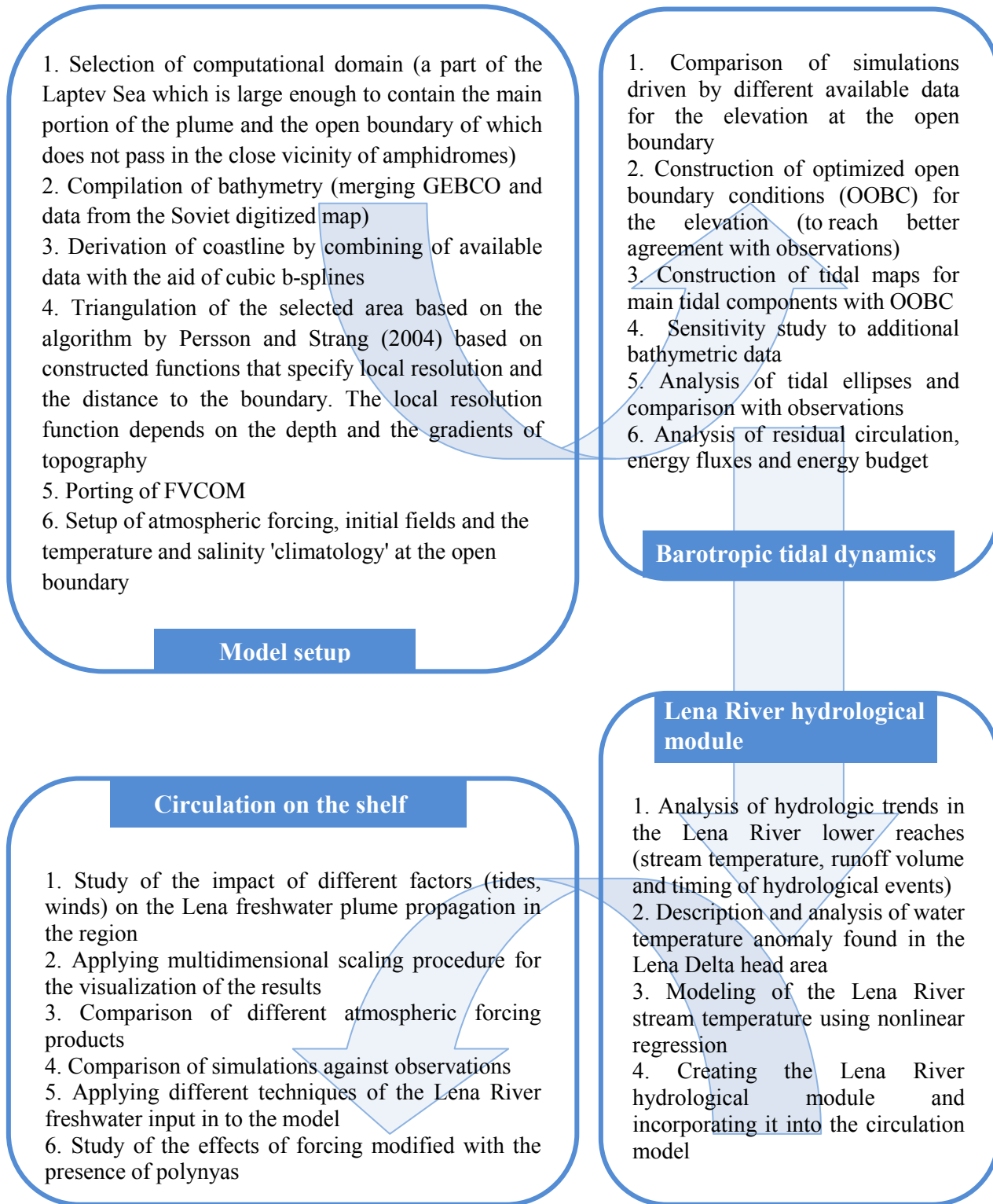
Fig. 2. The substeps of the main work directions.

5. Semidiurnal tides in the Laptev Sea Shelf zone in the summer season (Manuscript 1)

V. Fofonova,[1,2] A. Androsov,[2] S. Danilov,[2] M. Janout,[2] E. Sofina,[3,4] K. H. Wiltshire [1]

[1] Alfred Wegener Institute, Helmholtz Centre for Polar and Marine Research; Kurpromenade, D-27498 Helgoland, Germany;
[2] Alfred Wegener Institute, Helmholtz Centre for Polar and Marine Research; Bussestrasse 24, D-27570 Bremerhaven, Germany;
[3] St. Petersburg Branch, Shirshov Institute of Oceanology, Russian Academy of Sciences; Pervaya Linia 30, 199053 St. Petersburg, Russia;
[4] Russian State Hydrometeorological University; Malookhtinskii 98, 195196 St. Petersburg, Russia.

Abstract

Tidal processes play an important role in the dynamics of shelf circulation in the Laptev Sea. The Unstructured Grid Finite Volume Coastal Ocean Model (FVCOM) is used to simulate the tidal dynamics in the Lena Delta region of the Laptev Sea in ice-free barotropic case. The grid element size is ranging from 400 m to 5 km. The major semidiurnal tidal waves M_2 and S_2 are investigated with the M_2 being the most important in generating large sea level amplitudes and currents over the shallow areas. A correction to the tidal elevation at the open boundary is proposed which minimizes the discrepancy between the model prediction and observations. The observations include both recent mooring data and the standard set of tide gauge measurements used in previous studies. The comparison of results to known tidal solutions is carried out. The paper also discusses the residual circulation and energy fluxes and assesses the impact of additional bathymetric information.

Keywords

5.1. Introduction

The south-eastern part of the Laptev Sea, which includes the Lena Delta region, represents a large, shallow, estuarine area with dominant depths of about 10–30 m and complex shape of the coastline (Fig. 1). It forms a unique, plankton and zoobenthos rich, arctic ecosystem, characterized by high productivity supported by a powerful Lena River discharge (Sorokin and Sorokin , 1996).
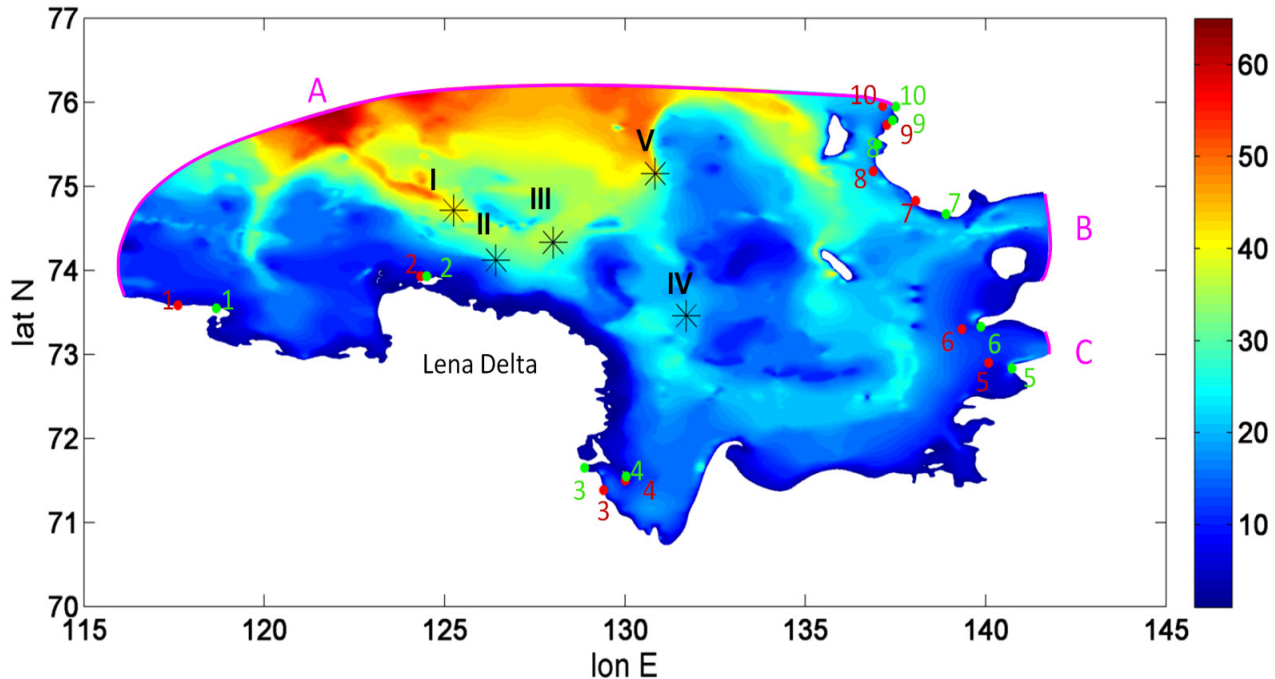

Fig. 1. Bathymetry of the selected domain (derived from GEBCO, resolution ~ 2 km), [m]. The numbered green and red points show the location of tide gauges where the amplitudes and phases are known. The green points correspond to the positions used by KP with some precision correction from the PSMSL data source. The red points are the positions of the stations used for verification AO-FVCOM. They deviate up to 40 km from the positions provided by KP. The asterisks show the mooring positions with known tidal ellipse parameters. The open boundary segments A, B and C are shown in pink.

A large number of observations available for the Lena Delta region suggest significant changes both in climatology and in ecosystem over the last fifty years (Bauch et al., 2009; Costard et al., 2007; Dmitrenko et al., 2008a; Hölemann et al., 2011). Given the large territory, the direct measurements are by far insufficient, calling for a modeling approach which would enable one to estimate the impact of different factors on the circulation dynamics and would lay the foundation for further ecosystem modeling. Tidally driven currents and mixing are important factors of such modeling.

Tides provide direct forcing to the Arctic marginal seas in all seasons (Lenn et al., 2011). The topographic features of the south-eastern part of the Laptev Sea make it very sensitive to tidally-induced mixing that dominates over the eastern Siberian Shelf (Kowalik and Proshutinsky, 1994;

21

Munk and Wunsch, 1998; Sofina, 2008). Tides may have a strong impact on marine ecosystems. The strong density contrast between the surface and bottom water would lead to reduced oxygen in the bottom layer if not the turbulent transport due to strong tidal currents over shallow water regions (Müller, 2008). The residual currents of barotropic motion play an important role in the transport of sediment, nutrients and organic matter in lagoons and estuaries, namely, in their exportation toward coastal seas (Valentim et al., 2013). For this reason, proper modeling of tidal dynamics is a prerequisite of any modeling efforts in the shelf part of the Laptev Sea.

While there are numerous modeling studies devoted to the dynamics of the Arctic Ocean, studies with focus on the coastal part of the Laptev Sea are virtually absent. In the Arctic the amplitudes of semidiurnal M_2 and S_2 and diurnal K_1 and O_1 tidal waves dominate over all tidal constituents (Kowalik and Proshutinsky, 1994). Numerical models simulating these constituents for the Arctic Ocean (AO) and its subdomains (e.g., Chen et al., 2009; Kowalik and Proshutinsky, 1993, 1995; Lyard, 1997) reveal that increased resolution helps to more accurately reproduce currents amplified over varying topography. Whereas the Russian Arctic coast zones, and the Laptev Sea in particular, are getting more and more in the spotlight, the still insufficient amount of observational data as well as the lack of modeling efforts with fine resolution over the shelf leaves many challenges. However, certain observational evidence has already been accumulated, leading to valuable insights in tidal dynamics (Dmitrenko et al., 2012; Janout and Lenn, 2013; Lenn et al., 2011).

The goal of this paper is to study the tidally driven circulation in the shelf zone of the Laptev Sea with focus on the Lena Delta region in ice-free barotropic case. We concentrate on the semidiurnal tidal waves M_2 and S_2, which will be simulated separately. The contribution from M_2 is the most important in the region, followed by S_2. According to AOTIM5 and TPXO7.1 (Padman and Erofeeva, 2004), the amplitude of the next largest semi-diurnal constituent N_2 is approximately 2-3 times smaller than amplitude of S_2 constituent on the open boundary of our region. The observations by Janout and Lenn, 2013 show a weak velocity signal of lunar elliptical tide N_2 only in the outer shelf area of the Laptev Sea. We therefore do not take it into account. The contribution of the K_1 and O_1 constituents in the domain is negligible based on observational data (Dmitrenko et al., 2012; Janout and Lenn, 2013).

Special attention is paid to the choice of open boundary conditions (OBC) for the tidal elevation for the investigated constituents. The OBC play the main role in achieving good agreement with observations in the limited modeling domain. It turns out that conditions derived from available

global or Arctic solutions have to be corrected, and we describe the procedure used. We also address in detail questions of energy balance and residual currents and carry out a comparison with available observations and model results. The model used for our studies is the Finite Volume Coastal Ocean Model (FVCOM), which has a solid record of practical applications (Chen et al., 2006; Rego and Li, 2010; Zhao et al., 2006) and works on unstructured meshes allowing variable resolution.

To validate the performance of the model we used data of tide gauges and moorings. Their locations are shown in Fig.1 superimposed on the bathymetry map of the domain under consideration. The comparison with accurate inverse solutions for AO and World Ocean AOTIM5, TPX06.2 and TPXO7.1 (Padman and Erofeeva, 2004) and tidal simulations for AO (Chen et al., 2009) and Siberian Shelf (Kagan et al., 2008a) has been also carried out.

The paper is organized as follows: In the next section we briefly describe data and model solutions we will use for comparison. Section 3 presents the description of our model and solutions used to impose boundary conditions on the model open boundary. In Section 4 we present and discuss tidal maps simulated for the M_2 and S_2 waves, which prove to be in a good agreement with observations, and also comparison with other simulations. We analyze ellipses of barotropic currents and the residual circulation induced by the M_2-tide. We extend the analysis further and consider the energy balance for the M_2 and S_2 waves and the sensitivity to the bathymetry. Section 5 presents the conclusions.

5.2. Available solutions and data

5.2.1. Tidal solutions

In this subsection we briefly describe tidal solutions for Global and Arctic Oceans and also for the Siberian Shelf, which will be used for comparison and to construct the OBC for tidal elevation. They include inverse solutions obtained by assimilating data of tide gauges and satellite altimetry (TPX06.2, TPXO7.1 and AOTIM5) and two solutions of forward 3D models for the Siberian Continental Shelf and Arctic Ocean.

We begin from the inverse models. The AOTIM5 (The Arctic Ocean Tidal Inverse Model) is based on Egbert et al. (1994) data assimilation scheme and presents an inverse solution with all available tide gauge data in the Arctic Ocean (Padman and Erofeeva, 2004). The Arctic Ocean Dynamics-based Tide Model (the numerical solution to the shallow water equations) was used as a 'prior' solution. This pan-Arctic 2-D linear model employs a 5-km regular grid and simulates 4 the

most energetic tides constituents (M_2, S_2, O_1 and K_1). Assimilated data consist of coastal and benthic tide gauges, between 250 and 310 gauges per tidal constituent, and also of available satellite altimetry data (Padman and Erofeeva, 2004). Model bathymetry is based on the International Bathymetric Chart of the Arctic Ocean (Jakobsson et al., 2008). AOTIM5 does not consider the effect of sea ice.

The TPXO7.1 and TPXO6.2 are global inverse tide models (Egbert et al., 1994; Padman and Erofeeva, 2004). The resolution of these models is $1/4^o$ x $1/4^o$. The TPXO7.1 and TPXO 6.2 assimilate TOPEX/Poseidon (T/P) and TOPEX Tandem satellite radar altimetry (available for the ice-free ocean between +/-66° latitude), and *in situ* tide gauge data in the Antarctic and the Arctic. The TPXO7.1 is considered as one of the most accurate global tidal solutions and recommended for using as a global model by Egbert, Erofeeva and Padman (EP).

Chen et al. (2009) presented the high-resolution unstructured grid finite-volume Arctic Ocean model (AO-FVCOM) with application for tidal studies. The horizontal resolution is ranging from 1 km in the near-coastal areas to 15 km in the deep ocean. The domain is divided into 40 sigma-layers. This model accurately resolves the irregular geometry of bays, inlets and islands in the Arctic coastal zone. But it shows rather large amplitude and phase differences between the modeled and observed semidiurnal tides along the Siberian Coast.

Kagan et al. (2008a,b) and Sofina (2008) presented the tidal model of the Siberian Continental Shelf (Kara, Laptev, East-Siberian and Chukchi Seas) based on a modified 3D finite-element hydrostatic model QUODDY-4. The ocean is considered homogeneous. The horizontal resolution varies from 2.57 km near the shore to 60.66 km in the open ocean. The water column is divided into 20 sigma-layers. Tidal elevation at the open boundary is determined by tidal forcing from the AOTIM5. The model takes into account the backward effect of shore-fast and drifting ice on the tidal dynamics. A comparison with observations on tidal gauges on the Siberian Continental Shelf of modeled tidal amplitudes and phases in the absence of sea ice shows smaller root mean square absolute and relative errors for this regional model than for the AOTIM5. These results also will be used in our analysis.

5.2.2. Observations

Observations of tidal currents over the Laptev Sea Continental Shelf are rare and fragmentary. The starting point for our analysis is tide gauge data obtained from http://www.ims.uaf.edu/tide/, the source organized by Kowalik and Proshutinsky (KP). These data are used by KP for verification of

their barotropic Arctic tidal model with sea ice (Kowalik and Proshutinsky, 1993,1994,1995). Note that the positions of these tide gauge stations were shifted up to 40 km for verification of AO-FVCOM by Chen et al. (2009) (see Fig. 1). The Buor-Haya Station will be excluded from our analysis because its coordinates as used in Chen et al. (2009), and provided by KP differ by approximately two degrees of latitude. In addition, the amphidromic points for the M_2 and S_2 constituents are located close to the Buor-Haya Station (Sofina, 2008), which leads to the high sensitivity of phase calculation to the position of this station. For our analysis we use coordinates provided by KP with some precision corrections obtained from Permanent Service for Mean Sea Level (PSMSL: http://www.psmsl.org/). We should mention that the large part (about 80%) of these data came from tide tables published in Russia in 1941 and their quality has never been evaluated and discussed (Chen et al., 2009). The recent research confirmed that significant corrections of amplitudes and phases for coastal stations are needed (Voinov, 2002). It should also be stressed that measurements on these stations can be done only within a couple of months due to presence of fast ice. However, these data allow constructing the major pattern of tidal dynamics in the region.

The other set of data we will use for analysis is based on several year-round oceanographic mooring records at different locations, designed to monitor currents and hydrography on the central Laptev Sea Shelf (Janout and Lenn, 2013). Based on these data, Janout and Lenn, 2013 (under revision) computed ellipse parameters of barotropic currents during the sea ice and open water seasons. Their results of barotropic tidal ellipses are based on vertically averaged ADCP profiles. Janout and Lenn, 2013 aimed to investigate the role of stratification on tidal structures, and in turn the importance of the sheared tidal currents on diapycnal mixing. But they also confirmed the theoretical study (Polyakov, 1994) that tidal kinetic energy in the domain considered is quantified sufficiently well by the barotropic tide. The moorings were operated as part of the German-Russian "Laptev Sea System" project since 1992. Each mooring was designed to remain at a safe distance below the sea ice, and was equipped with upward-looking Teledyne-RDI Workhorse Sentinel Acoustic Doppler Current Profilers (ADCP, 300 kHz), moored ~3 m above the bottom with a sampling frequency of 30 minutes and some moorings were equipped with an additional downward-looking 1200 kHz ADCP (Janout and Lenn, 2013).

For our analysis we choose five different locations (Fig. 1), which are situated in the selected region, and limited to the case of open water.

5.3. Model, input data and experiment descriptions

5.3.1. Model description

For simulations of tidal dynamics in the Delta Lena region of the Laptev Sea we use the Finite Volume Coastal Ocean Model (FVCOM), which solves primitive equations on unstructured meshes (Chen et al., 2006). The computational domain covers water depths up to 65 m (Fig. 1), with the minimum depth set to one meter. The domain was selected so as to avoid amphidromic points in the close vicinity of its open boundary (we relied on the results by Kagan et al., 2008a and Sofina, 2008), to be large enough to incorporate the central part of the Laptev Sea Shelf zone, yet small enough to keep moderate the ratio of largest to smallest elements of the grid. Simulations are performed on a high quality unstructured grid, which allows us to take into account the complexity of coastline and bathymetry. The grid was generated using the algorithm by Persson and Strang (Persson and Strang, 2004) and is composed of triangles that are close to equilateral. Elements sizes vary from 400 m near the coast to 5 km in the deepest area of the domain. The number of nodes in each horizontal layer is about 250000; the mesh contains six vertical sigma-layers. We use equally spaced sigma layers. Additional simulations with not equally spaced sigma layers have been also carried out, but with a smaller time step. We did not find any significant difference in dynamics in these cases. For vertical and horizontal mixing simulation we use the modified Mellor and Yamada level 2.5 and Smagorinsky turbulent closure schemes respectively. The multiplicative coefficient in the Smagorinsky parameterization is set to 0.005. FVCOM uses upwind implementation of momentum advection, so that large values of horizontal viscosity are not necessarily needed. As advection scheme, we apply the second order upwind scheme. The model used in this study employs the mode splitting method. The time step for external mode is 4.6 sec, the ratio of internal mode time step to external mode time step is 10.

To avoid errors due to the inconsistency between the character of equations and the specified open boundary conditions (prescription of tidal elevation only), a sponge layer has been introduced. It gradually turns off the advection of momentum and viscosity in the vicinity of the open boundary. After series of experiments we decided to use 70-km sponge layer to avoid instabilities in the vicinity of the open boundary and preserve the tidal dynamics inside the domain.

5.3.2. Input data

We used two sources of bathymetry data: GEBCO_08 (The General Bathymetric Chart of the Oceans) gridded bathymetry data - a global 30 arc-second dataset (http://www.gebco.net/data_and_products/gridded_bathymetry_data/) and data in the vicinity of the Lena Delta consisting of 27686 points from digitized Soviet map provided by Paul Overduin, with an average distance between the points of 800 m. The latter data set is utilized in the analysis of the sensitivity of tidal simulations to the details of bottom topography. For coastline construction, we combined the coastline derived from GEBCO bathymetry data with ~ 2 km resolution, which is largely consistent with the bathymetry, but lacks many details at the coast, and NOAA (The National Oceanic and Atmospheric Administration) coastline data with ~ 250 m resolution from World Vector Shoreline database (http://www.ngdc.noaa.gov/mgg/ shorelines/shorelines.html), which is too detailed for the mesh resolution we intended to use. The resolution of coastline obtained by us varies from 400 m to 800 m, depending on the local size of mesh elements. The GEBCO data, because of their smooth character, do not allow one to take into account certain essential coastline features. We, therefore, departed from the NOAA data removing, first, fragments with a too small local curvature radius (given by the minimum triangle side) and relaxing the coastline toward the smooth GEBCO data. Thus, for each local region optimization problem was solved. In the end, to further smooth the coastline we used cubic b-splines technique. Fig. 2 illustrates the result, which is close to both data sets where the coastline is smooth, but shows deviations over the intended part of the boundary.
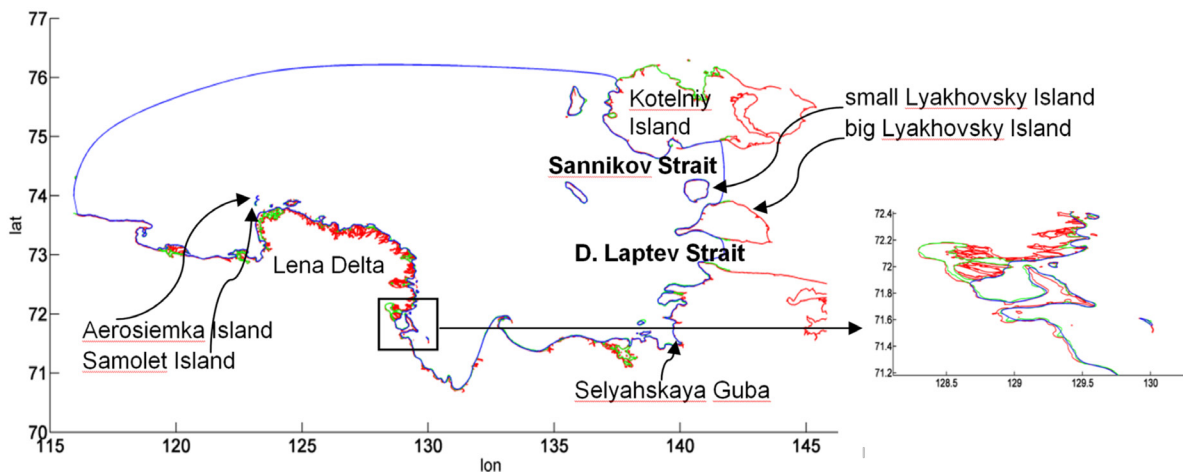

Fig. 2. The coastline of the computational domain. The red line corresponds to the NOAA data, the green one is GEBCO based and the blue one is the used coastline. It is constructed using both data sets, but drawn so as to have bounded curvature (using cubic b-splines), as shown in the right panel for a fragment of coastline.

5.3.3. Open boundary conditions derivation and experiment description

Specification of tidal elevation on the open boundary is central to modeling tides (we do not take the tidal potential into account because the model includes a rather long open boundary). It turned out that the amplitudes and phases of the elevation on the open boundary, taken from the inverse solutions, should be corrected near the coast (depth<10-15 m). For one thing, the inverse solutions predict different dynamics in the region of interest, as illustrated in Fig. 3. Indeed, the amplitude maps provided by these solutions differ substantially on the model open boundary, especially over the western part. The horizontal resolution of TPX06.2 and TPXO7.1 and associated inaccuracies in assumed bathymetry data limit the skill of their solutions in the coastal zone. Although AOTIM5 provides much better spatial resolution, it is still insufficient. Based on the available solutions, we tried to combine and adjust them at the open boundary so that the simulated elevation inside the domain reaches best possible agreement with the available observational data. We have 10 stations where the observed amplitudes and phase are available and also 5 stations with the information about barotropic ellipse parameters in the region considered. The information from 3 stations can be used directly because they are close to the open boundary. The rest can be taken into account indirectly, by doing simulations and analyzing their results. In a way, it was a simplified version of data assimilation procedure.
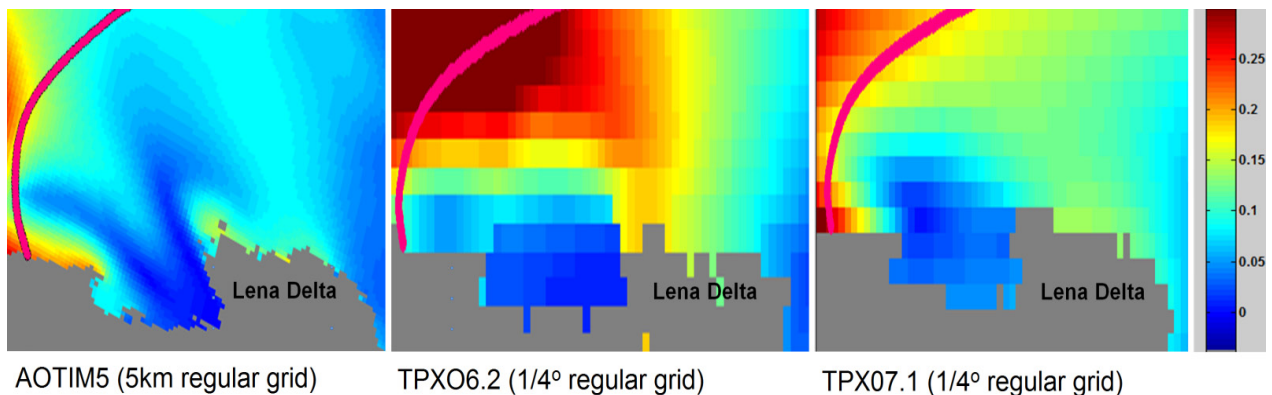

Fig. 3. The amplitude of the M_2 constituent in the Lena Delta region of the Laptev Sea, [m]. The maps are obtained using TMD toolbox provided by EP. The open boundary is shown in pink.

We used a two-step procedure to find the optimal boundary conditions (OBC). First, we derived the tidal elevation from the available inverse solutions of AOTIM5, TPXO6.2 and TPXO7.1, and analyzed to what a degree each of them leads to an accurate solution. For each of three cases of OBC, with the tidal elevation taken from AOTIM5, TPXO6.2 or TPXO7.1, the bottom drag coefficient was tuned to reach the best agreement with observations. The bottom drag coefficient

varies with depth as given by the second formula in the section describing user-defined setting in Chen et al. (2006). We slightly modified the bounds in this formula. The maximum and minimum of the bottom drag coefficient were chosen for each case of OBC.

On the second step, we, first, split the open boundary in segments (Fig. 1) and analyzed the impact of each of them on the amplitude and phase patterns. Carrying out numerous experiments, we selected the solutions on each segment that provided the best agreement with observations. They have been then additionally corrected by directly taking into account the information from the tide gauges situated near the open boundary, and further tuned then to improve the agreement with observational data at other locations. As a result we designed the corrected tidal elevation for the M_2 and S_2 constituents on the open boundary. Some other details will be provided below.

5.4. Results and Discussion

Our analysis will touch several aspects of tidal circulation. First, we present and discuss the simulated tidal maps and parameters of barotropic ellipses, comparing them against the available solutions and observations, and also the residual circulation. Next we will examine the impact of improved topography representation, which predict small, but systematic shift in tidal map, and will end with the discussion of energy balance and energy fluxes in the analyzed domain.

5.4.1. Tidal maps and parameters of barotropic ellipses

We begin the description from experiments forced directly by TPXO6.2, AOTIM5 and TPXO7.1. The best results for the M_2 constituent were obtained for OBC derived from TPXO7.1, with the bottom drag coefficient varying in the range from 0.003 to 0.005. Simulation with the OBC from AOTIM5 with the bottom drag coefficient varies in the range from 0.001 to 0.003 have nearly the same quality. The simulations based on TPXO6.2 boundary conditions are characterized by the largest phase errors compared to simulations based on TPXO7.1 and AOTIM5. This result implies that for semidiurnal tides, AOTIM5 and TPX07.1 provide a significantly better fit to the tide gauge data than TPXO6.2 (Padman and Erofeeva, 2004) for the M_2 constituent (Table 1). We observe that tidal dynamics simulated with OBC from any of inverse models as well as direct predictions of these models are markedly different in the south-western part of the domain for both M_2 and S_2 tidal waves. It is by all probability explained by bathymetry features in that zone (Figs. 1, 7), which were either not taken into account or not resolved in the AOTIM5, TPXO7.1 and TPXO6.2. Note also that this region in all these models is too deep.

In order to construct an optimal OBC for the M_2 constituent we used the amplitudes and phases from TPXO7.1, but with slightly reduced amplitude, as the zeroth-order approach. It allowed us to reduce the bottom friction coefficient to range from 0.001 to 0.003 and, respectively, to use the AOTIM5 data for a near coast correction. The correction was selected so as to optimize the agreement of simulated elevation with the observed amplitudes and phases near all open boundary segments (stations 1, 5, 6, 7, 9, 10 (Fig.1)). The TPXO7.1 was used as a base for optimal OBC, because the results of experiment forced directly by TPXO7.1 provide better agreement with known ellipses parameters in five positions (Fig. 1), compare to the results of experiment forced by AOTIM 5. The results of our simulations for the amplitudes and phases for the M_2 constituent are summarized in Table 1. The information on vector error is shown in Fig. 4. They indicate that a substantial improvement in agreement with observations is achieved for the amplitude at nearly all stations in case with optimal OBC. The last column in Table 1 and the rightmost bars in Fig.4 relate to our attempt to improve the agreement between our simulation and observations by slightly displacing the positions of observational points. We sought for position within 20 km radius where the simulated results agree better with observations (note that Chen et al. (2009) assumed even larger displacements). As it can be seen, the agreement can be significantly improved, which clearly reflects the impact of simulated positions of amphidromic points on the overall accuracy.

Table 1. Comparison of amplitudes (Am.) and phases (Ph.) from different models and observational data for the M_2 constituent. The asterisk indicates the shift in station positions up to 40 km compare to positions provided by KP, the double asterisk indicates the shift up to 20 km.

№	Name of station		Amplitude, cm (M_2)									
			Observ.	AO-FVCOM*	Siberian Shelf model	AOTIM5	TPX07.1	TPXO6.2	Model forced by AOTIM5	Model forced by TPXO7.1	Model with optimal OBC	Model with optimal OBC**
1	M. Terpiay-Tumsa	Am.	14.0	15.4	3.1	18.0	3.2	6.3	2.1	8.0	13.6	14.0
		Ph.	24	30	48	41	15	193	325	60	100	24
2	Dunay Isl.	Am.	15.0	9.5	16.0	12.6	11.4	18.5	6.4	15.6	14.2	15.0
		Ph.	120	128	125	115	155	144	109	149	124	120
3	Tiksi	Am.	13.0	11.7	19.5	2.7	6.6	1.7	14.7	14.5	17.8	16.7
		Ph.	69	40	55	69	46	88	67	98	84	74
4	Muostakh	Am.	13.0	9.7	16.4	1.1	6.2	1.5	12.7	12.4	15.3	13.8
		Ph.	36	41	70	15	69	108	63	88	76	58

#	Station											
5	Sviatoy Nos	Am.	5.0	5.3	7.2	1.2	6.0	1.5	2.1	4.0	4.6	5.0
		Ph.	150	164	157	287	148	306	198	167	158	150
6	Kigilliakh	Am.	5.0	5.1	7.3	2.1	4.3	1.8	1.8	5.0	4.8	5.0
		Ph.	231	218	149	225	200	208	289	222	222	231
7	Sannik. Pas.	Am.	5.0	11.6	7.7	3.1	1.3	1.2	5.5	3.2	6.2	5.0
		Ph.	30	18	51	27	15	229	10	29	45	30
8	Kieng Urasa	Am.	7.0	9.4	12.0	9.7	7.7	7.6	7.6	8.6	9.8	7.0
		Ph.	111	90	65	91	100	102	69	91	71	84
9	Tempa	Am.	15.0	20.9	18.8	16.8	13.3	14.5	12.6	12.7	14.9	15.0
		Ph.	93	79	83	80	97	96	55	92	63	75
10	Kotelniy	Am.	22.0	19.0	20.0	17.3	14.1	15.2	18.3	13.6	20.3	21.0
		Ph.	66	69	90	80	95	100	71	94	66	68
Error		Er_A		11.7	15.3	18.1	17.2	20.4	16.0	11.0	6.5	3.8
		Er_P		12	27	24	19	67	31	22	23	7

In Table 1 $Er_A = \sqrt{\sum_{i=1}^{N}(A_s(i) - A_O(i))^2}$ is the error of amplitude in the Euclidean norm (L^2 - norm), where A_s is the simulated amplitude and A_O the observed amplitude. $Er_P = \frac{1}{N}\sum_{i=1}^{N} D_P(i)$ is the average error of phase, $D_P(i) = \begin{cases} |P_s(i) - P_O(i)|, & |P_s(i) - P_O(i)| \le 180° \\ 360° - |P_s(i) - P_O(i)|, & |P_s(i) - P_O(i)| > 180° \end{cases}$, where P_s the simulated phase, P_O the observed phase, $P_s, P_O \in [0,360°]$ and $N = 10$ the number of stations. The error of phase is in L^1-norm (divided by N) for the convenience of calculation.
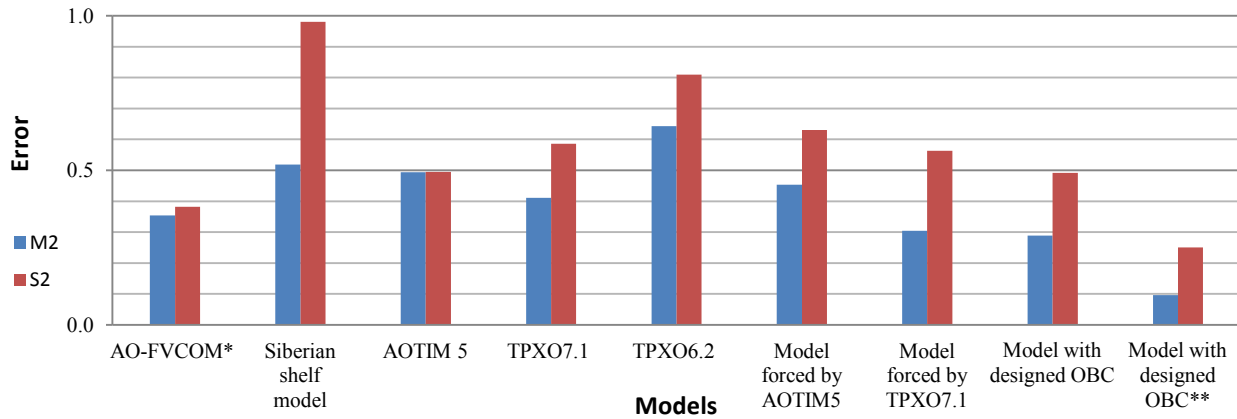

Fig. 4. The error of different models against coastal tide gauges for the M_2 and S_2 constituents. The single (double) superscript indicates that points where the simulated results have been taken may deviate up to 40(20) km from the station positions provided by KP.

The ordinate in Fig. 4 is the average error for both phase and amplitude (RMS vector error) computed as $Error = \frac{1}{N} \sum_{i=1}^{N} \left(\left(1 + \left(\frac{A_S(i)}{A_O(i)} \right)^2 - 2 \cdot \cos \left(\frac{P_S(i) - P_O(i)}{2} \right) \cdot \frac{A_S(i)}{A_O(i)} \right)^{\frac{1}{2}} \right)$.

The tidal map for the M_2 constituent with the optimally corrected OBC, providing the best agreement with observations, is presented in Fig. 5a. The S_2 constituent was treated in the same way. The optimal OBC for it were designed based on the same principles. Our simulated tidal map for the S_2 wave is shown in Fig. 5b. With exception for a degenerate amphidromic point in the S_2 case near the Lyakhovsky Islands (Fig. 2), other amphidromic points occupy close locations in cases of the M_2 and S_2 waves. Accordingly the Kelvin wave is a dominant factor in forming amphidromic points for both M_2 and S_2 constituents.
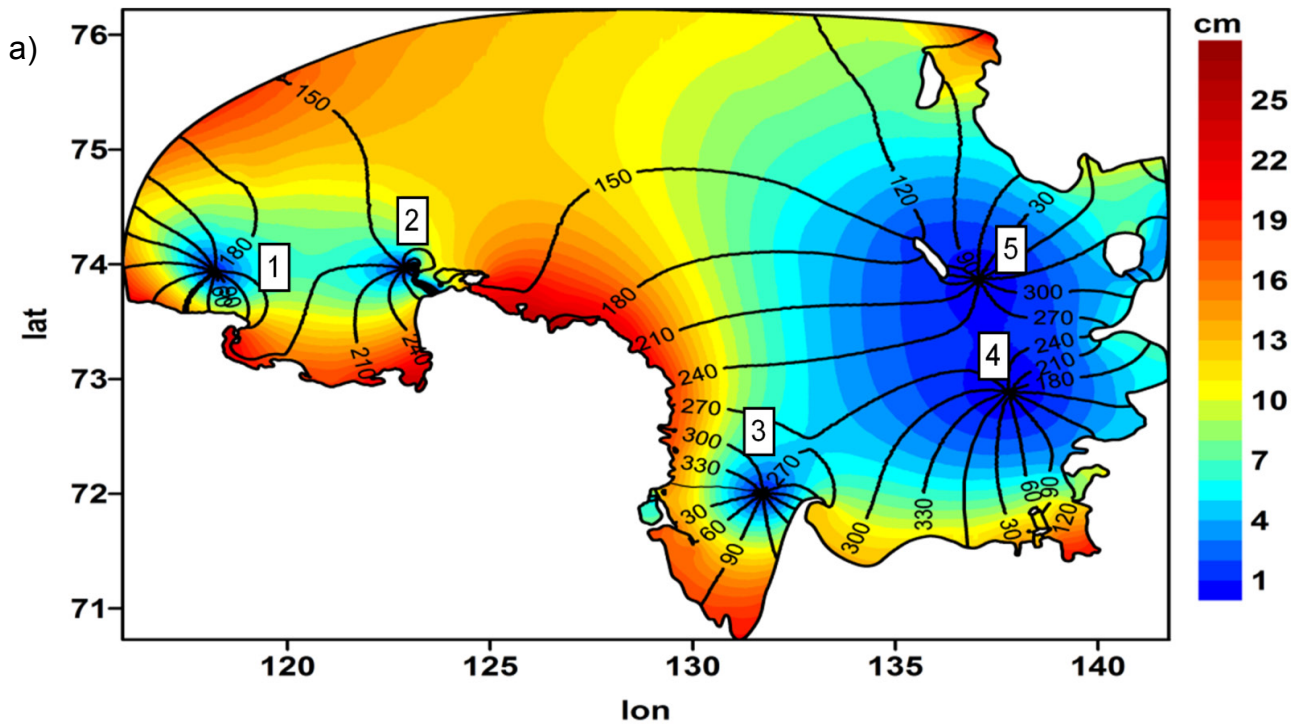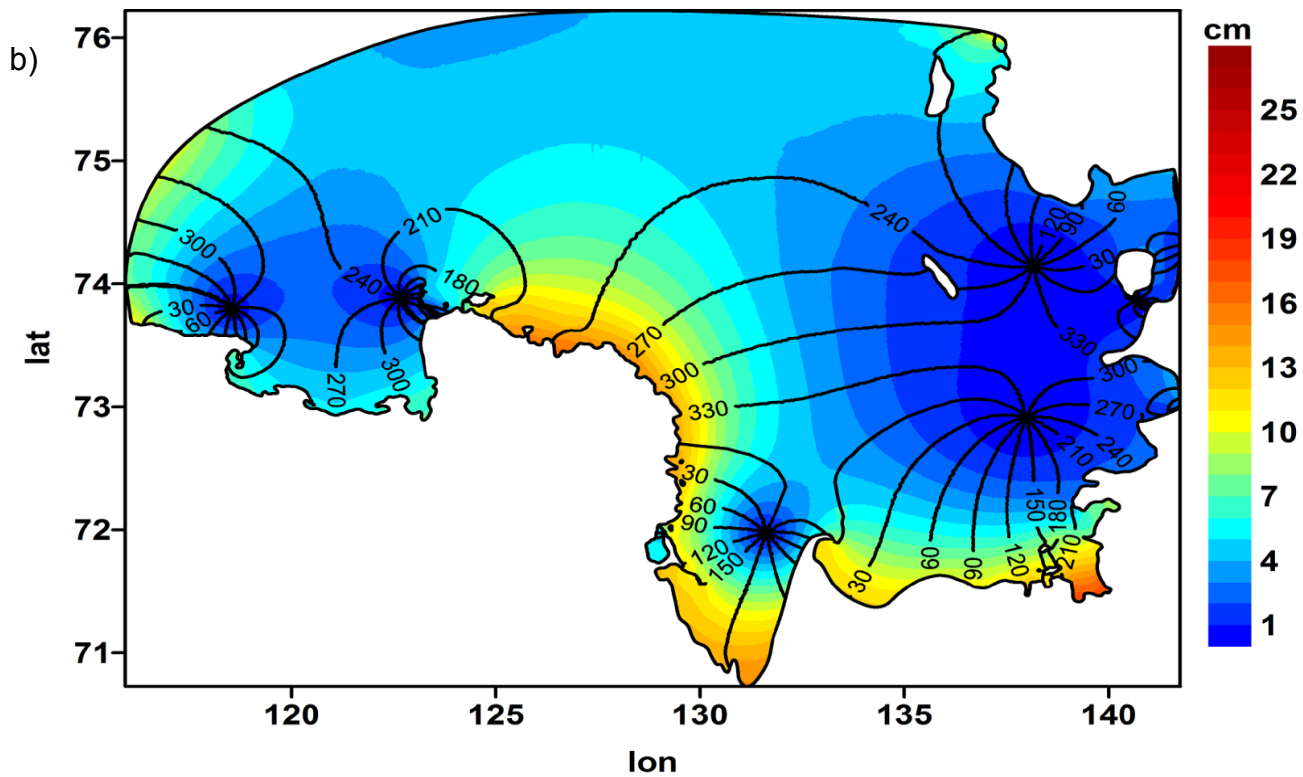
Fig. 5. The tidal map for the M_2 (a) and S_2 (b) constituents. Simulations use optimal boundary conditions for tidal elevation.

The results of comparison for the S_2 constituent with other models are presented in Fig. 4. For the S_2 wave, the data on M. Bykovsky Station are not available and the analysis is based on 9 stations. Note that in all cases in Fig. 4 the error for the S_2 slightly exceeds that for M_2 tide.

The simulated tidal map for the M_2 constituent (Fig. 5a) has many features in common with the empirical tidal map shown in Dvorkin (1970) and also with modeling results from Androsov et al. (1998), Chen et al. (2009), Dvorkin et al. (1972), Kagan et al. (2008a), Kowalik and Proshutinsky (1994), Lyard (1997), Padman and Erofeeva (2004), Polyakov (1994). It includes a "chain" of cyclonic amphidromes located near the coast. This picture can be explained with the Poincare waves originating from oblique reflection of the Sverdrup waves from the coast followed by an interference of the incident and reflected ones (Androsov et al., 1998; Nekrasov, 1990) with predominantly eastward propagating waves. The tidal waves with large amplitudes enter the region from the western part (Fig. 5a) of the open boundary fragment A (Fig. 1). They travel as the Kelvin waves along the coast, the contour lines of phase are perpendicular to the coastline (Fig. 5a). On their way they lose much of their energy and only a small portion reaches the East Siberian Sea through the Dmitry Laptev Strait (Fig. 2). We should emphasize that the positions of amphidromic points number 4 and 5 (Fig. 5a) directly depend on the condition on the open boundary segments C

and B (Fig. 1). The position of amphidromic point number 3 (Fig. 5a) is the most stable and largely coincides in all considered models. The amphidromic point number 1 can be degenerate or even disappear depending on conditions in the south-western part of the open boundary A. The amphidromic point number 2 depends on the condition in the western part of the open boundary A and can move far to the west, if amphidromic point number 1 is not present.

The positions and directions of rotation of phase around amphidromic points are similar to modeling results provided by Kagan et al. (2008a) and Chen et al. (2009) except for the apmhidromic point near the Aerosiemka and Samolet Islands (Fig. 2), which is not presented in these models. The numbers and positions of amphidromic points in our domain differ between our simulations and solutions of AOTIM5, TPXO6.2 and TPXO7.1. All they provide less amphidromes compared to Chen et al. (2009), Kagan et al. (2008a), and tidal maps obtained by us. The AOTIM5 provides the closest picture to the obtained tidal maps but with essentially different positions of the amphidromes. Due to this reason, the attempt to improve the agreement with observations by assuming that stations locations are shifted within some radius is not as efficient for the inverse tidal solutions as it was for AO-FVCOM, for example.

The ellipses of barotropic currents for the M_2 constituent are shown in Fig. 6 and the residual circulation for the western part of our domain is shown in Fig. 7.

In most areas the major axes of barotropic ellipses are less than $10\ cm\ s^{-1}$, but on the periphery of islands they can reach up to $50\ cm\ s^{-1}$. The most powerful is the western part of the domain, where amplitudes and major axes of barotropic ellipses are maximal (Fig. 6), which is in agreement with (Sofina, 2008). In general, the ellipses with clockwise rotation dominate in the region, as confirmed by the observations (Janout and Lenn, 2013) and modeling study (Padman and Erofeeva, 2004; Sofina, 2008). In the deepest part of the domain (depth>25m) the tidal current ellipses are nearly circular: the minor-to-major axis ratio may be as large as 0.9, the zones of change in the rotation direction are the exception.
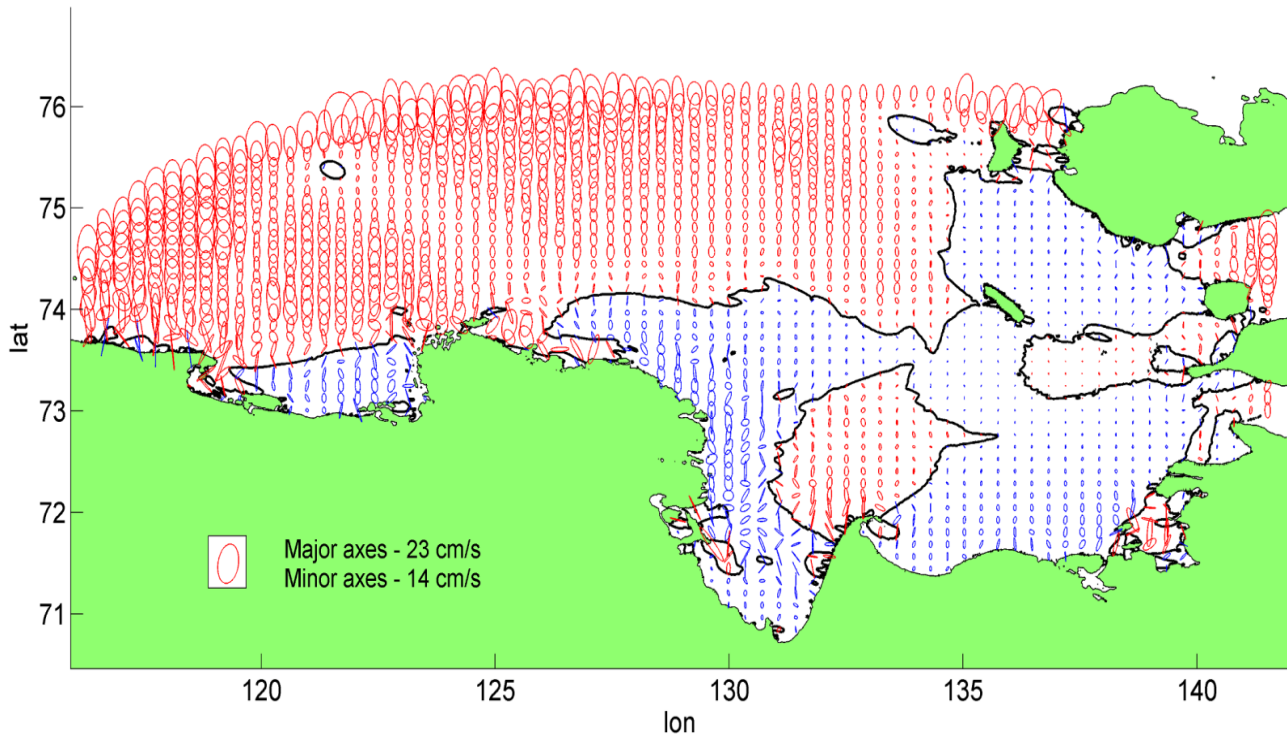
Fig. 6. Ellipses of barotropic velocities for the M_2 constituent, red ellipses have clockwise rotation, blue ellipses have counterclockwise rotation. The parameters of ellipses are interpolated on a regular grid. The black line marks the change in the rotation direction. Simulations use optimal boundary conditions for tidal elevation.

The residual currents are mainly shaped by bathymetric features and the Coriolis force (Fig. 7). Far from the shore the residual circulation has a vortex structure, the residual currents are also localized along coastal boundaries. Maximum residual currents ($10\ cm\ s^{-1}$) are reached on the periphery of islands. In general, residual currents are smaller than $2\ cm\ s^{-1}$. The residual circulation in the eastern part of considered domain, which is not shown in Fig. 7, is much weaker than in the western part. Only motion along coastal boundaries remains before Selyahskaya Guba (Fig. 2), where it forms a vortical flow.
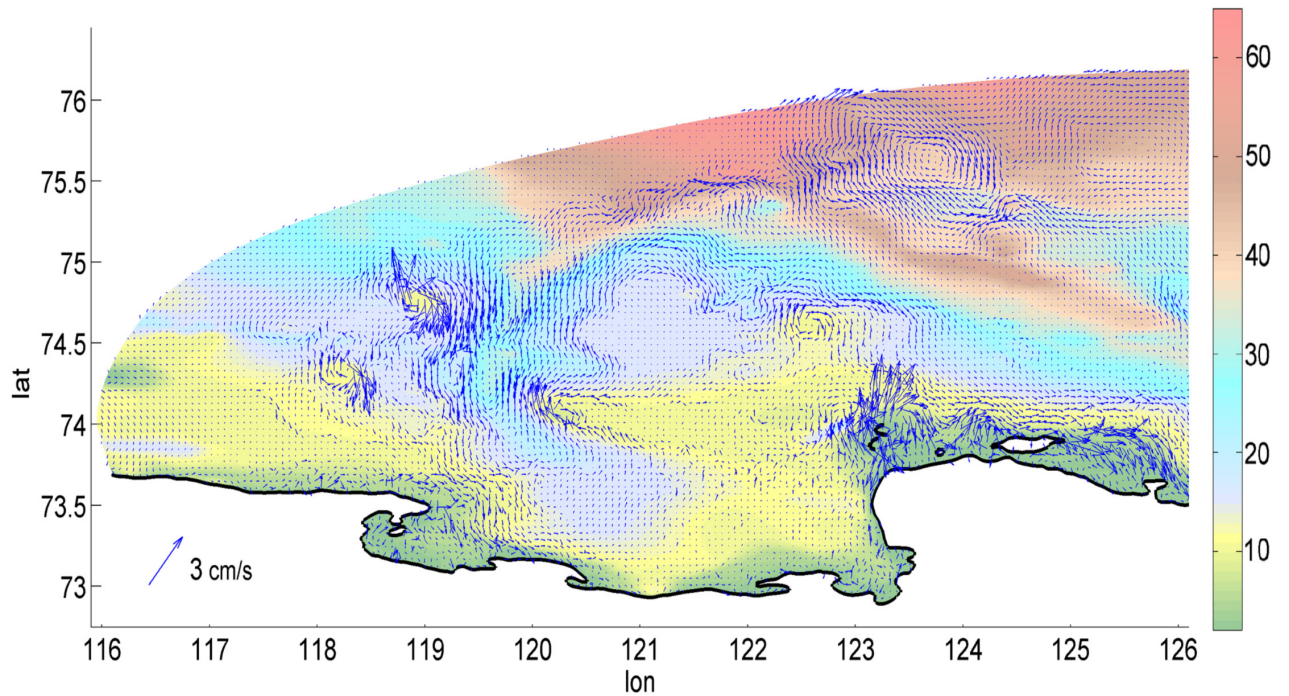
Fig. 7. Residual circulation for the M_2 constituent superimposed on bathymetry map, [m], for the western part of the considered domain, the vectors are interpolated on a regular grid. Simulations use optimal boundary conditions for tidal elevation.

We now discuss how the ellipse parameters in different models compare with observational data. The results are summarized in Table 2. Unfortunately, we did not have any information about ellipse parameters from the AO-FVCOM and Siberian Shelf model, so only inverse solutions will be considered in addition to the simulated one. The sense of rotation is provided by the sign of the minor axis, with the negative sign implying the clockwise (anticyclonic) rotation.

Table 2. Comparison of ellipse parameters from different models and observational data in open water season. "Maj." is the abbreviation for the major axes, M_2 (S_2), [$cm\ s^{-1}$], "Min." for the minor axes, M_2 (S_2), [$cm\ s^{-1}$], and "Inc." for the inclination, M_2 (S_2), [deg].

Coordinates of the stations		Major axes, M_2 (S_2), $cm\ s^{-1}$						
		Observ.	AOTIM5	TPX07.1	TPXO6.2	Model forced by AOTIM5	Model forced by TPXO7.1	Model with optimal OBC
125.25 74.71 (I)	Maj.	6.4 (2.6)	2.7(1.2)	4.3(2.5)	7.8(3.0)	6.4(5.5)	6.4(3.6)	5.3(3.7)
	Min.	-2.4(-1.4)	-1.2(-0.4)	-3.3(-1.4)	0.01(1.1)	-4.9(-3.6)	-3.8(-2.5)	-4.2(-2.4)
	Inc.	84(79)	92(108)	66(95)	66(78)	140(121)	86(136)	113(130)
128 74.33 (III)	Maj.	5.6(3.6)	2.8(1.1)	3.5(2.0)	5.2(1.1)	4.4(4.7)	6.3(2.4)	5.5(3.2)
	Min.	-0.1(-0.6)	-0.2(-0.2)	-0.9(-0.2)	0.6(0.6)	-2.2(-0.4)	-0.9(-0.4)	-1.2(-1)
	Inc.	85(91)	78(91)	68(80)	59(63)	97(91)	72(97)	77(93)
130.84 75.15 (V)	Maj.	5.4(2.8)	3.9(1.7)	4.8(2.6)	6.7(1.6)	4.8(3.6)	6.2(1.0)	5.5(3.3)
	Min.	-1.2(-1.0)	-1.4(-0.7)	-2.7(-1.0)	-1.4(0.2)	-3.3(-1.8)	-2.5(-0.2)	-3.1(-2.7)
	Inc.	55(59)	65(69)	58(76)	75(84)	75(79)	64(84)	60(64)
131.70 73.46 (IV)	Maj.	3.3(1.3)	1.4(0.7)	1.9(0.6)	1.7(0.6)	3.3(3.3)	3.2(2.0)	3.4(2.0)
	Min.	0.4 (0.7)	0.3(0.3)	0.2(-0.1)	0.2(0.1)	0.5(1)	1.6(0.4)	1.6(0.9)
	Inc.	115(104)	126(115)	111(121)	89(103)	110(114)	115(126)	123(112)
126.42 74.12 (II)	Maj.	6.9(4.3)	3.4(1.65)	3.6(2.2)	5.4(1.7)	6.0(7.2)	7.9(3.9)	7.5(4.5)
	Min.	0.1(-0.5)	-0.1(0.1)	-1.2(-0.3)	1.3(0.7)	-1.5(-0.1)	-0.3(-0.3)	-0.6(-0.5)
	Inc.	26(36)	107(123)	89(99)	72(92)	114(110)	96(115)	103(98)
Er_{axes_maj}			**6.3(4.1)**	**4.7(2.7)**	**2.9(3.9)**	**1.6(4.8)**	**1.5(2.6)**	**1.4(1.5)**
Er_{axes_min}			**1.2(1.3)**	**2.3(0.9)**	**2.8(3.3)**	**4.2(2.4)**	**2.4(1.5)**	**3.2(2)**
Er_{av}			**3.75(2.7)**	**3.5(1.8)**	**2.85(3.6)**	**2.9(3.6)**	**1.95(2.05)**	**2.3(1.75)**

In Table 2 Er_{axes} is the error of major (minor) axes in the Euclidean norm, Er_{av} the arithmetic average of the Er_{axes_min} and Er_{axes_min}.

For different OBC our model provides better agreement with major axes observations compared to all Arctic Ocean barotropic models respectively (Table 2, Fig. 8). It generally predicts a larger minor axis, but with the correct sign, than measured and obtained directly from different Arctic Ocean barotropic models, the same effect was shown by Chen et al. (2009). We tried to improve the agreement with observational data reported in Janout and Lenn (2013), by varying the bottom drag

coefficient. However, it turned out that the measures to improve the agreement for major axes impair the agreement for the minor axes for all stations, and vice versa.
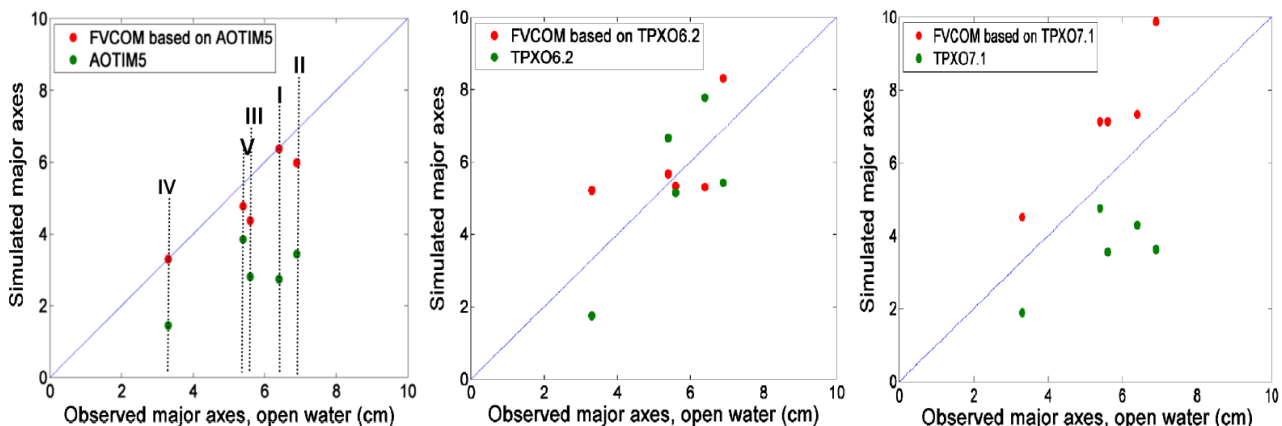

Fig. 8. Comparison of major axes in simulations based on the open boundary conditions from different inverse models and predicted directly by these models with observational data.

Noteworthy, our solutions with optimally designed OBC give one of the best arithmetic average of the errors for major and minor axes (Er_{av}) for the both M_2 and S_2 waves (Table 2). Note that comparably small errors characterize also the results derived directly from TPX06.2 for M_2 component, directly from AOTIM5 for the S_2 component and our simulations forced by TPXO7.1 solution (Table 2). Also for all our simulations the directions of rotation coincide with observational directions for both components. The exception is the sign of minor axis for the M_2 component at the second station (‖) (Fig. 1), which may be due to the proximity to the region with opposite rotation (Fig. 6). The inclinations for all solutions have nearly the same accuracy.

5.4.2. Sensitivity to bathymetry

The agreement of our simulations with observational data is further improved when topography derived from GEBCO is merged with the additional bathymetric data from digitized Soviet map covering the vicinity of the Lena Delta. The upper panel of Fig. 9 shows the modification of topography suggested by this additional data set. Broadly speaking, there is a large-scale pattern with regions that are shallower or deeper on average, but also there are important depth corrections near amphidromic point 2 (Fig. 5a). As follows from panel b, it leads to substantial local corrections.

Using this synthetic bathymetry, in the experiment with the M_2 constituent the error was reduced by nearly 25 percent (from 0.29 (Fig. 4) to 0.22). We have found that with a more realistic bathymetry the total energy of the system can change significantly.
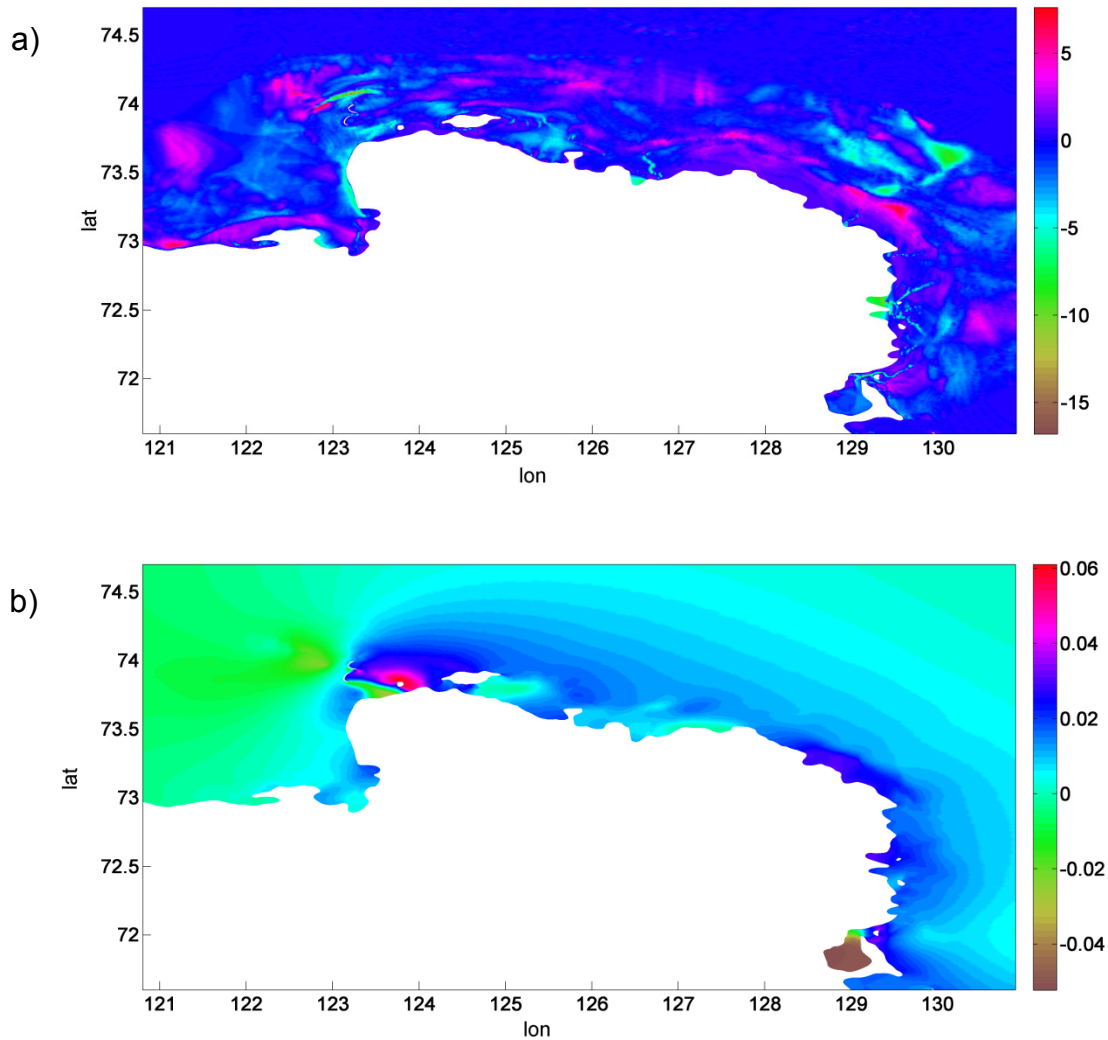

Fig. 9. a) The difference between GEBCO bathymetry and additional bathymetric data from digitized Soviet map, [m], b) The differences between amplitudes of the M_2 in simulations based on GEBCO and modified bathymetry, [m].

Numerous studies emphasize the importance of properly selected bottom friction in shallow regions (Lu and Zhang, 2006; Rego and Li, 2010). Our simulations indicate that using OBC derived from the global models (as TPXO6.2, TPXO7.1) may require to use a larger bottom drag coefficient than in the case when the tidal OBC are derived from regional model (AOTIM5). For assimilated models we can see the next imbalance: if in shallow part of the domain the results for amplitudes and phases have good agreement with observations it can lead to large errors for major and minor

axis in neighboring deep regions. Bottom drag, however, cannot be varied in wide limits. In the case considered, increasing the bottom friction coefficient 2.5 times results in the total energy reduction by 35 percent in experiment with the M_2 component. We continue with the analysis of energy balance. With larger value of bottom friction coefficient the time it takes the system to equilibrate obviously is decreasing.

5.4.3. Energy balance

The analysis of the energy budget provides an important insight into the evolution of energy in the model region.

The equation of energy for the vertically averaged equations has the form:

(1) $\quad \frac{\partial \bar{E}}{\partial t} + \nabla \cdot \left[\rho H \left(g\zeta + \frac{1}{2} |\bar{\mathbf{v}}|^2 \right) \bar{\mathbf{v}} \right] = -\rho r |\bar{\mathbf{v}}|^{3/2} + \rho \bar{\mathbf{v}} \cdot (\nabla \cdot (KH\nabla\bar{\mathbf{v}})),$

where $\bar{E} = \frac{1}{2}\rho(H|\bar{\mathbf{v}}|^2 + g\zeta^2)$ is the total energy per unit area, $\bar{\mathbf{v}} = \int_{-h}^{\zeta} \mathbf{v}\, dz$ is the vertically integrated fluid velocity, ζ the sea surface level, $H = h + \zeta$, h the water depth, ρ the water density, r the bottom drag coefficient, K the generally non-uniform eddy viscosity coefficient, g the acceleration due to gravity and $\nabla = \left(\frac{\partial}{\partial x}, \frac{\partial}{\partial y} \right)$ is the gradient operator.

After integration of eq. (1) over the region Ω with boundary $\partial\Omega = \partial\Omega_1 + \partial\Omega_2$, $\partial\Omega_1$ is the solid part of the boundary, $\partial\Omega_2$ the open boundary, taking into account the Gauss and Green formulas for divergence and Laplace operator respectively and condition of zero velocities at $\partial\Omega_1$, we obtain the mean energy balance equation:

(2)$\int_\Omega \frac{\partial \bar{E}}{\partial t} dx\, dy = -\int_{\partial\Omega_2} \left[\rho H \left(g\zeta + \frac{1}{2} |\bar{\mathbf{v}}|^2 \right) \frac{\partial \bar{\mathbf{v}}}{\partial \mathbf{n}} - \frac{1}{2} \rho KH \frac{\partial |\bar{\mathbf{v}}|^2}{\partial \mathbf{n}} \right] ds - \int_\Omega \rho r |\bar{\mathbf{v}}|^{3/2} dx\, dy -$

$\int_\Omega \rho KH \left(|\bar{\mathbf{v}}_x|^2 + |\bar{\mathbf{v}}_y|^2 \right) dx\, dy,$

where $\frac{\partial \bar{\mathbf{v}}}{\partial \mathbf{n}} = (\bar{\mathbf{v}} \cdot \mathbf{n})$, $\mathbf{n}$ is the outward normal to $\partial\Omega_2$, $\bar{\mathbf{v}}_x$ and $\bar{\mathbf{v}}_y$ the partial derivatives of $\bar{\mathbf{v}}$.

The first term on the right side of (2) is the total flux of energy across the open boundary, the second and third terms are the rates of energy dissipation due to the bottom friction and due to viscosity, respectively (see, e.g., Androsov et al., 1998, 2002).

The Fig.10 shows that the total energy (energy for the whole domain) for the M_2 component is approximately twice higher than that for the S_2 component. The result is in agreement with observational data on the Laptev Sea Shelf (Dmitrenko et al., 2008b, 2012). The number of simulated periods was dictated by the time of complete system equilibration. The difference in the

total energy between the two last periods is negligible (Fig. 10). There is some asymmetry between the half-periods in Fig. 10, which is linked to the presence of higher harmonics. In the western part of the domain, where tidal currents for both M_2 and S_2 are strong (Fig. 5), bathymetry features lead to intensification of the nonlinear effects and this is accompanied by asymmetry in the flows over the tidal period. However, the asymmetry is quite small in our study. Figure 11 shows the amplitudes of higher harmonics M_4, M_6, M_8, compare to the amplitude of M_2, and constant term (Z_0) at all coastal stations.
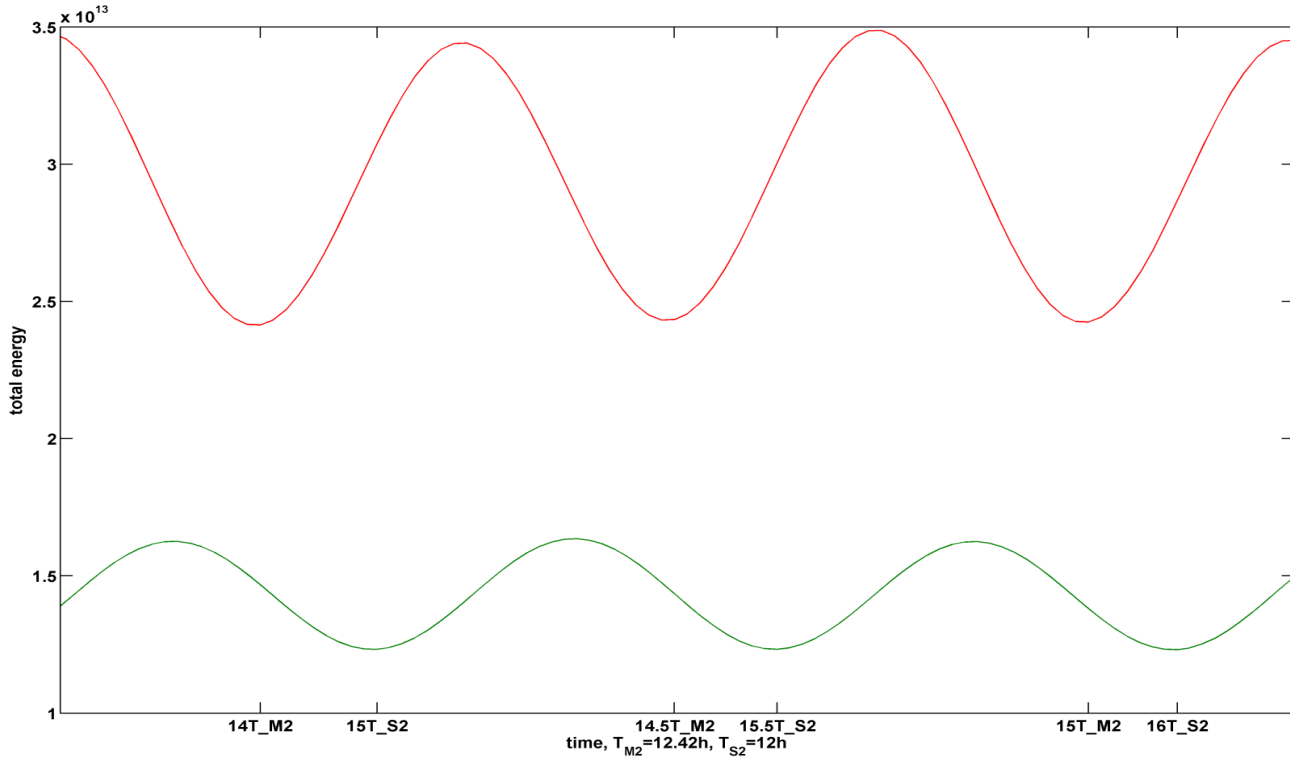
Fig. 10. The total energy, [J]: in red – for the M_2 constituent, in green – for the S_2 constituent.
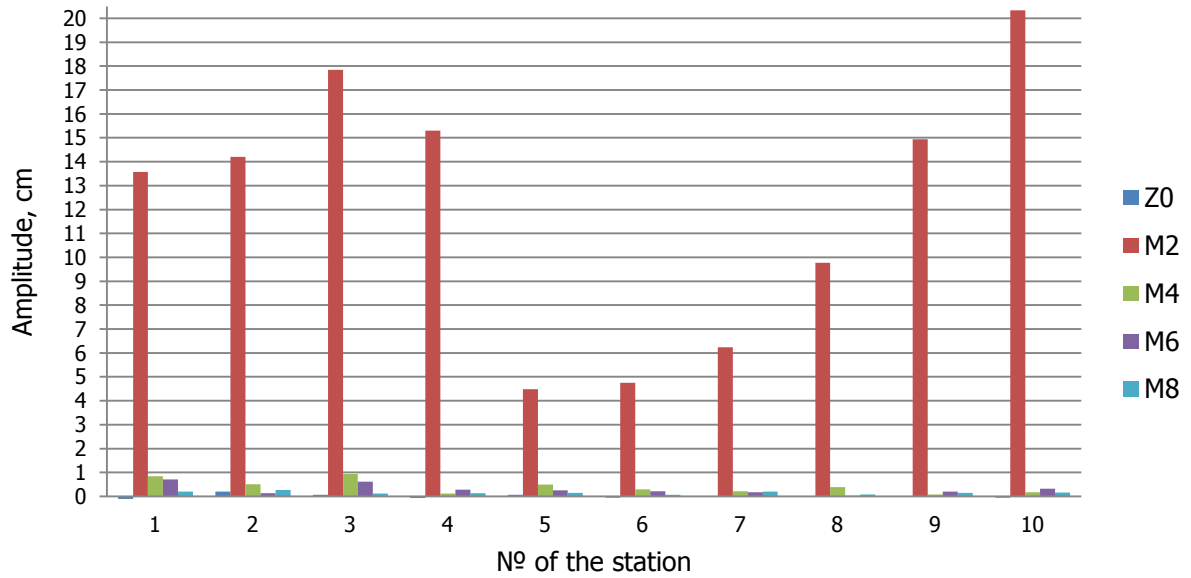
Fig. 11. The amplitudes of M_2, M_4, M_6, M_8 harmonics and Z_0 at all coastal stations.

Components of the energy equation (2) are presented in Fig. 12 for both M_2 and S_2 constituents. The magnitude of the energy budget residual in Fig. 12 is small indicating that the budget is fulfilled with high accuracy in numerical simulations. There is a balance between the temporal change of energy and energy fluxes through the open boundaries during the tidal cycle for both constituents. The horizontal turbulent exchange plays a minor role in energy budget; its contribution is smaller than the contributions of other components of the balance by a factor 10^4. As expected, the contribution of bottom friction is substantial because the fluid layer is relatively shallow over a large part of the computational domain.
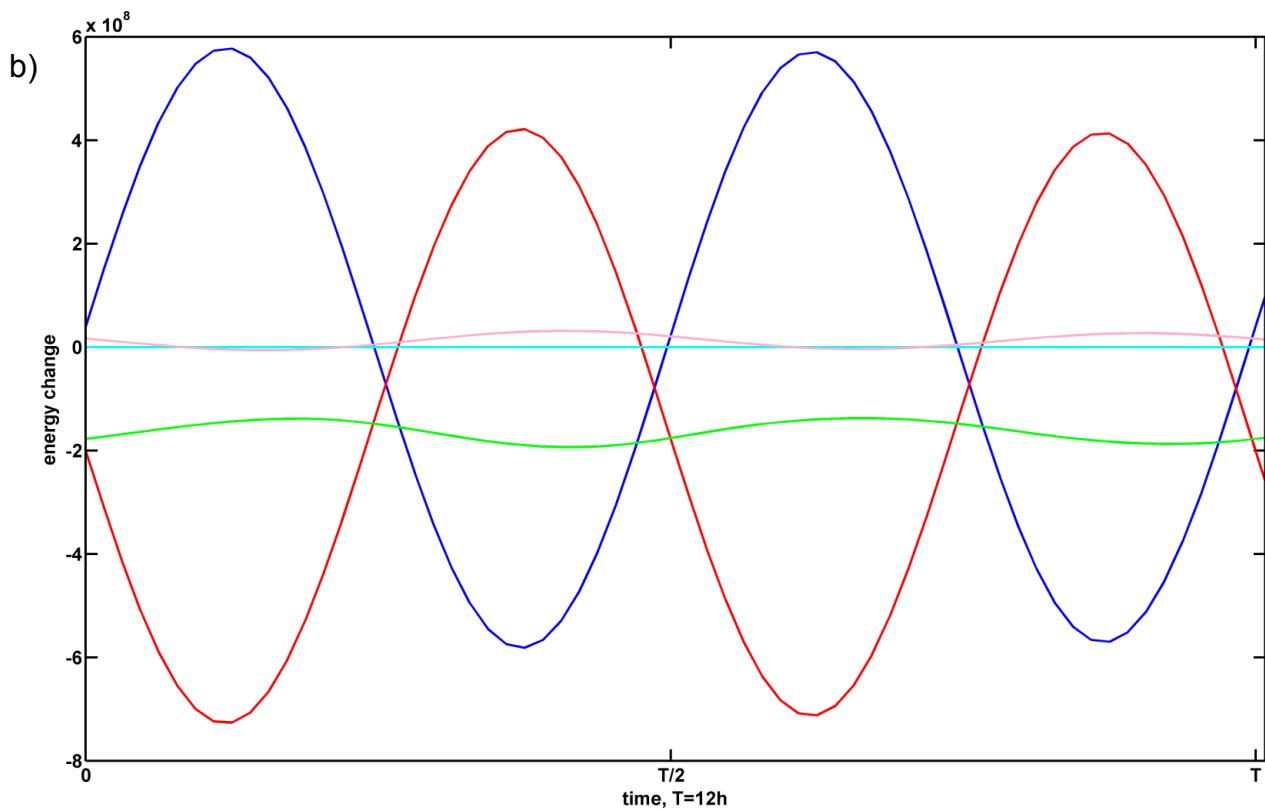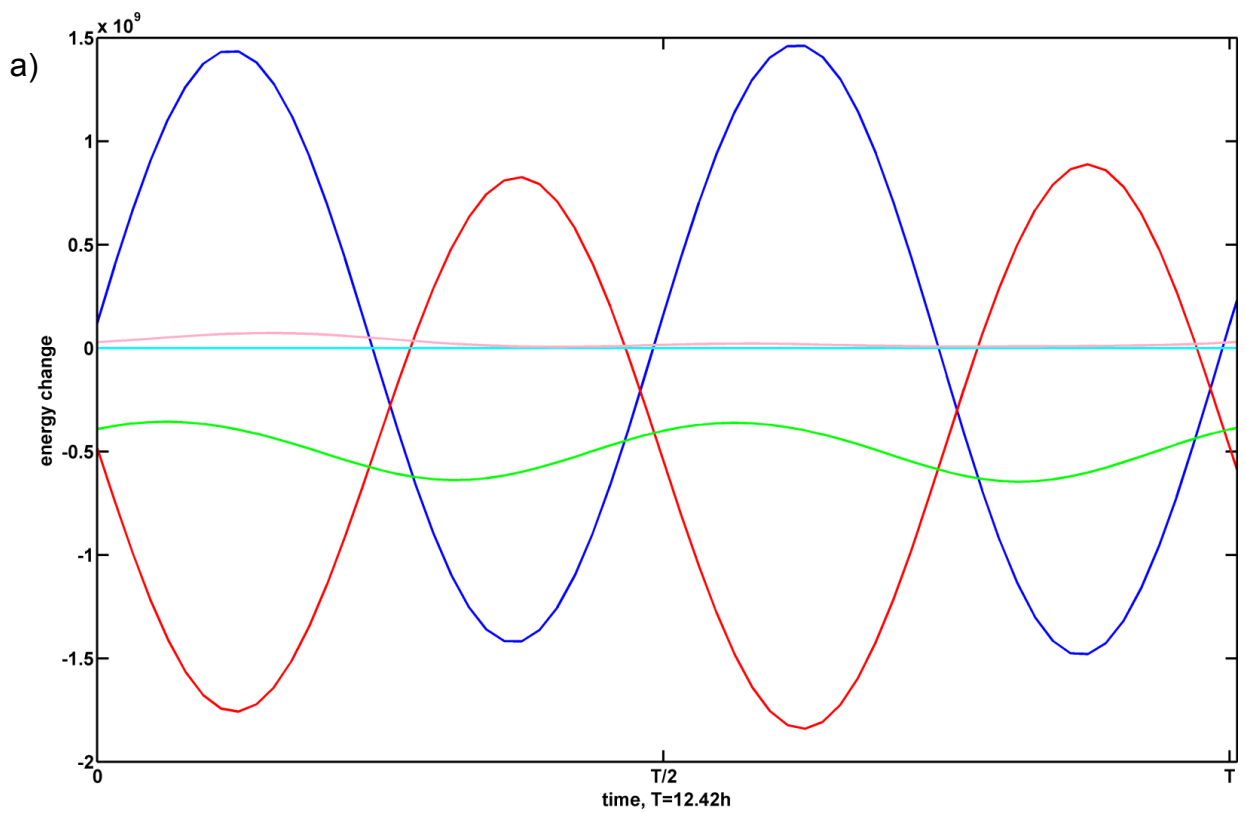
Fig. 12. Energetic budget, [W], in blue – energy change in time, in red – flow through the open boundaries, in green – bottom friction, in cyan – horizontal turbulent viscosity, in pink – the imbalance:
a) M_2 constituent, b) S_2 constituent.

43

Numerical computations generally do not conserve energy unless special measures are undertaken, and FVCOM code is not energy conserving. It has certain numerical viscosity, which is, by all probability, mostly the reason of small imbalance in our energy analysis. Although the imbalance is mostly due to numerical viscosity, it also contains other errors (time stepping, interpolation to the open boundary, etc.). Note, however, that the mean imbalance is more than 2 orders of magnitude smaller than averaged impact of bottom friction for both constituents considered here, and this is why FVCOM can safely be used for tidal simulations.

The tidal energy flux is estimated using the following definition (Crawford, 1984; Kowalik and Proshutinsky, 1993):

$(E_\lambda, E_\theta) = \frac{1}{T} \int_0^T \rho H \left(g\xi + \frac{1}{2} |\bar{\mathbf{v}}|^2 \right) \bar{\mathbf{v}} \, dt$, where E_λ, E_θ are the zonal and meridional components of the tidal energy flux vector, T is the tidal period.

The spatial patterns of energy flux for the M_2 and S_2 constituents are close to each other but have their own unique features (Fig. 13).

a)
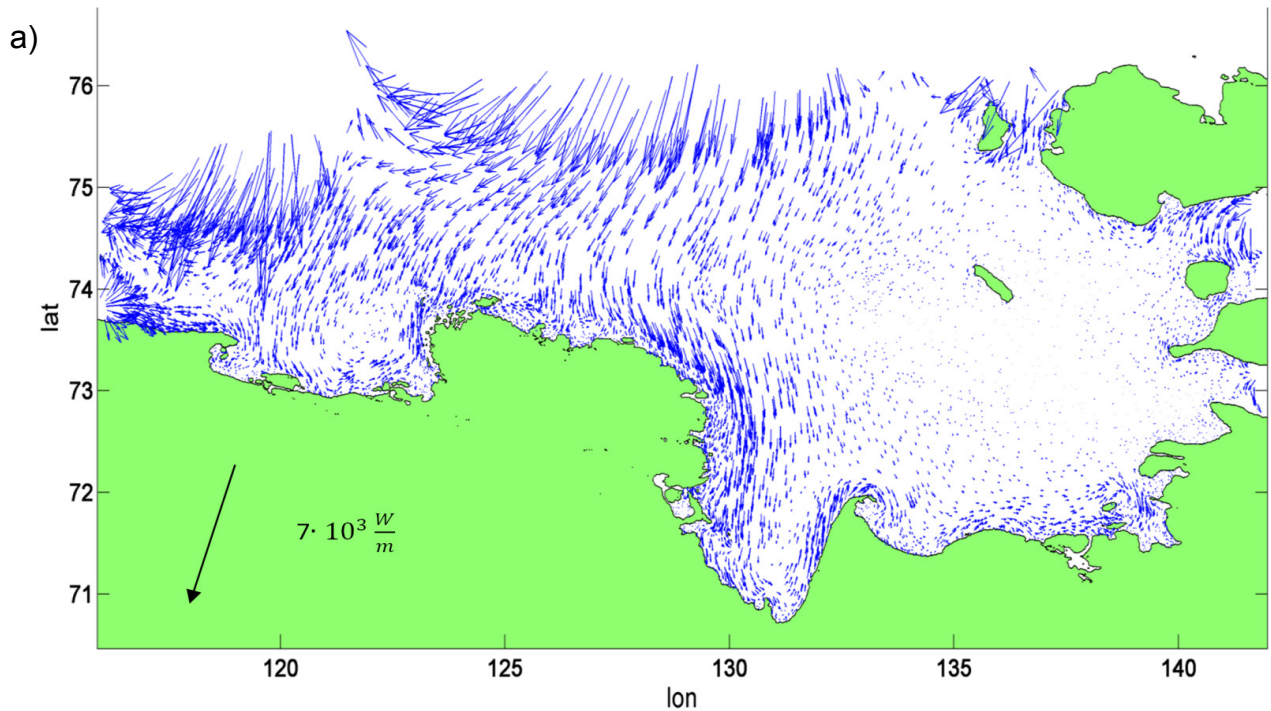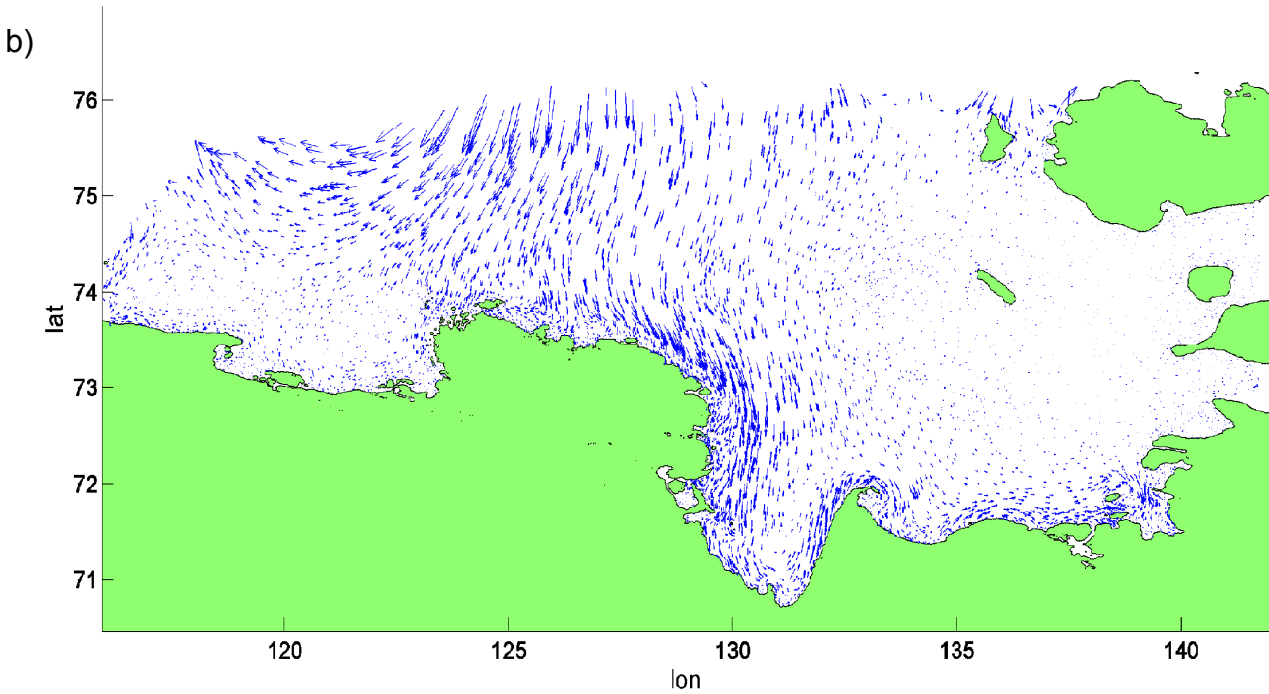
Fig. 13. The flux of tidal energy (E_λ, E_θ) for the M_2 (a) and S_2 (b) constituents. The vectors are shown for every 90th point of the instructed grid.

For both M_2 and S_2 constituents the tidal energy is largely supplied by the progressive tidal wave propagating to the coastal area from the central northern part of the open boundary segment A (the deepest area in our domain) (Fig. 1). An essential part of this energy goes directly to the south and also a significant part of energy leaves the domain little west. Also for both constituents the coastal energy flux comes from the west, but for the M_2 it is much stronger (Fig. 13). This flux propagates along the shore from the western part of the Laptev Sea, which has the biggest amplitudes (see Fig. 5 and e.g., Kagan et al., 2008a; Padman and Erofeeva, 2004). The M_2 constituent is characterized by a strong flux from the south-western part of the open boundary, partly deflecting from the region slightly to the south. In the western part of the domain the fluxes from different sides meet, especially for the M_2 tide, the resultant energy flux vectors have a high level of dissipation due to small depths and topography traps (Figs. 7, 13). As a consequence of the importance of these details, influenced by details in bottom topography, the Arctic Ocean and global tidal models on one hand and our simulations with the OBC derived from these models on the other hand provide different dynamics for the western part of the domain considered here. The zone in the vicinity of Lena Delta is a dissipation region for the M_2 and S_2 tides energy. In this region, the paths of the M_2 and S_2 tides energy fluxes are controlled by the large amount of small islands, complex

45

coastline topography and intricate bathymetry, with flushing through narrow channels. The eastern open boundaries have only a small impact on the tidal dynamics in the region for the both waves. The high-resolution simulations reveal many mesoscale patterns which vary greatly over the space and types. It is hard to compare in detail our energy fluxes with those in (Lyard, 1997), for the horizontal resolution and coastline geometry is different. However, the patterns have much in common. We made comparison with the patterns of energy fluxes by Chen et al. (2009), (their Fig. 8 and 9) and conclude that they agree well.

5.5. Conclusions

The barotropic tidal model for the Lena Delta region of the Laptev Sea established here provides a necessary first step to further modeling of the circulation and ecosystem dynamics in the area. This model accurately resolves the irregular coastal topography with a large number of small islands and narrow channels and also bathymetry features of this domain. It reproduces the major semidiurnal tidal waves M_2 and S_2, which are the most important in generating large sea level amplitudes and currents over the considered shallow area. For the domain under consideration a special procedure was developed for the construction of optimal OBC for tidal elevation for both components. These OBC were based on results of modeling studies and observations. The simulated tidal maps show an improved agreement with observations as compared to other modeling studies performed for a larger area. The model also provides important information about barotropic currents, residual circulation, which affects sediment and nutrients transport, and evolution of energy fluxes in the region. The residuals of the energy budget are small implying that the budget is nearly balanced in the numerical simulations.

The next step is to set up a full model for accurate simulation of water stratification and ice in the domain. This is the subject of ongoing work. However, the results obtained here will be relevant in that case too. Indeed, the stratification causes only small variations in the structure of the tidal sea level, especially in the shallow areas like our region (Polyakov, 1995). The tidal kinetic energy in the domain considered is quantified sufficiently well by the barotropic tide, as follows from observations (Janout and Lenn, 2013). However, Janout and Lenn showed a strong link between stratification and baroclinic tidal structures, which of course must be considered when looking into diapycnal mixing processes. The freshwater plume dynamics can in principle modify both the tidal elevation and vertical structure of tidal ellipses. However, the main Lena freshwater channels are in the eastern part of the Lena Delta (carrying about 89% of the total Lena feshwater to the Laptev Sea

(Magritsky, 2001)). The freshwater plume spreads towards the East-Siberian Sea or to the north depending on the atmospheric conditions in the summer (Dmitrenko et al., 2010a). According to the observations (Janout and Lenn, 2013) and our modeling results, the tides are weak in the eastern part of the domain where most of freshwater is directed. This leads us to expect that freshwater plum dynamics will not noticeably interfere with tidal dynamics. A more delicate issue is the impact of sea ice. The Arctic tides are sensitive to the presence of ice cover, and mixing in the Arctic shelf seas depends of sea-ice conditions (e.g. Kowalik and Proshutinsky, 1994; Lenn et al., 2011). In a more general context, the fixed ice cover should increase the dissipation, resulting in a general decrease in tidal amplitudes and velocities on the one hand and tidal phase delay on the other hand. It is confirmed by modeling results for the Laptev Sea (Kagan et al., 2008a). However, we will concentrate on the period when there is no fast ice or ice is absent at all in the domain considered. Modeling results (Kagan et al., 2008a; Kagan and Sofina, 2010) shows that drift ice causes minor restructuring of tidal maps in the region. The changes in amplitude do not exceed 1-3 cm, which is less than the root mean square of absolute errors of model equal 3.8 cm in the absence of sea ice when the observations are available.

Acknowledgments

6. Simulation of shelf circulation dynamics in the Laptev Sea (Manuscript 2)

V. Fofonova[1,2], Dr. S. Danilov[2], Dr. A. Androsov[2], Prof. M. Zhukov[3], Dr. O. Semenova[4], Dr. Paul Overduin[5], Prof. K. H. Wiltshire[1]

[1]Alfred Wegener Institute, Helmholtz Centre for Polar and Marine Research; Kurpromenade, D-27498 Helgoland, Germany;
[2]Alfred Wegener Institute, Helmholtz Centre for Polar and Marine Research; Bussestrasse 24, D-27570 Bremerhaven, Germany;
[3]Southern Federal University, faculty of Mathematics, Mechanics and Computer Science; Milchakova 8a, 344090 Rostov-on-Don, Russia;
[4]Russian State Hydrometeorological University, Department of Hydrology; Malookhtinsky prospect 98, 195196 Saint-Petersburg, Russia;
[5]Alfred Wegener Institute, Helmholtz Centre for Polar and Marine Research; Telegrafenberg A43, D-14473 Potsdam, Germany;

Abstract

The article describes the modeling processes of the shelf circulation dynamics in the Laptev Sea with focus on the Lena Delta region. We try to estimate the role of different factors such as heat exchange with atmosphere, Lena runoff and tidal forcing on the dynamics in the region. An unstructured-grid Finite Volume Coastal Ocean Model (FVCOM) is used as a modeling tool.

Key words

Laptev Sea, Lena Delta, shelf circulation dynamics, FVCOM

6.1. Introduction

The polar shelf zones are highly dynamic and diverse systems. They form a border between warm and fresh water of continental drain and the cold currents of the northern seas. In the Arctic shelf region, multiple river deltas accumulate organic carbon. They host a unique and very diverse northern fauna and flora.

Over recent years, the Lena delta region of Laptev Sea acquired a special focus since it can serve as an indicator of climate change. A large number of observations in this region suggest a strong climate and biological changes for the last fifty years (Bauch et al., 2009; Hölemann et al., 2011). Organized as a part of the International Polar Year (2007 – 2008), joint study by the National Research Center of France, University of Alaska (USA) and Melnikov Permafrost Institute (Siberian Branch of Russian Academy of Sciences) has found that the Lena water temperature at the middle reach in the flood period had increased by 2 ° C compared to the values of 1950 (Costard et al., 2007).

Based on the results of observations in the Lena Delta region (Russian-German expeditions «Lena-2007», «Lena-2008») and Laptev Sea (Russian-German expedition «BARKALAV-2007/TRANSDRIFT-XII», «POLYNIA-2008/TRANSDRIFT-XIII», «BARKALAV-2008/TRANSDRIFT-XIV») it was found that in summer 2007 a positive anomaly of temperature and negative anomaly of salinity were present in the central and eastern part of the Laptev Sea in the mixed layer. The same structure of temperature and salinity was observed in summer 2008, but the magnitudes of anomalies were smaller. A continuous temperature increase was also found for Atlantic water. Such a powerful inflow of warm Atlantic waters into the Arctic Basin was not observed for the entire period of instrumental observations since 1897.

The long-term analysis by Polyakov et al. (2008) of the surface salinity change in the Arctic Basin and Arctic Seas, including the Laptev Sea, showed that ice-related processes, freshwater runoff and the way it spreads under the influence of atmospheric processes play a key role in salinity changes (freshening) of the upper layer over the past decades.

Johnson (2001) modeling studies showed that atmospheric forcing greatly determines the direction of freshwater transport in the Laptev Sea. The observations have confirmed that the variability of summer surface salinity in the Laptev Sea is mainly governed by local wind patterns associated with positive and negative phases of atmospheric vorticity over the adjacent Arctic Ocean (Dmitrenko et al., 2005). It should be emphasized that the winter water dynamics has very small impact on riverine water pathways in the summer (Dmitrenko et al., 2010a). In the end of the winter

season (March-April) the surface hydrography pattern is nearly the same as in September modified by thermodynamic ice formation.

Driven by the need to explain and understand the processes in the Lena Delta, the main goal of this work is modeling of the shelf circulation dynamics in the Laptev Sea with focus on the Lena Delta region. Our more distant goal is the ecosystem modeling in the region, for which a model with consistent dynamics is a necessary step.

This note describes our results obtained while tuning the model so that it is able to simulate the climatic changes in the region, and studying with its help the variability of circulation under the action of atmospheric, tidal and run-off forcing. We examine the role of topography structure and temperature of freshwater runoff, characteristics of heat fluxes in determining the features of the temperature and salinity distributions in the region and the role of local wind pattern and tidal dynamics. Additionally, we estimate the impact of improved bathymetry representation on the shelf in the vicinity of Lena Delta on tidal dynamics and local temperature and salinity local. Numerical simulations were based on Finite Volume Coastal/Community Ocean Model (FVCOM; Chen et al., 2006).

6.2. Model description

We use FVCOM to carry out our simulations. It is developed for simulations of flooding/drying processes in estuaries and tidal-, buoyancy- and wind-driven circulation in the coastal region featuring complex irregular geometry and steep bottom topography. FVCOM is unstructured- grid, finite-volume, free-surface, prognostic, 3-D primitive equation coastal ocean circulation model (Chen et al., 2003; Chen et al., 2006).

Our model domain covers water depths down to 65 m (Fig.1). The minimum water depth in the model is 0.5 m. We use high quality unstructured grid, which allows us to take into account complexity of coastline, characteristics of the bathymetry and other peculiarities of the problem. The grid was constructed using algorithm described in Persson and Strang (2004). Elements sizes are vary from 400 m near the cost to 5 km at the open boundary. The mesh contains six vertical sigma-layers with 250000 nodes on each of them. FVCOM was run using spherical coordinates, with nudging temperature and salinity at open boundaries to external data. For vertical mixing and horizontal viscosity simulation we used the modified Mellor and Yamada level 2.5 and Smagorinsky turbulent closure schemes respectively. As advection scheme we used the second order upwind scheme. The FVCOM version employed in this study is time stepped by a mode splitting method

(Chen et al., 2009). The time step for the external mode is 4.6 sec for the barotropic case and 2.5 sec for the baroclinic case, the ratio of internal mode time step to external mode time step is 10.

6.3. Input data

The bathymetry data were taken from GEBCO (The General Bathymetric Chart of the Oceans; http://www.gebco.net/data_and_products/gridded_bathymetry_data/). For coastline construction we compared GEBCO bathymetry data and NOAA (The National Oceanic and Atmospheric Administration) coastline data (http://www.ngdc.noaa.gov/mgg/shorelines/shorelines.html). To smooth the coastline we used cubic b-splines technique (Fig.1).
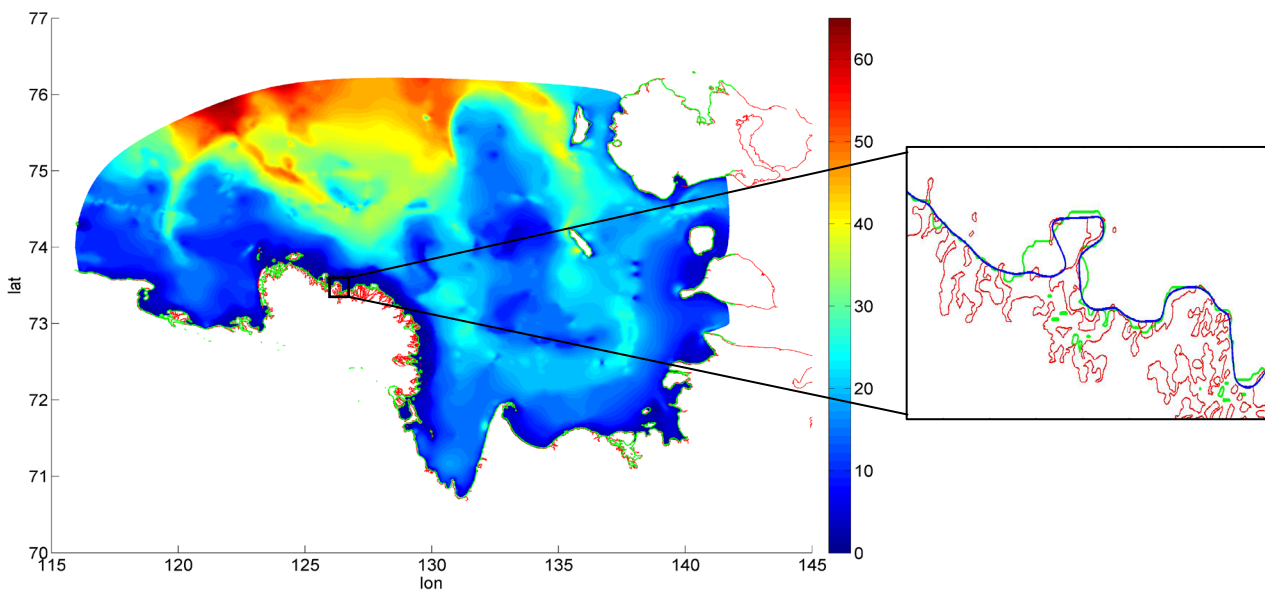
Fig. 1. The selected domain, bathymetry data from GEBCO (resolution of GEBCO grid is 30 arc-second), m. In red is shown coastline based on NOAA data, in green – coastline, which was obtained from GEBCO bathymetry data. On the right picture in blue is shown constructed coastline (smoothed using cubic b-splines technique).

The wind magnitudes and direction and radiation fluxes were taken from the regional, non-hydrostatic model provided by the consortium for Small-scale Modeling (COSMO). The time resolution of COSMO forcing is 1 hour. The COSMO model with included thermodynamic sea-ice module provides a high quality atmospheric forcing, which takes into account the presence of a thin layer of ice, and can be applied for short-range simulations (Steppeler et al., 2003; Schättler et al., 2008; Schröder et al., 2011). We used results from COSMO simulations with 5 km resolution

performed for the Laptev Sea area with and without assumption that the Laptev Sea polynyas are ice-free.

The temperature and salinity fields for initializing the model and for daily nudging on the open boundary were taken from Arctic simulations by R. Gerdes and P. Rozman with focus on the Laptev Sea region (Rozman et al., 2011). This model provides data, which are in a good agreement with long-term mean (1920-2008) surface salinity distribution for winter season (February-April) described in (Dmitrenko et al., 2010a) and salinity observation data for May, 2008 (provided by M. Janout). Also, the provided salinity/temperature patterns are close to the pattern of seasonal cycle from summer of 2007 to late winter/spring of 2008 shown in (Hölemann et al., 2011). This sea-ice model provides daily data for temperature and salinity field in the region for six vertical layers.

The input daily Lena runoff data, derived from observations, were provided by Hydrological Institute, St. Petersburg. The runoff temperature was set to either 0.5°C or 5°C, which present, according to Yang et al. (2002), Yang et al. (2005) and Costard et al. (2007), the approximately lower and upper bounds for mean temperature in the river mouth during May respectively. For assessment of the influence of local bathymetry on temperature and salinity patterns we used additionally bathymetry measurement data in Lena Delta region. The observation bathymetry data at 27686 locations (the average distance between points is about 800m) in close proximity to Lena Delta were provided by Paul Overduin (Alfred Wegener Institute, Potsdam).

The model is forced by tidal elevation prescribed at the open boundary from different models: TPX06.2, TPXO7.1 and AOTIM with Doodson correction. We paid special attention to tuning the conditions at open boundaries so as to obtain best agreement with the observational data. The model simulates the four most energetic tidal constituents: M_2, S_2, O_1, K_1 (Sofina, 2008; Lenn et al., 2011;Kowalik, 1993; Dmitrenko et al., 2012).

6.4. Tidal dynamics analysis

Observations of tidal currents over the Laptev Sea continental are rare and fragmentary. The starting point of the analysis was tide gauges data provided by Kowalik and Proshutinsky (KP) (can be downloaded from http://www.ims.uaf.edu/tide/). Based on observation data near the open boundary and features of different models we designed new open boundary conditions. To specify the correct open boundary conditions is one of the central problems of our modeling due to small depths in the area under consideration. We should emphasize that for the selected domain the amplitudes and phases on open boundary should be corrected near the cost (depth<10-15m) if they

are taken from any of models. The horizontal resolution of TPX06.2 and TPXO7.1 and associated inaccuracies in bathymetry data limit their skill in presenting the tidal features in the coastal zone. As concerns AOTIM (The Arctic Ocean Tidal Inverse Model), in addition to its 2D character, the linear assumption used in it makes it incapable of simulating residual currents (Chen et al., 2009).

The AOTIM was created based on (Egbert et al., 1994) data assimilation scheme by computing the inverse solution with all available tidal gauge data (Padman and Erofeeva, 2004). As a 'prior' solution was used the Arctic Ocean Dynamics-based Tide Model (the numerical solution to the shallow water equations). This pan-Arctic 2-D linear model is highly resolved (5-km regular grid), simulates 4 most energetic tides constituents (M_2, S_2, O_1 and K_1). Assimilated data consist not only coastal and benthic tide gauges (between 250 and 310 gauges per tidal constituent) but also available satellite altimeters (Padman and Erofeeva, 2004). Model bathymetry is based on the International Bathymetric Chart of the Arctic Ocean (Jakobsson et al., 2008). AOTIM5 does not include the effects of sea ice presence.

The TPXO7.1 and TPXO6.2 is a global inverse tide model developed by Gary Egbert and Lana Erofeeva at Oregon State University. The resolution of these models are $1/4^o$ x $1/4^o$. TPXO7.1 and TPXO6.2 assimilates 'TOPEX/Poseidon (T/P) and TOPEX Tandem satellite radar altimetry (available for the ice-free ocean between +/-66° latitude), and *in situ* tide gauge data in the Antarctic and the Arctic'. TPXO7.1 is one of the most accurate global tidal solutions.

 Chen et al. (2009) presented high resolution unstructed grid finite volume Arctic Ocean model (AO-FVCOM) in application for tidal studies. A spherical coordinate version of the instructed grid 3-D FVCOM was applied to the Arctic Ocean for tides simulation. The size of elements varies from 1 km in the near coastal areas to 15 km in the deep ocean; model resolves accurately the irregular coastal geometry. However, the largest amplitude and phase differences between modeled and observed tides were caused by the model errors along the Russian coast (Chen et al., 2009).

The designed open boundary condition provides better agreement with observation data compared to the case when the condition directly derived from AOTIM, TPXO6.2 or TPXO7.1 is used. The results from the tidal simulations for East Siberian shelf provided by Sofina have been also included in the analysis. Table 1 shows the results of comparison for M_2 constituent.

Table 1. The error of different models against coastal tide gauges for the M_2 constituent.

	AO-FVCOM with stations coord. corrections (R<40km)	East Siberian shelf model	AOTIM5	TPX07.1	TPXO6.2	Simulation based on AOTIM5	Simulation based on TPXO7.1	Simulation based on designed open boundary conditions	Simulation based on designed open boundary conditions with stations coord. corrections (R<20km)
$Error \cdot 10^2$	30.94	41.07	45.74	36.86	50.78	33.09	19.61	15.24	3.61

$$Error = \frac{1}{N} \sum_{i=1}^{N} \left(\left(1 + \left(\frac{S_{am}(i)}{O_{am}(i)} \right)^2 - 2 \cdot \cos(S_{ph}(i) - O_{ph}(i)) \cdot \frac{S_{am}(i)}{O_{am}(i)} \right)^{\frac{1}{2}} \right),$$

where S_{am}, S_{ph} - simulated amplitude and phase respectively, O_{am}, O_{ph} - observed amplitude and phase respectively, $N = 10$ - number of stations.
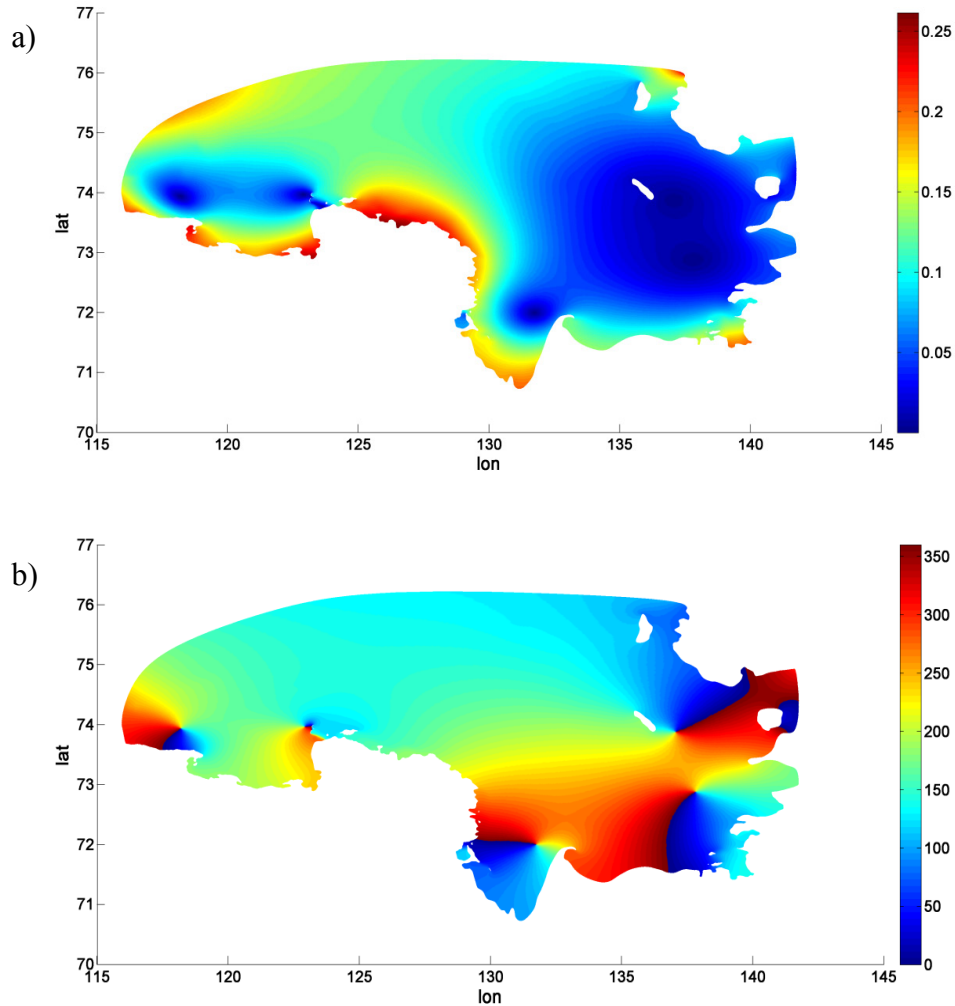
Fig. 2. The results of simulation with designed open boundary condition for amplitude and phase for M_2 constituent: a) Amplitude, m, b) Phase, deg.

6.5. Temperature and salinity patterns variability

We compare salinity and temperature fields in mixed layer under the ice in simulations with and without atmospheric forcing, tidal dynamics, with different temperatures of freshwater and using different techniques for freshwater input. We present here only a schematic overview of the results obtained.

The surface salinity to the north and west from Lena Delta is mainly determined by the local wind pattern. East of the Lena Delta, the temperature and salinity patterns are dominated by plume internal dynamics driven by freshwater discharge and accompanying changes in the sea surface height and density field in the presence of Coriolis force and are largely insensitive to the atmospheric forcing, this fact being reflected in the background hydrography (Dmitrenko et al. 2010a).

Tides play a significant role in water mass modification through vertical mixing of seawater properties in the mixed layer. In general, plume velocities induced by winds and plume internal dynamics exceed residual tidal velocities, especially east of the Lena Delta where tides are weak. Increasing the discharge water temperature influences only little the freshwater plume dynamics. It can, however, have some impact on the volume of net sea-ice melting, which is not considered here. Bauch et al. (2013) found that significant volumes of net sea-ice melting are observed only in case of river water spread to the central Laptev Sea. Their study showed that the local melting of the sea ice is coupled to river water. Note that the central-eastern Laptev Sea is a shallow region with the depth less than 20 m even north of 75.5˚. The shallowness of the region may assist northward propagation of temperature signal from Lena water to the north if northward winds dominate in the second part of the summer. The stable stratification in that time and presence of thin layer of fresher water strengthen the effect. Note that in 2008 in the middle of July the observational Lena water temperature near the mouth reached 20℃. We may hypothesize that if the freshwater plume spreads to the central Laptev Sea and not towards the East-Siberian Sea, the warm water of Lena River would lead to active ice melting in the adjacent area and a corresponding decrease in albedo and changes in heat flux balance.

The change in the structure of heat fluxes (COSMO data with and without open polynyas) and in runoff temperatures do not significantly influence the propagation of the freshwater plume whereas the temperature pattern is changed in the whole mixing layer (Fig. 3). The temperature anomalies in the mixed layer mainly in the northern part of the Lena Delta vicinity if they are independent of salinity anomalies can be mainly explained by characteristics of heat fluxes.
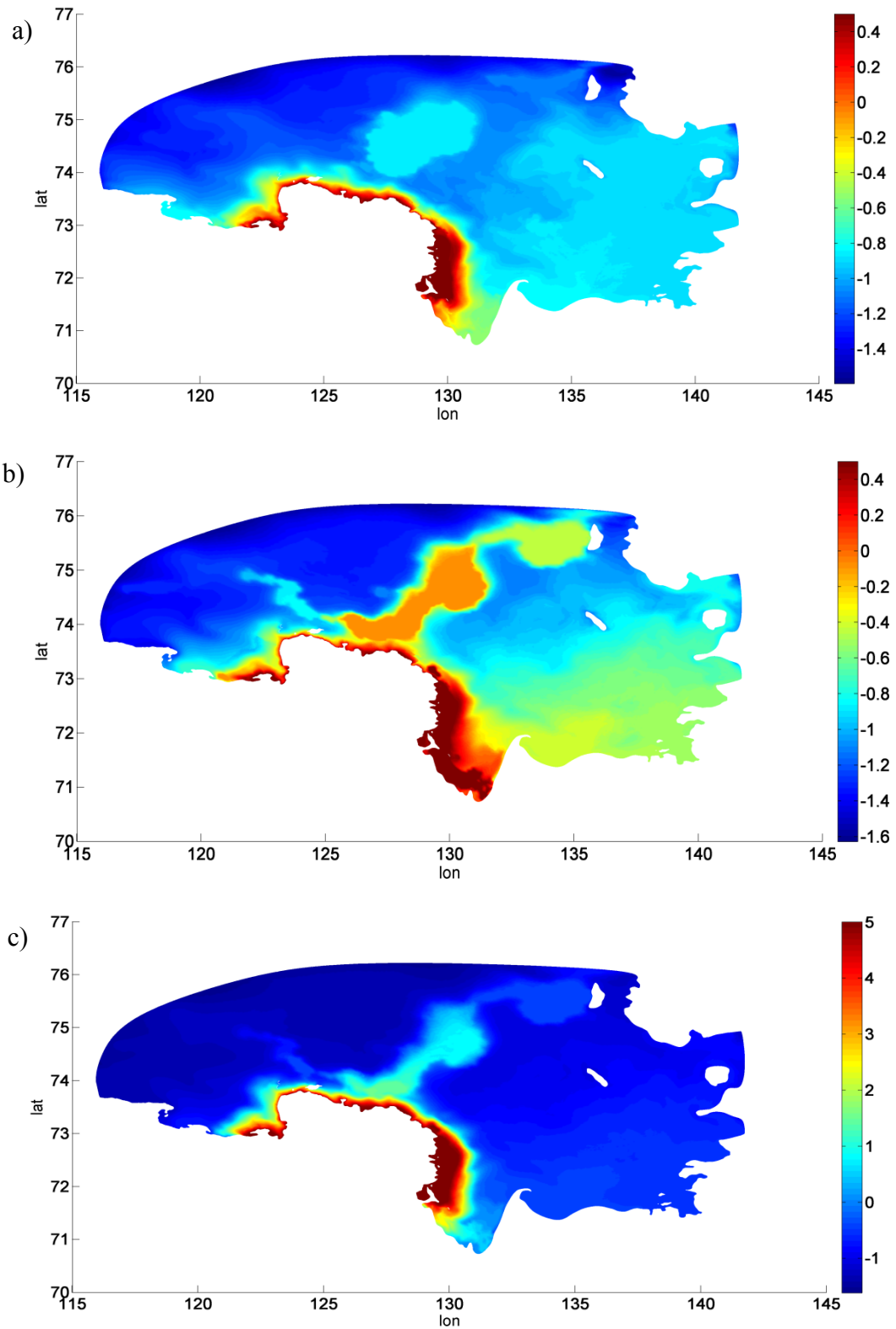
55

Fig. 3. The surface temperature fields [°C] at the end of May, freshwater runoff input from the boundary.
a) atmospheric forcing from COSMO with polynyas closed by thin layer of ice, the runoff temperature
is 0.5 °C, b) same as in a), but with open polynyas, c) same as in b) but for the runoff temperature of 5 °C.

Because of weak winds in the region in the summer period, the details of the Lena runoff distribution over the Delta channels influences the simulated salinity patterns. That is why we tried to follow observations and local bottom topography in prescribing it. The Delta of Lena and its channels are not resolved in the model, so the Lena discharge distribution can be accounted for only approximately. We used two techniques to distribute the total volume runoff. In the first case the freshwater input was implemented as a boundary condition on the Lena Delta boundary. The spatial runoff structure followed the description in Magritsky (2001) with positions derived from the auxiliary topography. In that case, the freshwater is input through 1552 mesh edges so as to model the observed spatial distribution. In the second case, the freshwater input was added over some vicinity of the Lena Delta boundary, depending not only on spatial runoff structure, but on the depth too. The second technique allowed us to avoid anomalous water elevation in Lena Delta zone (maximum runoff in 2008 was observed at the end of May), to form the main freshwater channels and estimate the degree of influence of bathymetry data. In that case the freshwater input organized via the nodes (Chen et al. 2006), the amount of nodes, over which the freshwater is supplied, is 35198. The way how the Lena discharge is implemented is leading to certain differences, mostly at short simulation times, as can be seen comparing the left and right columns of Fig. 4. These differences become less pronounced in longer runs. The advantage of distributing the discharge over close vicinity of boundary is smoother elevation anomalies. The gradient of elevation may be rather high in the vicinity of channels if the discharge is implemented as the boundary condition.
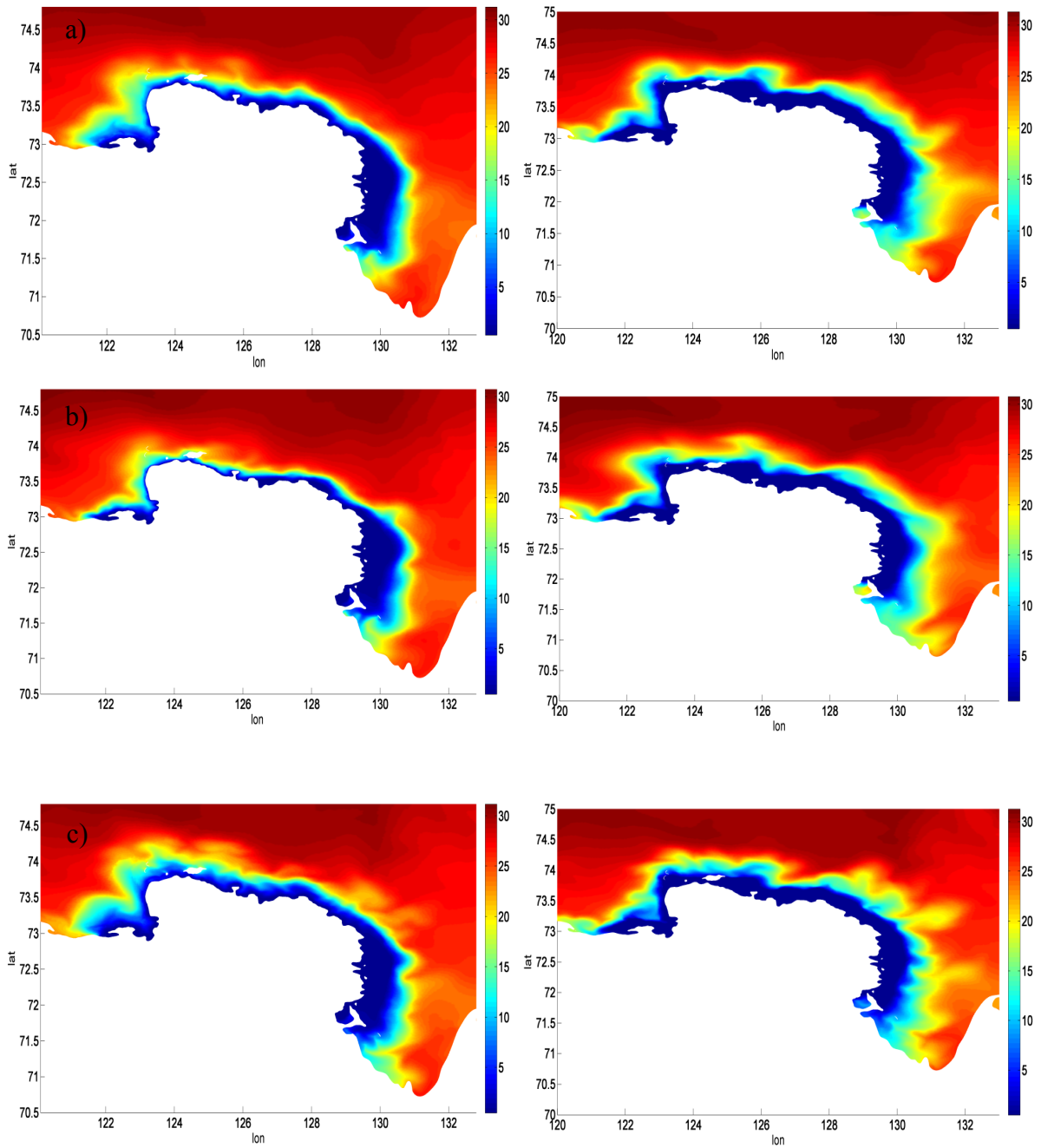
Fig. 4. (a) Surface salinity distribution simulated for the middle of May, 2008. (b) Same as (a), but in the absence of COSMO atmospheric forcing. (c) Same as in (a), but in the absence of tidal dynamics. The runoff is implemented as boundary condition (left column) and as distributed over some vicinity of the boundary (right column).   Salinity is in practical scale.

7. Impact of wind and tides on the Lena River freshwater plume dynamics (Manuscript 3)

V. Fofonova,[1, 2] S. Danilov,[2] A. Androsov,[2] M. Janout,[3] M. Bauer,[5] P. Overduin,[4] P. Itkin,[2]
 K.H. Wiltshire[1]

[1] Alfred Wegener Institute, Helmholtz Centre for Polar and Marine Research; Kurpromenade, D-27498 Helgoland, Germany;
[2] Alfred Wegener Institute, Helmholtz Centre for Polar and Marine Research; Bussestrasse 24, D-27570 Bremerhaven, Germany;
[3] Alfred Wegener Institute, Helmholtz Centre for Polar and Marine Research; Building Nordseevilla-1, D-27570 Bremerhaven, Germany;
[4] Alfred Wegener Institute, Helmholtz Centre for Polar and Marine Research; Telegrafenberg A43, D-14473 Potsdam, Germany;
[5] Trier University, Department of Environmental Meteorology; Behringstraße 21 (Campus II), D-54286 Trier, Germany;

Abstract

The Lena plume dynamics in the Lena Delta region of the Laptev Sea are explored in simulations performed with the Finite Volume Coastal Ocean Model (FVCOM) on a mesh with the horizontal resolution from 0.4 to 5 km and vertical resolution of 11 sigma-layers. The impact of winds and tides on the Lena plume propagation is analyzed by applying different sources of atmospheric forcing and the switching on/off tidal dynamics. East of the Lena Delta the plume dynamics are found to be rather insensitive to the detail of forcing, being driven mostly by the internal dynamics. Northward plume excursions are wind driven, and model skill in simulating them depends on the available wind forcing.

Key words

Laptev Sea Shelf; Lena Delta; freshwater plume; tidal dynamics

7.1. Introduction and motivation

Rapid climate change affects polar seas. The processes observed in the coastal and shelf regions are of particular interest, because of ice retreat, permafrost thawing and increase in river runoff temperature and volume influence local ocean circulation and ecosystem dynamics. One of the areas of recent focus is the Lena Delta region of the Laptev Sea, which was a subject of numerous observational studies over the past few years (Russian-German expeditions Lena-2007, Lena-2008, BARKALAV-2007/TRANSDRIFT-XII, POLYNIA- 2008/TRANSDRIFT-XIII, BARKALAV-2008/TRANSDRIFT-XIV). The interest in this area is partly motivated by the fact that the Lena River provides approximately 70% of the total runoff to the Laptev Sea.

Available studies indicate that the region is undergoing substantial changes. Costard et al. (2007) found that the water temperature in the middle reaches of the Lena River in its flood period had increased by 2°C compared to the values of 1950. Indeed, 2007 was the warmest year in terms of air temperature in entire Russia since the late nineteenth century (Bulygina et al., 2014; Ashik et al., 2010). Strong polynya activity in the Laptev Sea in spring 2007 led to more summertime open water and therefore warmer sea surface temperatures in the Laptev Sea (Hölemann et al., 2011). The expeditions in September, 2007 to the Laptev Sea and Lena Delta region discovered the largest positive anomaly of surface temperature for the entire period of observations and negative anomaly of salinity in the central and eastern parts of the Laptev Sea compared to the climatic mean (Dmitrenko et al., 2010a; Hölemann et al., 2011). A similar structure for temperature and salinity fields was observed in the middle of summer 2008, but with smaller anomalies. Note that local processes in the Laptev Sea may have a basin-wide impact on the thermohaline structure of the Arctic Ocean (e. g., Johnson and Polyakov, 2001; Dmitrenko et al., 2005; Krumpen et al, 2013).

The Lena River freshwater plume propagation is a key process defining the dynamics of the Laptev Sea region in the summer. It influences stability of the water column and modifies vertical mixing. Accordingly the factors that influence the plume behaviour are of interest. Atmospheric winds and tidal mixing can be considered to be the main driving factors, and the existing observational studies do largely confirm this (Dmitrenko et al., 2005, 2010b, 2012; Janout and Lenn, 2014). While there is general agreement on the factors governing the plume dynamics, there are still many questions concerning particular details of the relative importance of tides and winds as factors determining the plume spreading. This study aims at exploring some aspects of the observed plume variability. It is based on numerical simulations performed with the Finite Volume

Coastal/Community Ocean Model (FVCOM; Chen et al., 2006) on a mesh covering the Lena Delta region of the Laptev Sea (see Fig. 1).
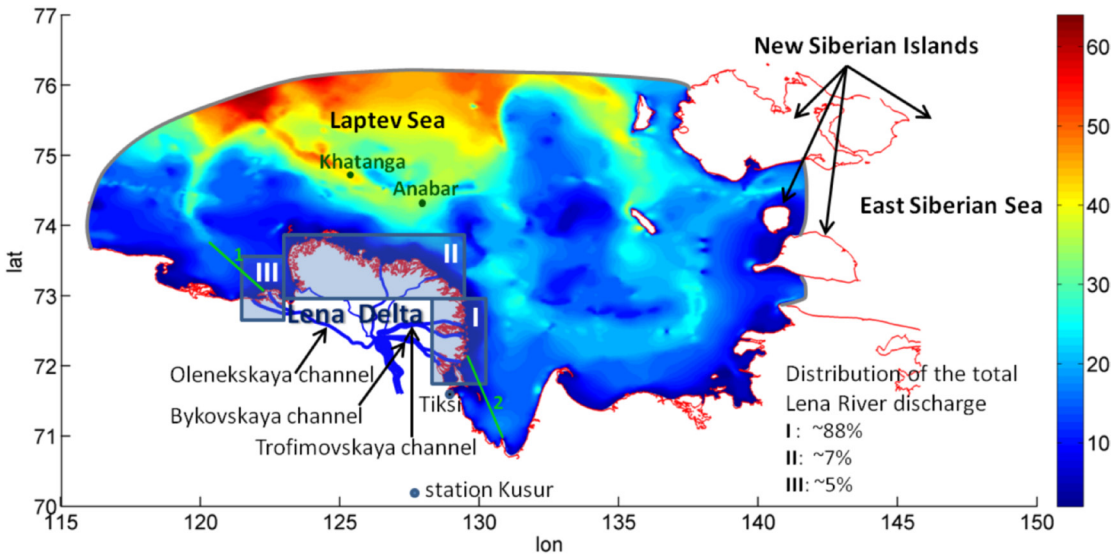

Fig. 1. The model computational domain. Colours show the GEBCO topography, [m], and the red line indicates the coastline derived from the NOAA database. The cross sections (1, 2) used for the analysis are drawn in green. The two green dots indicate the Khatanga and Anabar mooring positions. The transparent rectangles visualize the freshwater discharge distribution according to Magritsky (2001) and Bolshiyanov et al. (2013). The open boundary segments are shown in grey. Tidal elevation is prescribed there, and temperature and salinity are nudged to that of a large-scale model.

We compared simulations forced by different atmospheric forcing products including local, regional (Arctic) and global ones. The study concentrates separately on May, 2008 (for which all forcing products are available) and on a longer period from May to September, 2008 (only regional and global forcing). To verify the model we used the observational data available for 2008. We focused only on the inner shelf part of the Laptev Sea and relax temperature and salinity at the open boundary to a daily mean output of a large-scale ocean circulation model. Based on historical records of bottom layer temperature Dmitrenko et al. (2010b) found that only the Laptev Sea outer shelf is affected by the Arctic Ocean Atlantic water boundary current transporting warm and saline water from the North Atlantic. We did not explicitly consider sea ice in this study, because the model domain is essentially covered by movable ice or is ice free within the period we are interested in, but took into account the freshwater flux due to ice melting in long simulations. The modeling results by Kagan et al. (2008a), Kagan and Sofina (2010) showed that drifting ice causes minor restructuring of tidal maps in the region. The changes in amplitude did not exceed 1-3 cm, which is less than the root mean square of absolute errors of model equal to 3.8 cm in the absence of sea ice when the observations are available.

61

The article is organized as follows. Section 2 presents a short description of the related work. Section 3 describes the model setup, including model configuration, mesh design, input data and forcing. The experiments, together with their results, are described in Section 4. Sections 5 and 6 contain Discussion and Conclusions, respectively.

7.2. Background

While the large-scale ocean circulation in the Arctic is controlled by the balance between the Siberian High and the Icelandic Low (Johnson and Polyakov, 2001), the observations show that the variability of summer surface salinity in the Laptev Sea is mainly governed by local wind patterns (Dmitrenko et al., 2005). Generally, a prevailing cyclonic circulation in the summer leads to propagation of the Lena water to the east, creating a negative salinity anomaly east of the Lena Delta and farther to the East Siberian Sea, and a positive anomaly north of the Lena Delta. In contrast, a prevailing anticyclonic circulation leads to negative salinity anomalies north of the Lena Delta (freshwater is advected toward the north), and a corresponding salinity increase eastward. For example, according to Abrahamsen et al. (2009), the atmospheric circulation was cyclonic over the Laptev Sea in summer, 2007, with winds having an on-shore component. The mean sea-level atmospheric pressure (SLP) from National Centers for Environmental Prediction (NCEP, Kanamitsu et al., 2002) in July-September showed a low-pressure area centered over the eastern Laptev Sea near New Siberian Islands (Dmitrenko et al., 2010a) (see Fig. 1 for domain geometry). In 2008, the atmospheric circulation was anticyclonic from the middle of July to the middle of September, dominated by two SLP highs located over the western Laptev Sea near Severnaya Zemlya Archipelago and over the northeastern East Siberian Sea (Dmitrenko et al., 2010a), implying the northward plume propagation. Nevertheless, direct wind measurements in the region are sparse, and it is difficult to judge in general how well the actual winds are represented by the available forcing products.

Despite the fact that the atmospheric forcing modifies local salinity and temperature patterns, the surface salinity distribution over the shelf area east of the Lena Delta stays qualitatively similar, with standard deviation between two and four (here and below salinity is in practical scale) (Dmitrenko et al., 2010a).

Tidal dynamics provide a mechanism for turbulent mixing in estuaries and on continental shelves and influence temperature and salinity patterns (Androsov et al., 1998; Dmitrenko et al., 2012). The eastern Siberian shelf, consisting of the Laptev and East Siberian Seas, is rather shallow,

with an average depth of about 20-30 m (Dmitrenko et al., 2008a). Its shallow character makes it sensitive to the tidally induced mixing (Simpson et al., 1996; Lenn et al., 2011), yet the precise role of tidal mixing has not been quantified. The contribution from M_2 tide is the most important in the Laptev Sea shelf region, followed by S_2 (see, e.g., Padman and Erofeeva, 2004; Chen et al., 2009). The barotropic tidal dynamics induced by M_2 and S_2 waves in the domain of interest was analyzed by Fofonova et al. (2014). According to AOTIM5 (The Arctic Ocean Tidal Inverse Model) and TPXO7.1 (TOPEX/POSEIDON global tidal model) (Egbert et al., 1994; Padman and Erofeeva, 2004) the amplitude of the next largest semi-diurnal constituent N_2 is approximately 2-3 times weaker than the amplitude of S_2 at the open boundary of the domain. The observations by Janout and Lenn (2014) reveal a weak velocity signal of N_2 tide only in the outer shelf area of the Laptev Sea. The contribution of K_1 and O_1 waves, which are the main diurnal constituents in the region (Kowalik and Proshutinsky, 1994; Kagan et al., 2008b), is rather small in the domain according to observational data (Dmitrenko et al., 2012; Janout and Lenn, 2014).

7.3. Model setup

7.3.1. Model and mesh

Numerical simulations were performed using FVCOM (Chen et al., 2003, 2006). This is a prognostic, 3-D primitive equation coastal ocean circulation model using unstructured triangular meshes. The Mellor and Yamada level 2.5 turbulence scheme was applied to parameterize vertical diffusion and viscosity, and the Smagorinsky parameterization was used for the horizontal viscosity. The first order upwind scheme was selected to advect the temperature and salinity fields. The model employs the mode splitting method, with the time steps for the external and internal modes of 4,6 s and 46 s, respectively. They were dictated by stability requirements on the mesh we used.

The domain selected for simulations is shown in Figure 1, where colours represent the bottom topography derived from the General Bathymetric Chart of the Oceans (GEBCO, http://www.gebco.net/data_and_products/gridded_bathymetry_data/). In selecting the domain we have been guided by the requirement that it should be large enough to trace the propagation of the Lena freshwater plume and small enough to minimize the computational efforts. The open boundary was drawn in order to avoid the amphidromes in its close vicinity. Their positions were estimated from the tidal map simulated by Kagan et al. (2008a) and Sofina (2008). The GEBCO_08 gridded bathymetry with 30 arc-second resolution was used as a basic bathymetry data for the whole domain. However, this does not provide sufficient information on the location of small freshwater

channels in the vicinity of the Lena Delta. It was taken from the Soviet topographic map (http://www.geospatial.com/store/type/series/term/2000003/text/russian-nautical-charts/) representing the vicinity of the Lena Delta, digitized at an average resolution of 800 m. Since it resolves the channels, the map was also used in constructing the freshwater inflow distribution. The coastline was derived from the GEBCO bathymetry data and the National Oceanic and Atmospheric Administration World Vector Shoreline database (NOAA, http://www.ngdc.noaa.gov/mgg/shorelines/shorelines.html) with the resolution of approximately 2 km and 250 m, respectively. Guided by both, we constructed the coastline with 400 m to 1 km resolution using cubic b-splines technique, as detailed in Fofonova et al. (2014).

A high quality unstructured grid was generated by the algorithm by Persson and Strang (2004). The element size function was based on the square root of bathymetry (phase speed of long surface gravity waves) and its gradient. Additionally, the mesh was refined in the main directions of the Lena freshwater plume. The element sizes vary from 400 m near the coast to 5 km in the deepest part of the region. Such coastal resolution already allows one to take into account some details of actual coastline and bathymetry. The surface mesh contains approximately 250000 nodes, and there are 11 sigma layers in the vertical direction. Their thickness follows a parabolic function with the highest vertical resolution near the surface and bottom.

7.3.2. Initialization and forcing

The temperature and salinity fields for initializing the model and for daily nudging on the open boundary were taken from the North Atlantic/Arctic Sea Ice - Ocean Model (NAOSIM) simulations run at 1/12 degree spatial resolution (Fieg et al., 2010; Rozman et al., 2011). The NAOSIM grid covers the whole Arctic Ocean and part of the North Atlantic. NAOSIM is forced by daily NCAR/NCEP atmospheric reanalysis data (Kanamitsu et al., 2002). The river runoff is implemented as a virtual salt flux (Prange and Gerdes, 2006). The points where this negative salt flux is applied are distributed evenly along the eastern coast of the Lena Delta. The salinity simulated for 2008 shows a good qualitative agreement with the long-term mean (1920-2008) surface salinity for the winter season (February-April) described in Dmitrenko et al. (2010a). The surface and bottom salinity used to initialize our simulations are shown in Figure 2. They are rather uniform along the open boundary and do not necessarily represent the actual water masses there. It may affect the initial phases of our simulation during which the stability of water column depends largely on the initialization.
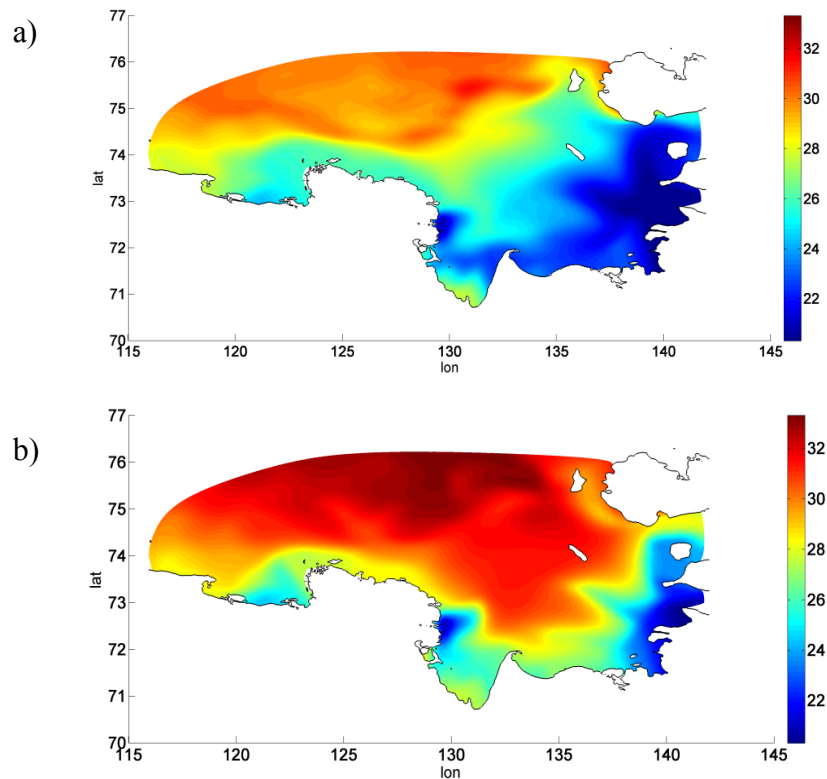
Fig. 2. Initial of salinity fields (10th of May, 2008 at 00:00:00), in practical scale, for a) surface layer and b) bottom layer.

For May, 2008, we had an opportunity to use the wind fields and radiation fluxes from a regional non-hydrostatic model provided by the Consortium for Small-Scale Modeling (COSMO). The COSMO model, which included a thermodynamic sea-ice module, provides a high quality atmospheric forcing, allowing one to take into account the presence of a thin layer of ice, and can be applied for short-term simulations (Schättler et al., 2013; Schröder et al., 2011; Steppeler et al., 2003). The sea ice concentration in this model is derived from AMSR-E (The Advanced Microwave Scanning Radiometer - EOS) sea ice concentration (SIC) data. The ice thickness is set to 1m at positions where AMSR-E SIC is above 70% (Schröder et al., 2011). We used hourly fields from COSMO simulations with 5 km resolution performed for the Laptev Sea area for two cases differing by the representation of the Laptev Sea polynyas (ice-free or ice-covered, the positions where AMSR-E SIC is below 70% are set to 0 cm and 10 cm ice, respectively). We note that the simulations of the Laptev Sea polynya dynamics by an ocean model driven by forcing provided by COSMO are closer to AMSR-E than the simulations driven by 6-hourly NCEP Reanalysis 1 (spatial resolution of 1.875°), NCEP Reanalysis 2 (spatial resolution of 1.875°) and GME (Global Model of the German Weather Service) (spatial resolution of 0.5°) (Ernsdorf et al., 2011). The COSMO

65

simulations for the Laptev Sea region were not available for the rest of the summer season in 2008. For this reason, we used them only for short May simulations. In longer simulations, (covering the entire period from May to September, 2008) the forcing derived from the operational European Centre for Medium-Range Weather Forecasts (ECMWF, http://data-portal.ecmwf.int/) atmospheric model was used. The data from ECMWF have spatial resolution approximately 40km. Additionally, for the comparison of different atmospheric sources against each other and available observations, we used the NCEP Reanalysis 2 product (http://www.esrl.noaa.gov/psd/data/gridded/data.ncep.reanalysis2.html).

The amplitudes and phases of tidal components on the open boundary were derived from AOTIM5 and TPXO7.1 (Egbert et al., 1994; Padman and Erofeeva, 2004) with corrections as described by Fofonova et al. (2014). These corrections noticeably improve the agreement of modeled tidal maps with available tide gauge data. The model simulates the most energetic semi-diurnal and diurnal tidal constituents: M_2, S_2, O_1, K_1.

7.3.3. Lena River discharge and freshwater input from ice melting

For all our simulations we used mean daily water discharge and temperature data from the basin outlet Kusur Station. The observed daily Lena runoff data were provided by the State Hydrological Institute, St. Petersburg (http://www.hydrology.ru/). The observed daily water temperatures were provided by the Center of Hydrometeorology and Environmental Monitoring in Tiksi. The information about the total freshwater distribution over the freshwater channels was taken from Magritsky (2001) and Bolshiyanov et al. (2013) (Fig. 1) and used accordingly in the model. The detailed bathymetric data available for the vicinity of the Lena Delta allowed us to adjust the positions of even very small freshwater channels. The freshwater is input through 1552 mesh segments of the Lena Delta boundary in order to simulate the observed spatial distribution.

We did not take into account the freshwater flux due to ice melting in short runs covering only May, 2008, but added the melt freshwater in long runs covering the period from May to September, 2008. The reason was that according to satellite observations (S. Willmes, personal communication) in May, 2008 ice occupied almost the entire Laptev Sea, except for a small zone of polynyas. Note also that land fast ice might be present close to the Lena Delta in May, which leads to changes in the geometry of the coastline. It generally breaks up when the freshwater runoff reaches its maximum (Bauch et al., 2009). In 2008 the daily maximum flow formed at the end of May according to observation, so the fast ice was absent for the most of integration time. We assumed that during May,

2008 the ice over most of domain is thin and moveable so that momentum flux is approximately transferred to the ocean. The sea ice presence is accounted for in the heat fluxes between the atmosphere and ocean, and freshwater due to ice melting is accounted for in long runs. Note that in August and September the Laptev Sea is more often almost ice-free (Alexandrov et al., 2000).

For the long range simulation (May-September) we distributed the freshwater due to ice melting in period from June to the middle of August according to AMSR-E sea ice concentration data provided by T. Krumpen and S. Willmes (Willmes et al., 2011), as additional precipitation. The thickness of the ice in different zones was obtained from observational data for the late spring 2008 and the description by Alexandrov et al. (2000). The information about sea ice export across the Laptev Sea boundaries and sea-ice melt water budget for 2008 was taken from Krumpen et al. (2013) and Bauch et al. (2013), respectively.

7.4. Results

7.4.1. Description of experiments

To address the relative role of tidal and wind forcing in the Lena River freshwater plume dynamics we performed a series of "short" runs simulating May, 2008. In the first subset of these runs we used COSMO, ECMWF and NCEP forcing alluded to earlier to learn about the impact of the difference in the wind forcing on the plume propagation. We compared the winds from these sources with available observations. In the second subset, we either turned off tidal forcing, or COSMO atmospheric forcing or both to trace their impact on the freshwater plume dynamics.

One-month simulations are too short to give a full answer about the impact of atmospheric forcing on the Lena freshwater distribution. We therefore carried out longer-term (May-September, 2008) simulations, driven by the ECMWF forcing. The long-term simulations also allowed us to make a comparison with observations and verify the model. In addition, we carried out several barotropic (but multilayer) runs to clarify the role of residual circulation of summary tide.

7.4.2. The effect of different wind sources

Wind forcing is a key factor determining the surface salinity variations in the Lena Delta region of the Laptev Sea. Since the COSMO forcing possesses the finest resolution and is produced in simulations with a special focus on the area, it was natural to consider it as the basic one. Since it was available only for May, 2008 and not for the summer season, we selected this month to learn about the impact of different forcing products. According to COSMO results, a very unstable and

heterogeneous pattern of winds at 10 m was observed in May, 2008. The invasions of strong winds from the continent were frequently associated with the onset of local circulation along the coast of the Lena Delta both from the west to east and vice versa. Such wind pattern locks the plume on the western or eastern sides of the Delta, since the Ekman transport and surface velocity are expected to be 90 and 45 degrees to the right. In general, the wind pattern simulated by COSMO for May, 2008 was characterized by the dominant westward and west-northward winds. Such winds act to enforce the plume spreading to the west and north in the north-western part of the Lena Delta vicinity. Figure 3a shows surface salinity snapshot at the end of May. The maximum wind speed over this domain reached 6.3 m/s, the minimum - 1.9 m/s with a mean value of 4.06 m/s according to COSMO. This range of magnitude is broadly in line with the norms of the region's climate. In the late spring and summer winds with speeds smaller then 3-4 m/s are prevailing. Strong winds exceeding 20 m/s are not observed in the summer (Dobrovolsky and Zalogin, 1982).

In order to see the uncertainty associated with the wind sources, we also simulated the May, 2008 circulation with winds at 10 m from ECMWF and NCEP-DOE Reanalysis 2. The surface salinity simulated in these runs is shown in Figure 3b,c. While the results of the simulations look qualitatively similar, there are noticeable differences in detail. One of the main reasons for this is the stronger and more homogenous winds from the large scale reanalysis products. Winds contribute in two ways: directly, through modifying transports, and indirectly, through modifying the vertical mixing. The average wind speeds given by ECMWF and NCEP-DOE Reanalysis 2 for May, 2008 are, respectively, about twice and more than twice as high as the COSMO wind speed. This leads to stronger mixing induced by wind, especially in the case of NCEP-DOE Reanalysis 2 forcing. While Figure 3b shows stronger plume propagation west of the Lena Delta, which is the consequence of stronger winds in ECMWF forcing, simulations in Figure 3c display stronger plume confinement to the Lena Delta vicinity despite even stronger winds in this case. The explanation is that in the case of NCEP-DOE Reanalysis 2 forcing presented in Figure 3c we obtained a largely mixed water column, in contrast to the other cases. For the same reason, rather counterintuitively, the plume looks most confined in Figure 3c over the central part of the Delta.
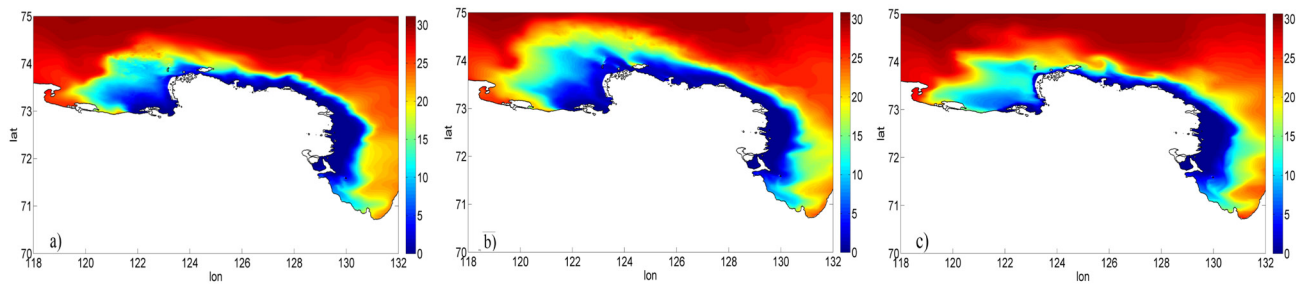
Fig. 3. (a) Surface salinity distribution, in practical scale, simulated at the end of May, 2008 with COSMO atmospheric forcing. (b) Same as in (a), but with ECMWF atmospheric forcing (c) Same as in (a), but with NCEP-DOE Reanalysis 2 atmospheric forcing.

We stress that since observational data in this region are scarce, they are insufficient to constrain the global and regional Arctic atmospheric models in order that their wind patterns may deviate at small scales from actual winds. However, NCEP-DOE Reanalysis 2 and ECMWF data show largely similar wind pattern, and their wind direction agrees well with that of COSMO. We compared the winds used by us with three-day averaged observed surface wind at the Tiksi (Fig. 1) hydrometeorological Station (http://www.aari.ru/main.php?lg=1). This comparison shows that COSMO provides the most realistic wind for the area. For our long-term runs we chose the ECMWF forcing, because the wind amplitudes of the NCEP-DOE Reanalysis 2 deviate more from COSMO and observations.

The differences in spreading patterns, caused by differing forcing, indicate that the availability of accurate wind forcing data is a prerequisite to reliable modeling of plume propagation. While on the early phase of plume propagation shown in Figure 3 the plume dynamics is to a large extent driven by the freshwater front which follows the shape of the Delta, the front will be deformed with time, and differences among the cases driven by different forcing may become more dramatic. We did not explore these issues in detail here, because we have found that long simulations driven by ECMWF forcing lead to reasonable agreement with observations.

7.4.3. The effect of tides and wind on plume propagation

To investigate the influence of tidally induced mixing on the plume dynamics, we analyzed the Brunt– Väisälä (BV) frequency in all short runs forced by COSMO fields with a closed polynyas assumption. Although within the plume area density anomalies are determined mostly by salinity, the BV frequency also takes into account the effects of temperature. For the analysis we chose two cross-sections in the Lena Delta zone located in the areas with the strongest freshwater input, as shown in Figure 1. Section 1 is located in the area where tides are strong, but freshwater input

69

makes just a fraction of the total freshwater input. Here we expect the influence of winds and tides to be more noticeable than for section 2 located in the eastern part of the Delta. This section crosses the main part of the plume, so the water mass properties are only governed by the freshwater input, and are expected to be less sensitive to the external factors. The four rows in Figure 4 show the BV frequency patterns at these cross-sections with superimposed isohaline lines. They refer to the cases of no tides and wind, no wind only, no tides only and the case of full forcing. For section 1 (left column), tides are responsible for mixing around the freshwater front, causing its to spreading diffusively, therefore, the isohaline 27 shifts seawards, and close to the coast the freshwater penetrates deeper. If the tides are off, but wind forcing is applied, the situation changes dramatically: wind-induced transport leads to the formation of a thin freshwater layer at the surface, as indicated by the flat lines of low salinity. The result is the increased stability of the surface layer and suppression of mixing there. Adding tides (to recover full dynamics) now adds mixing, as indicated by the position of the line with salinity 27, and also by deepening of the line with salinity 20. The high stability of the surface layer prohibits mixing there. Thus, we concluded that it is mainly the impact of wind that determines the plume propagation.
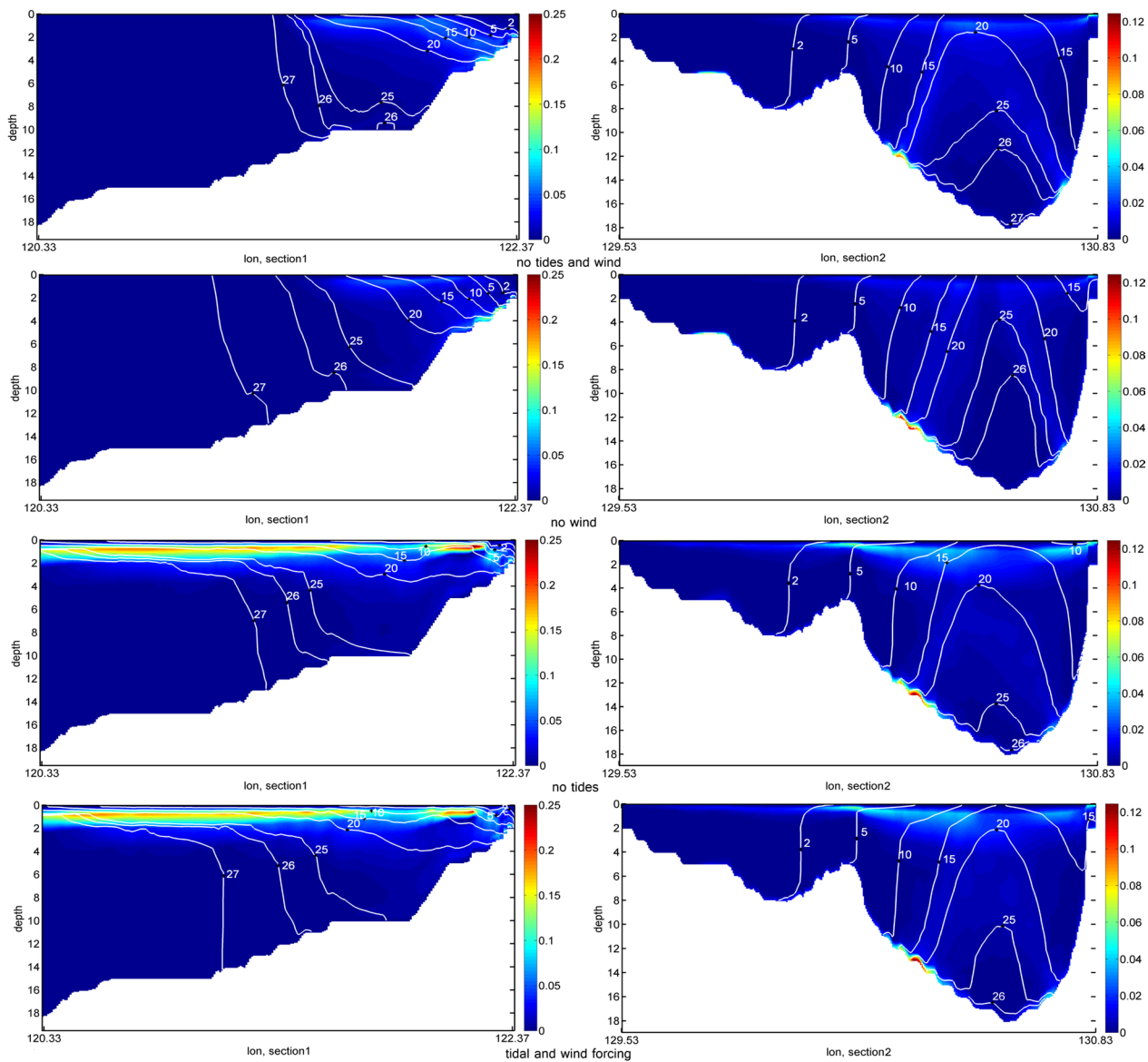
Fig. 4. The Brunt–Väisälä frequency (colours) and isohaline lines (white) in sections 1 (left) and 2 (right) by the end of May, 2008. From top to bottom: no forcing (only freshwater plume internal dynamics); only tidal forcing; only COSMO atmospheric forcing (polynyas are closed); full wind and tidal forcing.

In section 2, as expected, the effects were similar, but much less expressed. Tides increased mixing, but their action was only noticeable in the central part of the section, and the position of the freshwater front on the left did not change. Adding winds created a lens of fresher water at the surface, yet it was weaker, because of the lack of appropriately directed winds in May, 2008. Tides only slightly changed it, which is understandable, because they are only strong east of the Delta where the plume remains fresh over its full depth even in the absence of tides. Thus, patterns in section 2 remain qualitatively similar and are dominated by the dynamics driven by the density

71

contrast between the freshwater plume and the ambient water and accompanying entrainment. This is true for the entire area east of the Lena Delta, where the salinity (and temperature, not shown) patterns are largely insensitive to the detail of atmospheric forcing. This insensitivity is also confirmed by observations (Dmitrenko et al., 2010a). The presence of tides in that zone affects plume spreading to some extent by augmenting its mixing with ambient water (Fig. 4, right column). This behaviour is explained by the mere strength of the runoff in the eastern zone of the Lena Delta, which leads to high velocities in the region. The Trofimovskaya duct (dumps on the average 65% of river water), located north of Bykovskaya (dumps on the average 22% of river water) in the eastern part of the Lena Delta (Fig. 1), has a pronounced southern direction due to the action of the Coriolis force and entrains the freshwater from the Bykovskaya duct. In our case, we see this dynamics even in the short-term runs, because the maximum daily flow in 2008 occurred in late May. For this reason, the largest part of the freshwater plume stays in the eastern part of the domain with any type of atmospheric circulation.

In contrast, the plume propagation in the western and northern parts of the Lena Delta region in the absence of wind is very limited (Fig. 4, left panels). In the western part of the Delta the plume stays close to the coastline and is partly mixed by tides. In the northern part of the Delta the alongshore plume propagation to the east is partly supported by the residual circulation, which is about 1 cm/s for the summary tide. The pattern of residual circulation for summary tide resembles that for M_2 tide presented in Fofonova et al. (2014), with only a slight increase in some places.

The residual circulation of the summary tide is less than $0.8\ cm\ s^{-1}$ in the eastern part of domain, where most of freshwater plume is directed (see Fig. 1). Since typical velocities associated with the baroclinic plume dynamics are about $8\ cm\ s^{-1}$ there, we concluded that the main mechanism of tidal influence in the freshwater plume zone was through tidally induced mixing. By diagnosing the vertical diffusivity coefficient in simulations with and without tides, we concluded that tides increased it up to $0.001\ m^2 s^{-1}$ in areas characterized by a high vertical shear due to tidal velocities. The map of the shear due to M_2 tide was obtained from barotropic simulations and is shown in Figure 5. It is mostly the immediate vicinity of the Delta that is affected by tidal mixing.
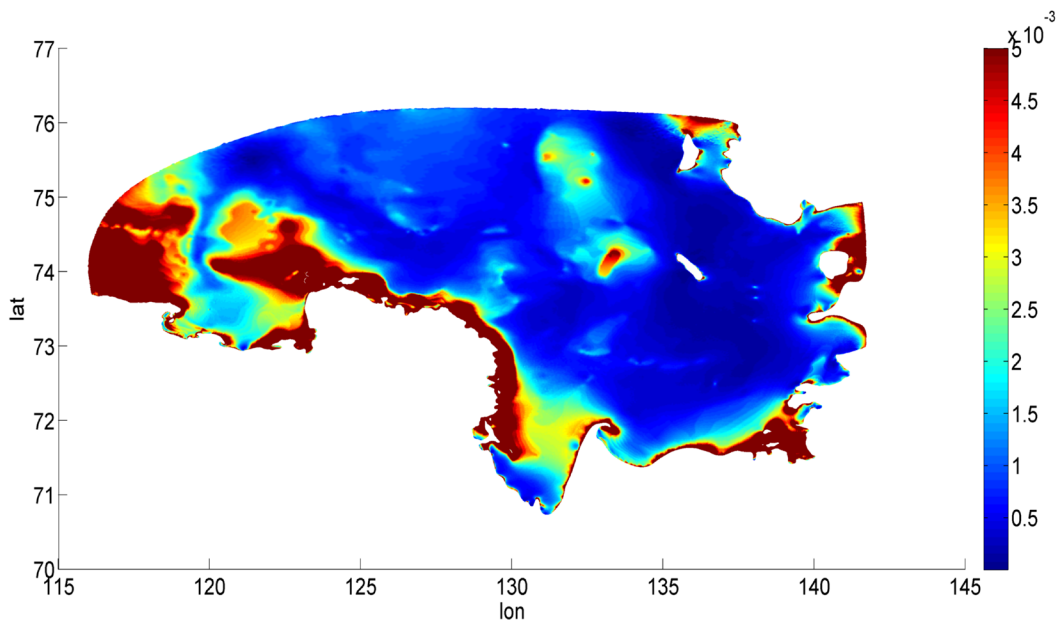
Fig. 5. The mean vertical shear induced by M_2 wave at the moment of maximum kinetic energy, [1/s].

7.4.4. Long-term plume simulations

We remind that the long-term simulations cover the period from the beginning of May to the end of September, 2008. They are driven by the ECMWF atmospheric forcing and additional freshwater forcing which accounts for ice melting. For this certain time period observational data are available, and our goal here is to compare model results against observations. We will use the moorings Khatanga and Anabar (Fig. 1) to compare the simulated near bottom temperature and salinity for the whole considered period from May to September, 2008. The velocity data from these moorings had been used to verify the barotropic version of the model (Fofonova et al., 2014). The conductivity-temperature-depth (CTD) observations over the eastern Laptev Sea shelf in September, 2008 from RV Ivan Kireev (September, 2008, expedition TRANSDRIFTXIV) will be used for the detection of plume propagation extent by the end of September and for the comparison of observed temperature and salinity profiles with simulated results.

7.4.4.1. Temperature and salinity at mooring locations

Figure 6 displays the simulated and observed near-bottom temperature and salinity at Khatanga and Anabar moorings for the duration of simulations. The moorings are located in the deep part of the domain, where large variations at the bottom are not expected. The observations and simulations

agree well in general, the simulated salinity repeats the dynamics of observed salinity during the whole summer season.
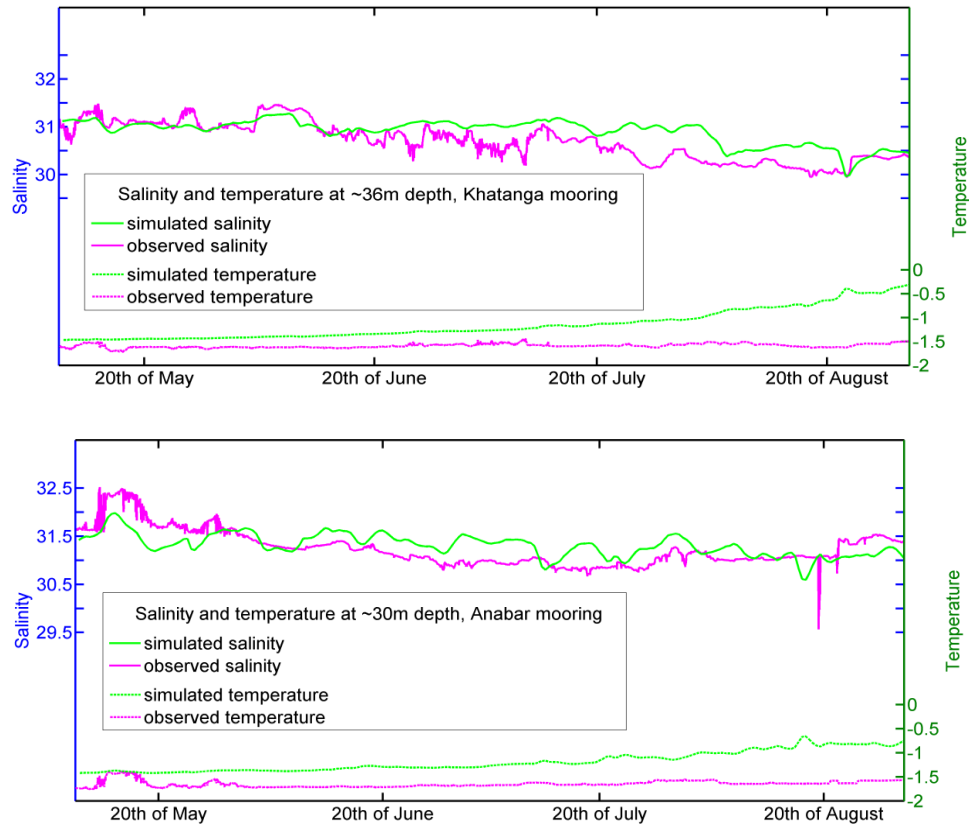
Fig. 6. The observed and simulated near-bottom temperature, [°C], and salinity, in practical scale, at Khatanga and Anabar mooring positions.

However, the bottom temperature gradually increases in simulations at both stations, which disagree with observations showing the lack of such a trend over the season. Taking into account the good agreement of salinity values, one may guess that the reason should not be linked to the model ability in simulating the plume dynamics. Since by the end of September the surface freshwater signal reaches the mooring locations (see below), one expects stable stratification in the upper layer, which should block the penetration of the temperature signal from the surface. The cause of this drift will be addressed in a future work.

7.4.4.2. Plume propagation

Although we have mentioned earlier that the plume characteristics east of the Delta do not show strong sensitivity to forcing, over a wider area and on a longer time period surface salinity may vary in wide limits during the season owing largely to variable winds. According to the
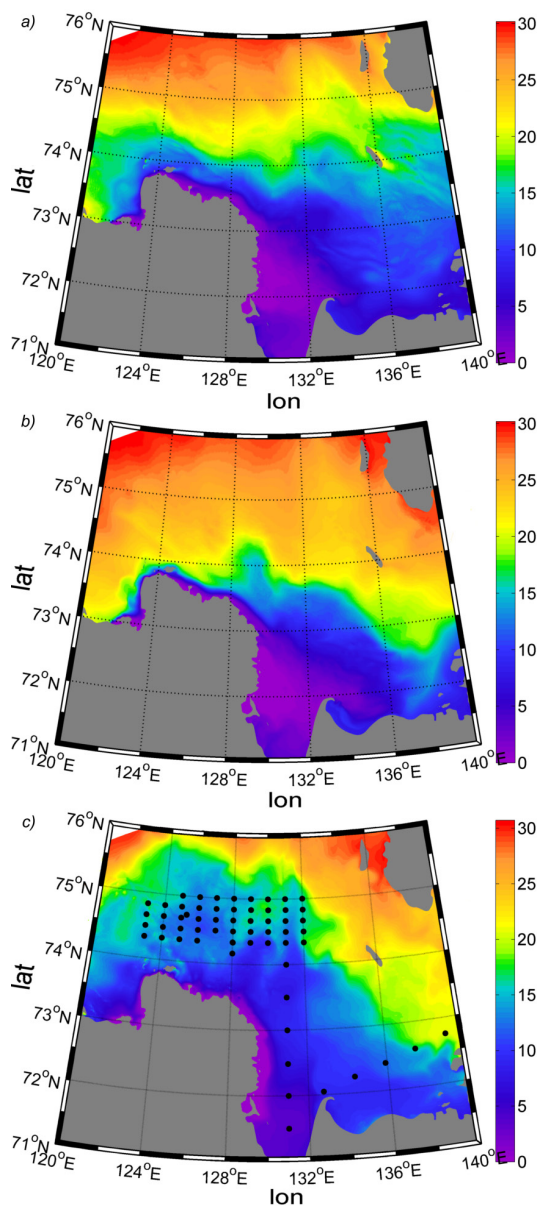
Fig. 7. Simulated surface salinity, in practical scale, driven by ECMWF atmospheric forcing on 22d of July (a), 26th of August (b) and 19th of September (c). The black dots in panels c) indicate the positions of CTD measurements available to us. The pattern in (c) has to be compared with the map of observed surface salinity obtained in Dmitrenko et al. (2010a).

ECMWF data, June and the beginning of July were dominated by the southward and south-eastward winds, July was dominated by westward winds changing at the end of July to strong eastward winds. From the end of August till the middle of September the prevailing circulation was anticyclonic, triggering the offshore propagation from the western and central parts of the Delta. Figure 7 demonstrates three snapshots of the Lena River freshwater plume extent during the summer season (June-September) with ECMWF forcing.

We note that in the eastern part of the domain northward winds were weaker and less frequent than southward winds in June and August. This explains the difference in Figures 7a (22 July) and 7b (26 August), showing much more confined salinity distribution over the eastern part of the domain by the end of August. Generally, eastward alongshore winds strengthen the freshening and warming effect over the shelf east of the Lena Delta. It leads to the appearance of larger temperature and salinity anomalies compared to the climatological mean. In September strong northward winds were present (Fig. 7c), modifying surface salinity distribution most significantly over the central part of the domain. Once again, we reiterate that knowledge of winds is a prerequisite to the seamless modelling of plume dynamics, and that it is only the area that is rather close to the Delta that shows the least temporal variability.

Figure 8 presents a more detailed comparison of the simulated temperature and salinity patterns against CTD observations in September, 2008. Its left and right panels show the observed and simulated temperature (bottom) and salinity (top), respectively. The locations of CTD stations are shown by black dots in Figure 7c. We see that the model manages to capture the northward plume

propagation and demonstrates rather encouraging agreement with the observations. However, there is difference in detail. First, the model does not fully explain the layer with nearly 10 meters thickness with salinity as low as 10 in the observational data. The most probable reason for overestimated salinity is excessively strong winds of ECMWF forcing, which causes strong mixing in the shallow zone. In our simulations we obtained a nearly homogeneous water column in the south-east part of the domain in September, which is especially well pronounced in the temperature profiles (Fig. 8, right panel). Observations, in contrast, show much thinner mixed layer, and bottom temperatures remain low. Over the deeper part (where most of CTD profiles are available), the model simulates a too deep surface mixed layer too, as is seen from the temperature profiles. It also simulates warmer bottom layers, consistent with what we have seen in Figure 6. This hints that an additional reason for the discrepancy can be too high vertical mixing in the model on its own, which would explain the warming. Note also that due to rare northward wind events in June-August in the forcing driving the model, the propagation of freshwater signal offshore is rather limited (Fig. 7a,b), in order that the surface layer with high stability over the deep part of the domain is absent for the most of the simulation time.

Despite the discrepancies we concluded that the model can be used for simulating the circulation in the domain of interest, especially if one takes into account by far insufficient data to better constrain the forcing fields. We also note that there are many other sources of possible errors, such as, for example, estimated meltwater signal and its spatial details or initial conditions.
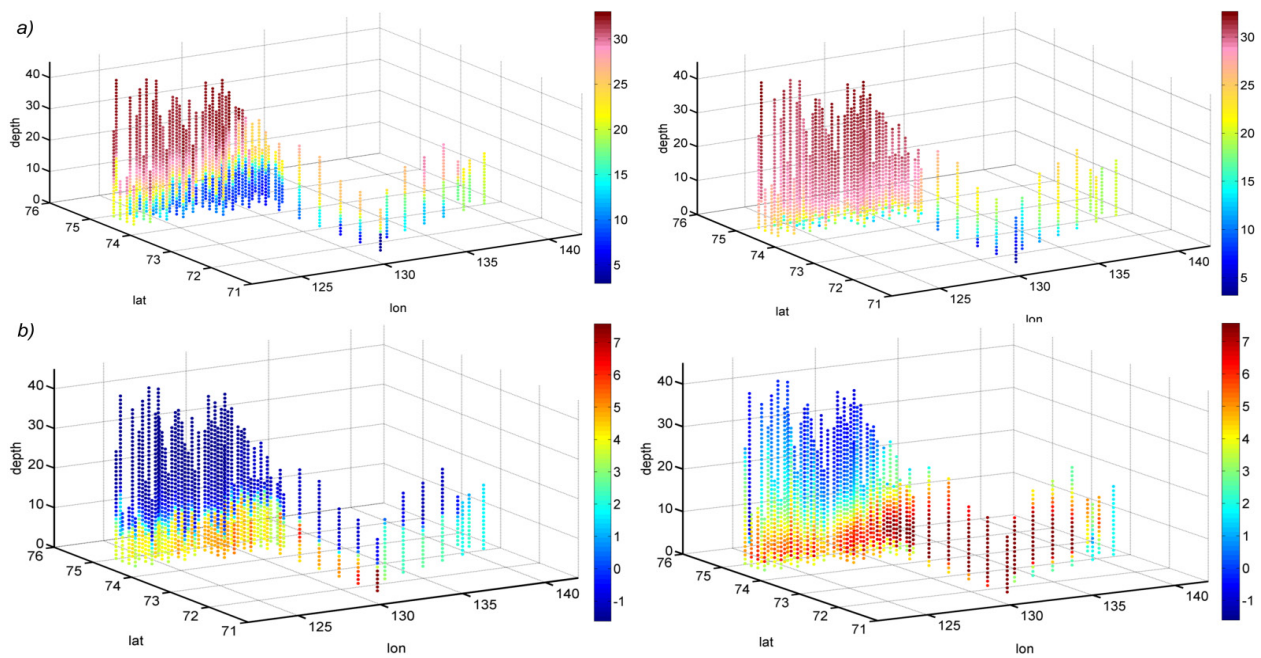
Fig. 8. The simulated (right panels) versus observed (left panels) temperature, [°C], and salinity, in practical scale, for September, 2008: a) salinity profiles; b) temperature profiles.

7.5. Discussion

The Lena runoff water temperature used here might be slightly higher than it is in reality. We used observational temperatures from the Kusur basin outlet station situated 200 km to the south from the Lena Delta head area. However, our additional simulations showed that the change in the heat fluxes (COSMO forcing with and without open polynyas) and in runoff temperatures does not significantly influence the propagation of the freshwater plume, but influences the horizontal temperature pattern, which penetrates the whole mixing layer. These results are in agreement with Ebner et al. (2011) and Hölemann et al. (2011).

Due to weak winds in the region in the summer period, the details of the Lena runoff distribution over the Delta channels influence the simulated salinity patterns. That is why we tried to follow observations and local bottom topography in prescribing this distribution. We stress the necessity of including the runoff from the northern and western parts of the Lena Delta. Attributing the runoff to only the strongest freshwater channels in the eastern part of the Lena Delta mouth would lead to significant errors in salinity and temperature patterns to the end of summer close to the northern and western parts of the Lena Delta, especially when circulation is anticyclonic. Note that plume spreading, accompanied by weak summer winds, creates strong surface stratification and influences vertical mixing. This also means that the simulations results are very sensitive to the vertical mixing setting, and additional work is required to study possible accompanying effects.

One of the important questions is the impact of initial conditions. One of the reasons for choosing the summer 2008 as a modeling period was the availability of initial conditions for temperature and salinity fields which have reasonable agreement with available observations. The shelf waters below the pycnocline in the southern Laptev Sea inner shelf preserve for at least one seasonal cycle from summer to late winter/spring season of the following year (Bauch et al., 2009; Dmitrenko et al., 2010a). At the end of the winter season (March-April) the surface hydrography pattern is nearly the same as in September, modified by ice formation. The ice formation and small Lena River freshwater impact provide at the end of the winter season surface salinity increase of ~5 (Dmitrenko et al., 2010a). In the NAOSIM model, used by us to initialize the simulations, the total freshwater input from the Lena River enters the ocean through the eastern part of the Delta, where two of the most powerful freshwater channels are situated (Fig. 1). For our purposes it means that the NAOSIM results can be successfully used if eastward winds dominated in the previous summer. In summer 2007, cyclonic patterns of atmospheric circulation were prevailing over the Laptev Sea

with an on-shore wind component. Accordingly, the NAOSIM resulting temperature and salinity patterns for spring 2008 have a quite good agreement with observations (Dmitrenko et al., 2010a). However, the weak initial stratification can be also one of the reasons of too mixed water column in our simulations.

7.6. Conclusions

In this article, based on simulations performed with FVCOM on a fine-resolution mesh covering the shelf part of the Laptev Sea, we studied how the Lena River freshwater plume propagation was affected by atmospheric forcing and tides for the warm season of 2008. We used atmospheric forcing provided by local high-resolution model (COSMO) and the regional (ECMWF) and global (NCEP) products. In a series of short-term simulations and long-term simulation we demonstrated that east of the Lena Delta neither the existing winds nor tides define the simulated pattern, which is largely governed by its internal dynamics linked to the freshwater discharge. Also, for this reason, the largest part of the Lena freshwater plume stays in the eastern part of the domain with any type of atmospheric circulation. In general, the pronounced cyclonic atmospheric circulation in late spring/summer season, characterized by eastward wind domination, strengthens the freshening effect over the shelf east of the Lena Delta. The details of offshore plume propagation depend on prevailing winds, and in short runs are most obviously west of the Delta. Tides are important in providing mixing but less so in determining the pattern of horizontal distribution east of the Lena Delta, where the bulk of the freshwater plume is detected every summer. The residual circulation associated with tides contributes to the eastward plume propagation along the northern part of the Delta. It is rather small east of the Lena Delta, compared to the typical plume velocities.

The fact that the largest part of plume remains east of the Lena Delta does not exclude variability. Our long-term (May-September) simulations confirmed that the atmospheric forcing (winds) largely defines the Lena freshwater plume excursions into the Laptev Sea. While in the middle of the summer season in 2008 the plume spreading pattern was similar to the one observed in 2007, at the end of August and September the plume propagation to the north due to northward winds according to simulations and observational data. For the period from May to September, 2008 we simulated the patterns that are largely in agreement with the observations. However, we only partly reproduced the observed pool of low salinity water in the central Laptev Sea. It is most probably linked to the too strong winds provided by ECMWF forcing and model vertical mixing

parameterization, to a lesser extent to the lack of northward winds in the product and errors in the freshwater contribution due to ice melting.

To conclude, this study demonstrates that it is feasible to simulate the Lena River plume dynamics, but stresses that the knowledge of true winds is a prerequisite of simulating the plume excursions into the Laptev Sea. There are several directions the model should to be augmented both to provide more realism and to allow for longer simulations. First and foremost, it needs to be coupled with a sea ice model and should take into account the fast ice, which effectively modifies the coastline at the beginning of May. Vertical mixing parameterization requires a special focus too. It will be addressed in a future work.

8. The stream temperature characteristics of the Lena River at basin outlet in the summer period (Manuscript 4)

V. Fofonova[1*], M. Kraineva[2], D. Yakshina[2], N. Tananaev[3], N. Volkova[4], K.H. Wiltshire[1]

[1]Alfred Wegener Institute, Helmholtz Centre for Polar and Marine Research; Kurpromenade, D-27498 Helgoland, Germany;
[2]Institut of Computational Mathematics and Mathematical Geophysics, Siberian Branch of the Russian Academy of Sciences (SBRAS); Lavrentiev avenue 6, 630090 Novosibirsk, Russia;
[3]Igarka Geocryology Laboratory, Permafrost Institute, SBRAS; I microrajon 8a, 663200 Igarka, Russia;
[4]State Hydrological Institute; II Linia 23, 199053 St. Petersburg, Russia;

Abstract

The stream temperature characteristics of the Lena River at basin outlet during the summer season (June–September) are considered. The analysis is based on a long-term data series covering the period from the beginning of observation (1936) to the present time at Kusur station and complementary data at several stations downstream and one station upstream. These additional data are rarely used, but their analysis is critical for understanding processes in the basin outlet area. A surface water temperature anomaly is found to exist between Kusur station and the beginning of the Bykovskaya Channel (delta head zone) during open water season from July to September; the differences between the stream surface temperatures at Kusur station and 200 km downstream to the north have almost always been negative for the considered period since the beginning of observation. The description of this anomaly and its basic analysis are presented. To sort the problem out, we consider the observational data in terms of the hydrology and morphology of the Lena River Delta and main channel area, including data on permafrost conditions under the river channel. The ability of water temperature observational data to represent the mean stream temperature is discussed. The measurements at Kusur station fail to do this. Rather, they reflect thermal conditions of the Lena River in general. Recent stream temperature estimates for the Lena basin outlet area are also given.

Keywords

8.1. Introduction

The Lena River is one of the largest rivers in the Arctic and has the largest delta. Permafrost underlies 78–93% of the watershed, with continuous permafrost extending south to 50°N (Zhang et al., 1999). Observational data available for the Lena River suggest an on-going change in climate and biological factors over the last 50 years (e.g. Kraberg et al., 2013; McClelland et al., 2006; Yang et al., 2002). Costard et al. 2007 found that the Lena water temperature in the flood period had increased at Tabaga station by up to 2°C, as compared to the values in 1950, and that this increase had contributed to coastal erosion and modified the chemical water composition. Most biological communities and species are very sensitive to changes in water temperature and water chemistry (Conlan et al. 2005; Kraberg et al., 2013). Restructuring of an ecosystem may follow such changes. Water mass characteristics at the Lena River basin outlet are particularly important for dynamics of the Laptev Sea and the Arctic Ocean as a whole (e.g. Dmitrenko et al., 2008; Morison et al., 2012; Yang et al., 2005). The Lena River Delta has a large number of freshwater channels, the three largest of which empty into the Laptev Sea on average 65%, 22% and 5% (Trofimovskaya, Bykovskaya and Olenekskaya channels respectively) of the total river discharge (Magritskiy, 2001) (Fig. 1); the mean annual runoff volume of the river from 1935 to 2012 was about 539 km^3 (http://www.r-arcticnet.sr.unh.edu). However, given the large territory of the Lena River basin and its outlet area in particular, direct measurements pertaining to the river are still insufficient. The high complexity of the region adds to the problem. As a result, the existing analyses of stream temperature and other discharge characteristics at the basin outlet are fragmentary and cannot provide the full picture of the dynamics in the region.

The goal of this paper is to analyse the available data on the water temperature of the Lena River at the basin outlet in the summer period (June–September). The analysis is based on long-term data series at Kusur station from the beginning of observations to 2011, and additionally at several downstream stations and one upstream station (see Section 1.2.1 for details). These additional data are rarely used, but their analysis is critical for understanding the complexity of processes in the region. The analysis reveals the existence of a surface water temperature anomaly between the Kusur gauging station (GS) and the beginning of the Bykovskaya channel during the open water season (from July to September) (Fig. 1). The description of this anomaly and factors that may be responsible for it is a particular focus of this paper. To sort the problem out, we consider the observational data in terms of the hydrology and morphology of the Lena River delta and main channel area, including data on permafrost conditions under the river channel.
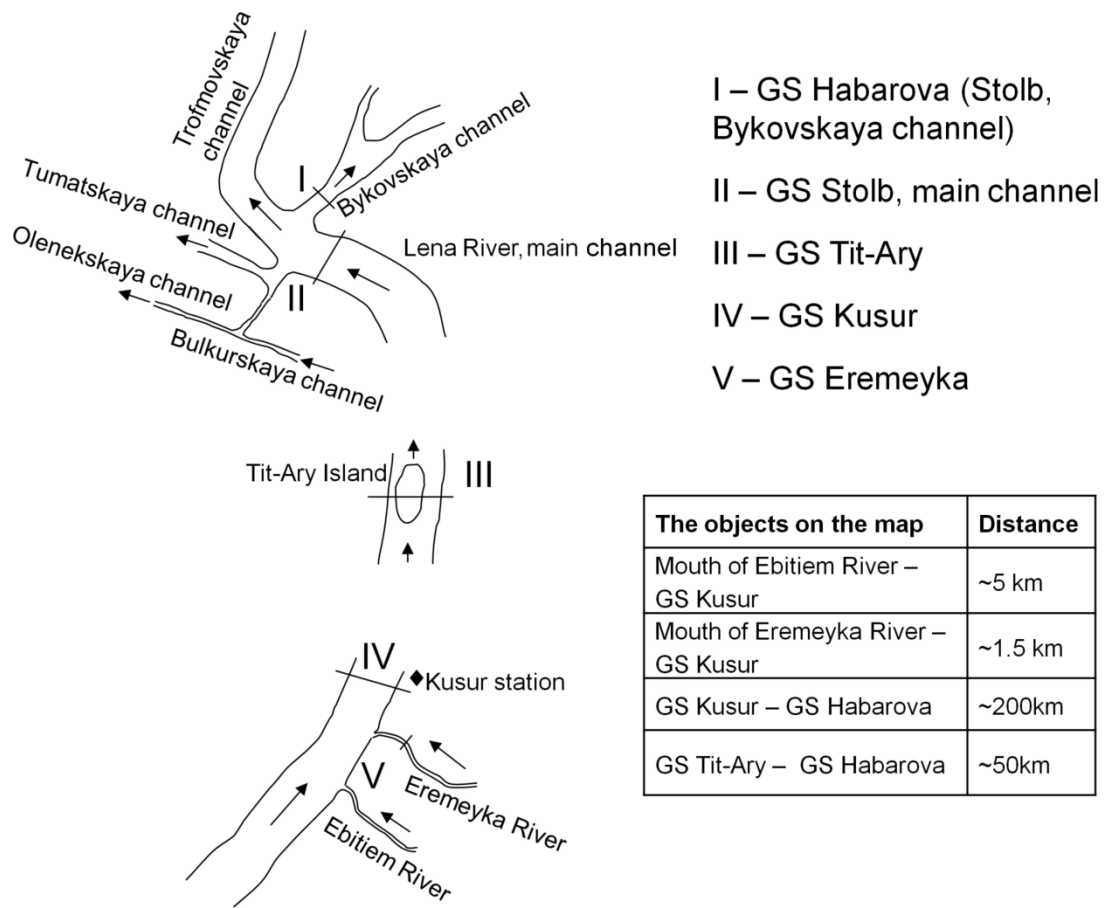
Fig. 1. The scheme of gauging station locations.

In recent literature, the data on the Lena discharge and water temperatures at the Lena Basin outlet are, as a rule, taken at Kusur station (e.g. Costard et al., 2007; Liu et al., 2005; Peterson et al., 2002; Yang et al., 2002; Yang et al., 2005), situated ~200 km to the south of the delta head (Fig. 1). In this paper, we discuss to what extent the water temperature observations at this station represent the mean stream temperature. We show that the water temperatures measured at Kusur station fail to represent the mean but do reflect the thermal conditions of the Lena River in general.

The paper is organized as follows. Section 1 presents a description of the data set used in this work, the hydrological stations and measurement techniques. The description of the surface temperature anomaly and analysis of data are presented in Section 2, and, in Section 3, we provide discussion.

8.2. Description of hydrological stations, measurement techniques and available data set

In this section we list the data available and used and the measurement techniques. We also describe the GS where these data have been collected.

8.2.1. Measurement techniques and available data

Since the late 1930s, relevant data from hydrological observations in the Siberian region, such as discharge, water temperature, ice thickness, dates of ice events (ice cover formation and decay), are controlled and stored by the Russian Hydrometeorological Service. They are available in hydrological yearbooks in local centres of hydrometeorology and environmental monitoring and are partly available on the web (http://www.r-arcticnet.sr.unh.edu). Table 1 lists the data available from the Russian Hydrometeorological Service used in this study. We also use CTD (Conductivity, Temperature, and Depth) data on water temperature profiles for several days in August 2011 at the cross-section of Habarova GS (Stolb, Bykovskaya channel) and Stolb main channel, located 4.5 km upstream from Stolb Island. These data were collected during the Lena cruise of 2011 which was a Russian-German venture.

Table 1. The available data used in this work.

Station	Data type	Time resolution	Observation period
Kusur	Surface water temperature	daily	2002-2011
		10 days	1936-2011
	Surface air temperature	daily	2002-2011
	Date of maximum daily water temperature within the year		1936-2011
	First ice appearance date in fall		1986-1999, 2000-2007
Habarova	Surface water temperature	daily	2002-2011
		10 days	1951-2011
	Surface air temperature	daily	2002-2011
	Date of maximum daily water temperature within the year		1951-2011
	First ice appearance date in fall		1986-1999, 2000-2007
Eremeyka	Surface water temperature	daily	2002-2011
		10 days	1974-2011
	Surface air temperature	daily	2002-2011
Tit-Ary	Surface water temperature	monthly	1981-1990

The Russian Hydrometeorological Service carries out measurements of water and air temperatures two times per day, at 8 a.m. and 8 p.m. Until 1993 in the USSR, the stream temperatures were measured at regional hydrologic stations on a 10-day basis (the 10th, 20th, and 30th days of each month) and were taken twice, at 8 a.m. and 8 p.m., on each observation day (State Hydrologic Institute, 1961). Measurements of the surface water temperatures covered from the end of spring, when the water temperature is close to zero, to the fall, a few days after the freezing of the water surface. The observations were made for flowing water; a cup with a thermometer was placed approximately 0.5m below the water surface for five to eight minutes and retrieved carefully for a quick recording of temperature.

8.2.2. Description of gauging stations

In this section we briefly describe the GSs referred to in this work (Fig. 1).

8.2.2.1. Kusur (70.70ºN/127.65ºE)

Kusur GS is located near Kusur Village at the site of the station carrying the same name (Fig. 1). The width of the River here is 2.4 km on average for the summer season. The catchment area is about 2.43 million km^2. The distance from the headland is 4,083 km. Measurements of stream surface temperatures are performed at the right bank of the Lena River. The transverse profile of the riverbed in the area of Kusur GS is shown in Fig. 2. Kusur GS has been operating since 1936 (Hydrological Yearbooks; http://www.r-arcticnet.sr.unh.edu).
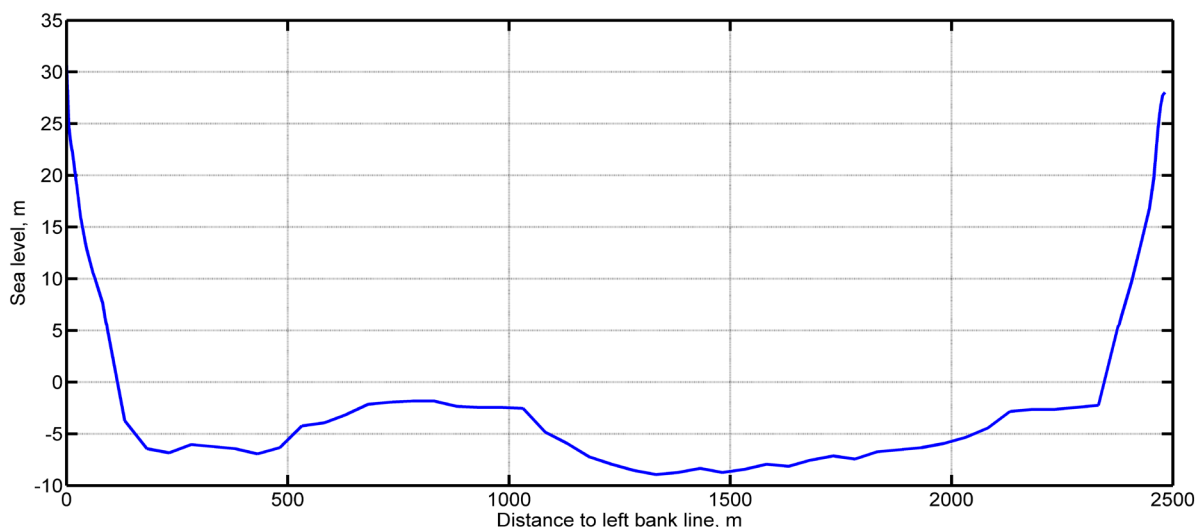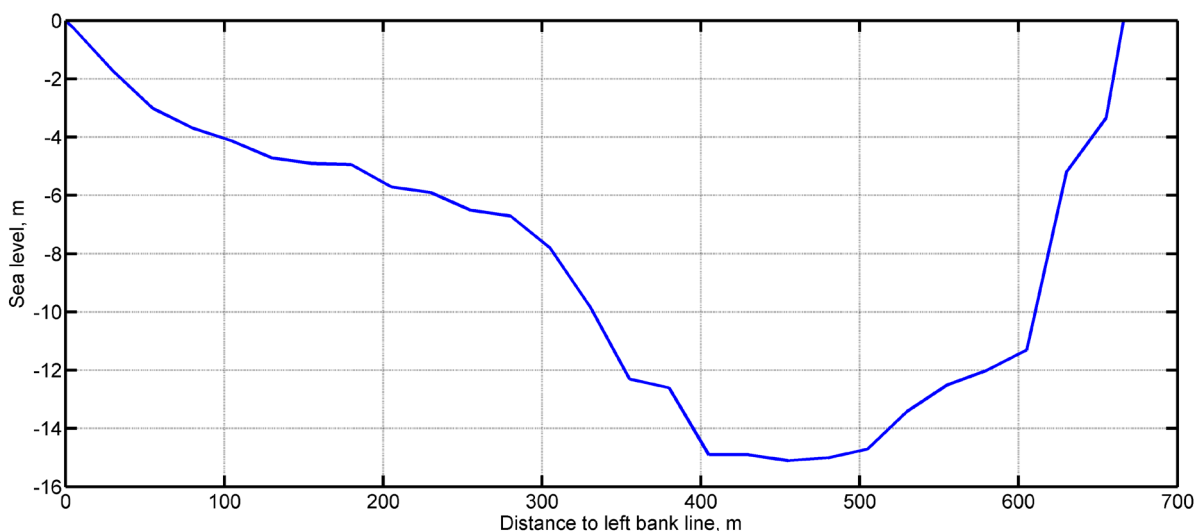
Fig. 2. The transverse profile of the riverbed in the area of GS Kusur based on observations in 2012, first decade of June, [m].

8.2.2.2. Habarova (Stolb, Bykovskaya Channel, 72.42ºN/126.72ºE)

Habarova GS (Stolb, Bykovskaya channel) is situated in the area of the delta head at the beginning of the Bykovskaya channel (Fig. 1) on the territory of Stolb polar station, 7.7 km downstream from Stolb GS main channel. The width of the channel at the cross section of Habarova GS is up to 1.0 km. Measurements of stream surface temperatures are performed on the right channel bank. The transverse profile of the riverbed in the area of Habarova GS is shown in Fig. 3. Habarova GS has been operating since 1951 (Hydrological Yearbooks; http://www.r-arcticnet.sr.unh.edu).

Fig. 3. The transverse profile of the riverbed in the area of GS Habarova based on observations in 1991, last decade of November, [m].

8.2.2.3. Tit-Ary (71.99ºN/127.09ºE)

Tit-Ary GS is situated on the right side of Tit-Ary Island, which consists of alluvial deposits. The river channel, with a width of about 12 km, is divided into two branches by the island. The island is 20 km in length, 7 km in width and 30 m in height and is located 1.2 km from the fairway. The left branch is shallow. Water temperature is measured on the right side of the island. The Tit-Ary GS operated for 15 years from 1976 till 1990 (Hydrological Yearbooks; http://www.r-arcticnet.sr.unh.edu).

8.2.2.4. Eremeyka (70.41ºN/127.24ºE)

The Eremeyka River is a right inflow of the Lena River with a catchment area of 9.70 km^2. The station is located 2 km upstream from the mouth. Water temperature is measured at midstream. Eremeyka GS has been operating since 1974 (Hydrological Yearbooks; http://www.r-arcticnet.sr.unh.edu).

8.3. Stream temperature characteristics at the basin outlet

8.3.1. Surface water and air temperatures analysis

In this section, we focus on long term data for surface air and water temperatures at Kusur GS, which are usually taken as representative for whole basin outlet zone, and Habarova, situated in the delta head area, 200 km downstream from Kusur GS (Fig. 1).

The tendencies in surface water temperatures measured at Kusur GS and Habarova in the summer period (June–September) are different. The statistically significant trends exist only for August at Kusur GS (with a probability of 96%) and for June at Habarova GS (with a probability of 93%), indicating a temperature increase of 1.3°C for both stations since the beginning of observations (Fig. 4).
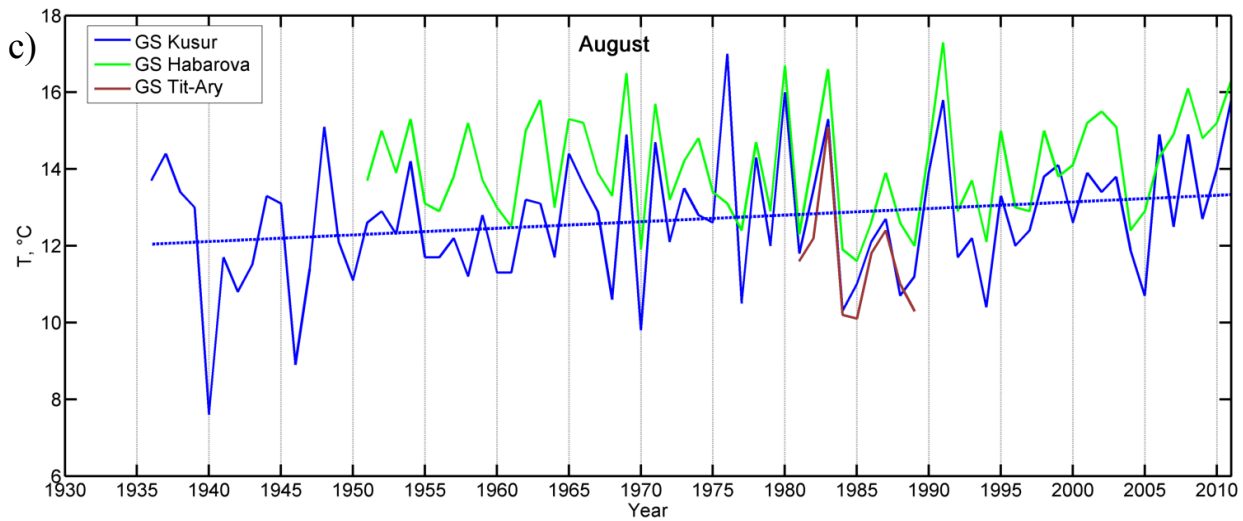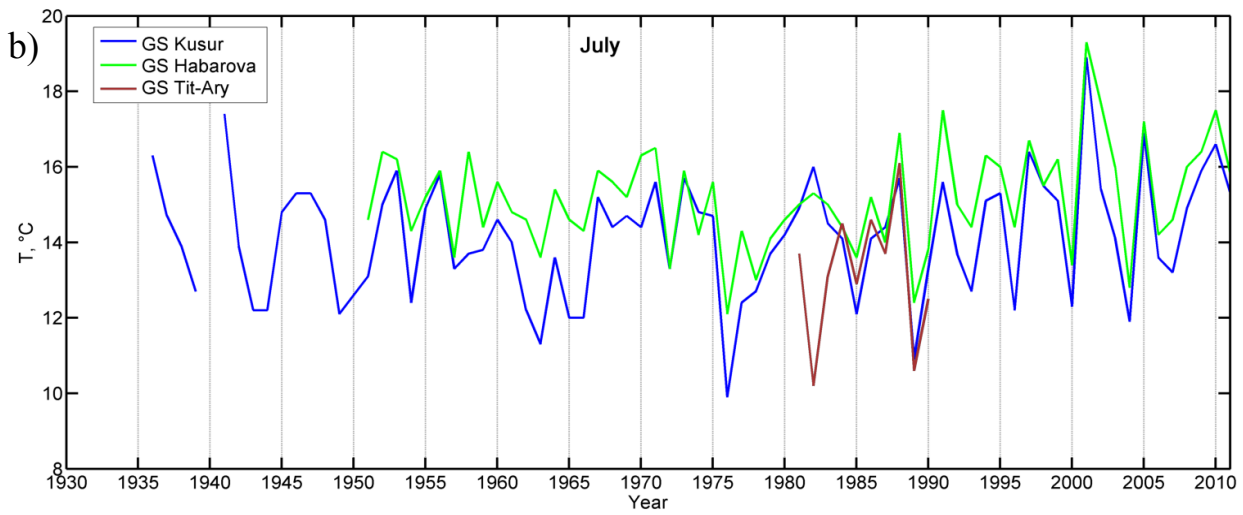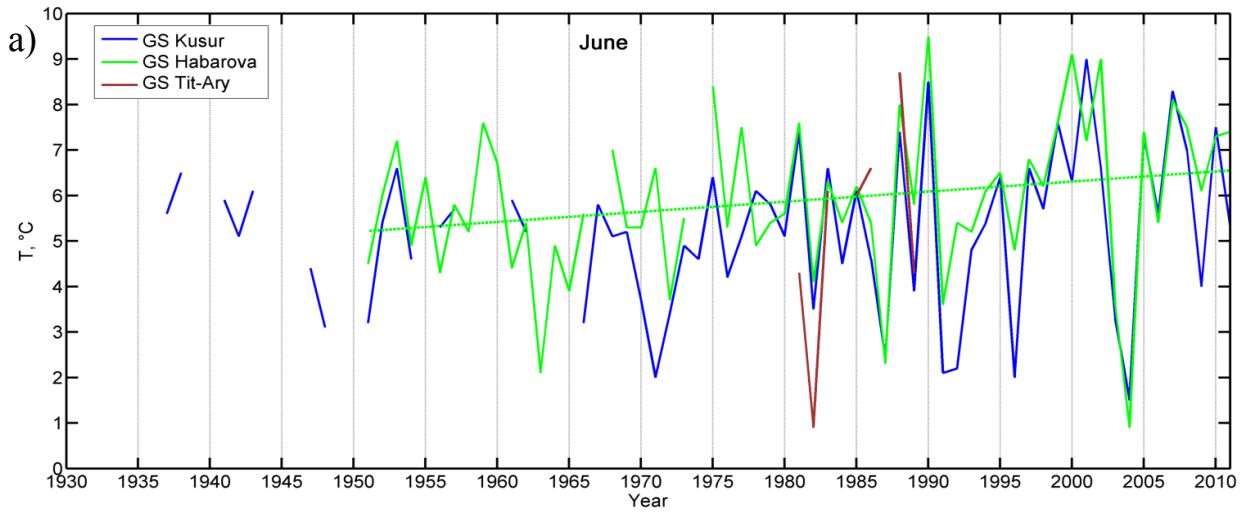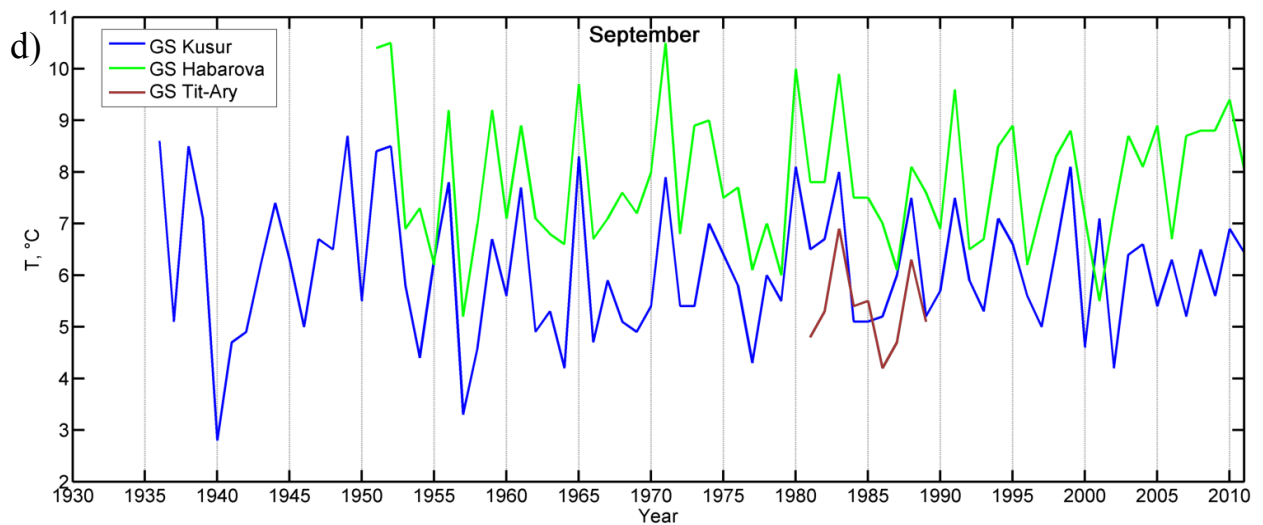
Fig. 4. The mean monthly surface water temperature measured at GS Kusur, Habarova and Tit-Ary from 1936 to 2011: a) June, b) July, c) August, d) September. The lines show the trends existing with more than 90% of probability.

Due to a high amplitude of mean stream temperature fluctuations from year to year, there is no guarantee that these trends are reliable. There are no trends for the mean August and September surface temperatures at Habarova GS or for the mean June and July surface temperatures at Kusur GS (Fig. 4). The mean summer stream temperatures at both stations do not have significant trends, but the regression lines have some slopes (Fig. 5).
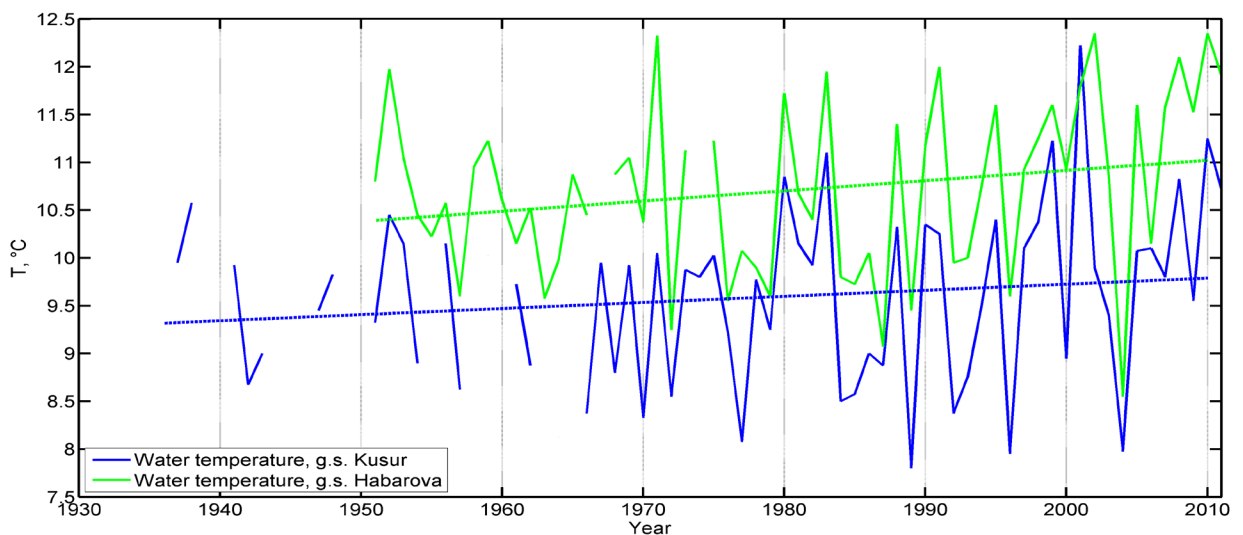
Fig. 5. The mean summer (June-September) water temperature at GS Kusur and Habarova. The regression lines are dashed. Their slopes are significantly different from 0 with 72.6% and 88.4% probabilities for GS Kusur and Habarova respectively.

The above estimates at Kusur station are consistent with the results in Yang et al. (2005). However, we would like to stress that the difference in the behaviour of stream temperatures at Habarova GS and Kusur (Figs. 4 and 5) indicates that measurements at Kusur GS cannot be directly taken for analysis of water temperature changes *in the mouth area.*

The fluctuations of mean *monthly* water temperatures in the surface layer usually follow the dynamics of mean air surface temperatures in the area closely (e.g. Johnson, 2003; Hammond and Pryce, 2007). This is confirmed by Fig. 6. It shows that the correlation between monthly air temperatures at Kusur GS and Habarova follows the correlation between monthly water temperatures, and monthly water and air temperatures have the same dynamics at these stations. We can observe some evident exceptions for water/air temperature correlation at Kusur GS for August and September (Fig. 6). However, this can be explained by air temperatures not shown by us upstream from Kusur GS. A strong association between monthly stream temperatures at Kusur GS and monthly air temperatures in the Lena River basin outlet area has been shown by Liu et al. (2005). For August and September, their results are statistically significant at the 99% confidence level. They have also shown that the correlations between stream temperature and precipitation are very weak and statistically insignificant.
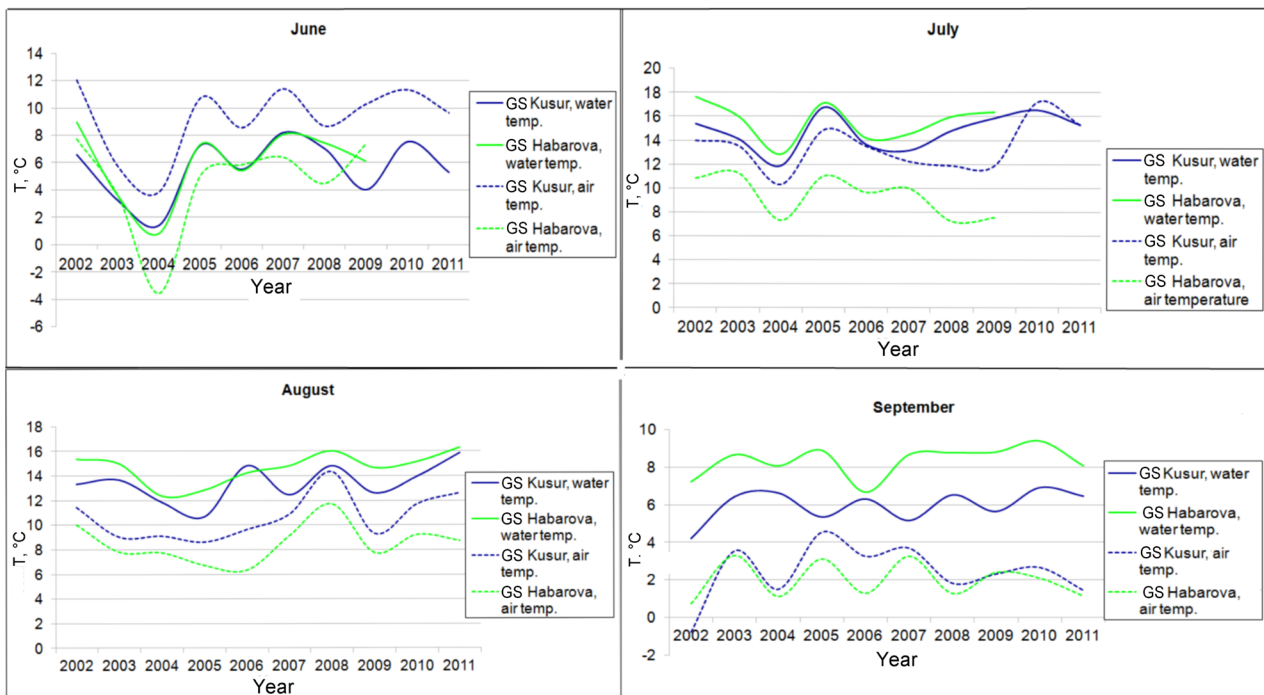

Fig. 6. The mean monthly surface air and water temperatures at GS Kusur and Habarova for the summer season for each year from 2002 to 2011.

89

For both Habarova GS and Kusur the mean monthly surface air temperature is below the water temperature for the period from July to September (Fig. 6). In summer season, the Lena River accumulates a large amount of heat upstream from Kusur GS, especially at the lower and middle reaches (Antonov, 1961). Figure 7 indicates that the skin water layer is much colder, by more than four degrees, than water at half-meter depth at Habarova GS and Stolb main channel (Fig. 1), despite the very high level of turbulent pulsations.
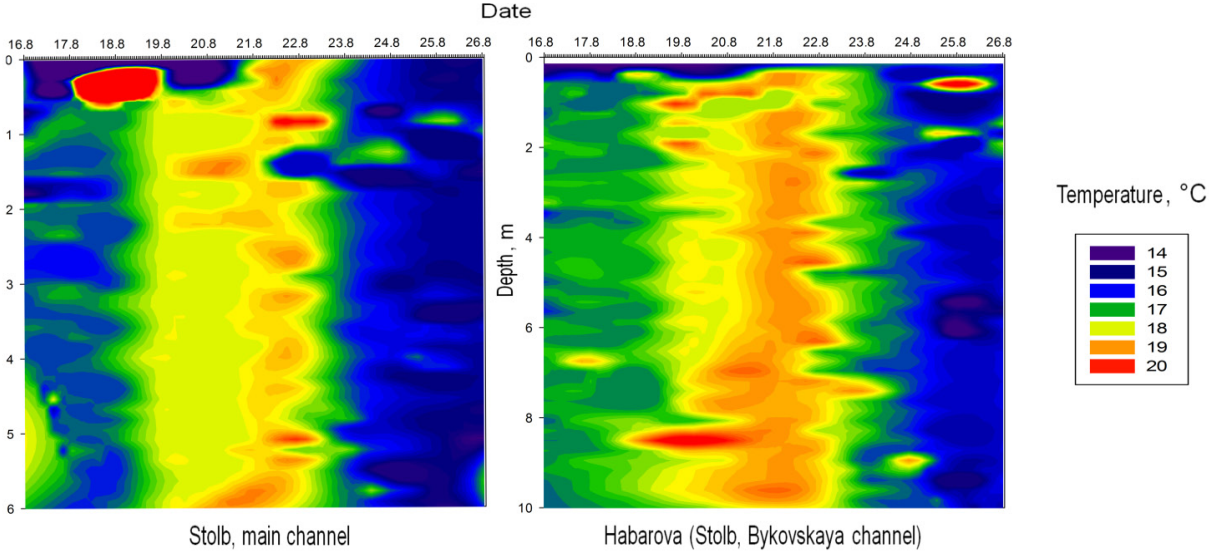
Daily mean air temperature in August, 2011													
Date / Station	16.8	17.8	18.8	19.8	20.8	21.8	22.8	23.8	24.8	25.8	26.8	16.8	17.8
Stolb, main channel	8	6.4	7.8	11.1	13.1	12.2	8.2	4.9	4.2	No data	No data	8	6.4
Habarova (Stolb, Bykovskaya)	8.1	6.5	6.2	7.8	13.5	11.9	7.5	4.9	3.6	3.5	4.8	8.1	6.5

Fig. 7. Stream temperature profiles and mean surface air temperatures on a corresponding date. The water temperature measurements were carried out at midstream, at 10.30 a.m., in the same time every day. The surface air temperature was measured twice per day, at 8 a.m. and 8 p.m., and then averaged. Depth is counted down from the free surface.

Exactly due to the highly turbulent character of the stream and its active cooling under the influence of the atmosphere, a strong correlation between fluctuations of mean water and surface air temperatures is observed.

Unfortunately, we do not have observations of mean monthly surface air temperatures in the region during the 20th century. This could help to analyse the reasons for the differences in the trends. The available air surface temperature data for the short period from 2002 to 2010 show the same tendencies for both stations, but they are not significant.

8.3.2. Surface temperature anomaly description and its analysis

Typically, the water temperature in the Lena River gradually decreases toward its mouth in the summer months due to the river's south-north orientation (e.g. Liu et al., 2005; Zotin, 1947). The presence of a deep valley and wide-open areas to the north and northwest, together with being surrounded to the south by the Lena-Vilui lowlands, facilitates unhindered entry of cold air masses from the north and west to the Taimyr Peninsula and the Laptev Sea (Burdikina, 1961). However, the surface water temperatures measured at Habarova GS for all years of observation are on average much higher for the summer season than at the main-stream Kusur station (Figs. 4, 5, 6 and 8) located much further upstream (Fig. 1). Figure 8 also clearly shows that the difference between water temperatures at Habarova GS and Kusur grows from June to September every year. In other words, the formation of the anomaly follows the decrease in temperature. Taking into account the behaviour of the amplitude of the anomaly (differences between water temperatures at Habarova GS and Kusur) during the period from June to September (Figs. 4, 5, 6 and 8), the amplitude of the anomaly does not have significant trends for the summer season from year to year. Below, we discuss the possible causes of this anomaly.
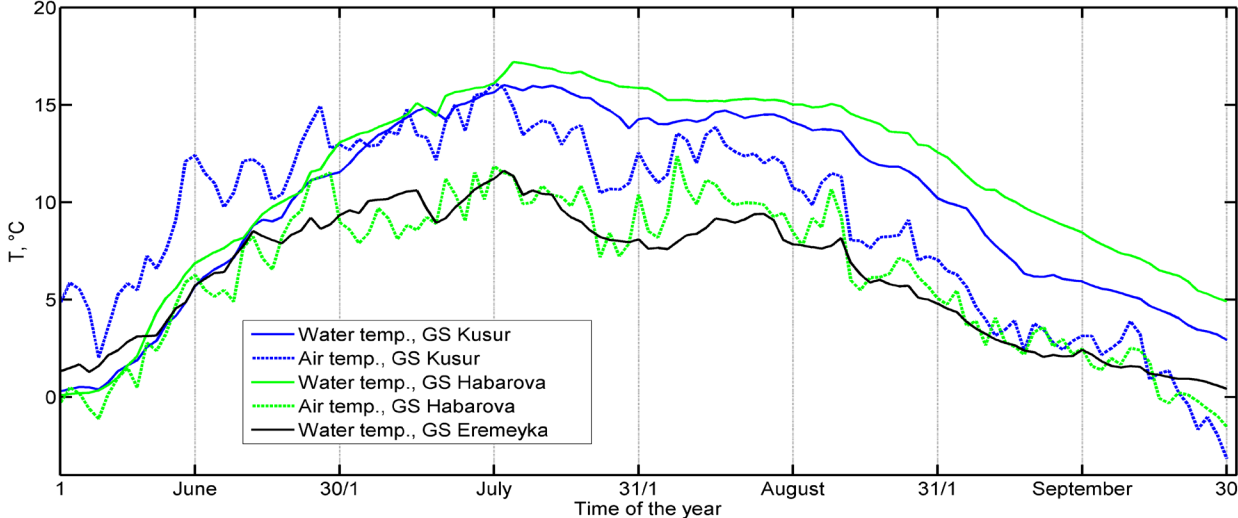

Fig. 8. The mean daily surface air (2m) and water temperatures measured at GS Kusur, Habarova and Eremeyka for the summer season (2002-2011). The mean surface air temperatures measured at GS Kusur and Eremeyka can be assumed equal based on observations.

91

a) The anthropogenic factor as a possible explanation should be discarded immediately given the very low population density in the region and the absence of industrial facilities and dams.

b) The difference in river-atmosphere heat exchange could be a possible explanation. However, surface air temperature naturally decreases when moving from south to north in the summer months. And yet, as indicated by Figs. 6 and 8, the air temperature for the whole area from Kusur GS to Habarova GS appears to be below the water temperature measured at Habarova GS for the period from July to September. One of the main factors, which determine the river water 'temperature level' is also heat accumulated by the river upstream. *Thus, the two important factors, the monthly surface air temperature and the heat accumulated upstream from Kusur GS, which should largely explain the mean monthly stream temperature values, fail to do so at Habarova GS.*

c) The possible reason for this puzzling disagreement could be the non-representativeness of measurements at one or both the stations. We should stress that water temperature measurements at both station are taken near the right riverbank. The stream temperature measured near the bank does not always correspond to the true mean stream temperature. This highly depends on local conditions like inflows with different temperatures upstream, the shallowness of the water layer or other coastal effects. On the other hand, for large rivers, vertical and lateral mixing is often very strong during a high discharge period (e.g., Sridhar et al., 2004) and is expected to homogenize the temperature distribution. However, several hydrological notes from the 1930s, 1950s and 1980s (http://www.r-arcticnet.sr.unh.edu) mention the possibility that surface water temperature measurements at Kusur GS lack representativeness. The differences between the weighted average and near coast stream temperatures ranged from 1 to 6 degrees and always remained positive. Based on observations in 1936, the mean ratio of these temperatures was found to be 1.2 for the warm season (June–September) (Reinberg, 1938; Zotin, 1947). Taking into account the technique of measurements and the river bed profile (Fig. 2), which shows a sharp increase in depth near the shore, we can assume that the main reason for non-representativeness is the influence of cold water from two small inflows, the Ebitiem (Ebetem) and Eremeyka Rivers. The mouths of these rivers are located approximately 5 km and 1.5 km upstream from Kusur GS respectively, (Balashov and Tamarskiy, 1938). The cold water from these rivers does not fully mix with the relatively warm water of the Lena River, probably due to the configuration of the current in the region. The central bar at Kusur GS (Fig. 2) and a chain of

small islands upstream divide the cross section of the Lena River into two branches (Reinberg, 1938). We should mention here that Fig. 2 shows the water level in the period of flood peak. The water level has a mean amplitude of about 17m during the summer period from June to September (http://www.r-arcticnet.sr.unh.edu) so that the central bar (Fig. 2) may influence the current after the flood peak at the end of May/June. The mean annual volumes of the Ebitiem and Eremeyka runoffs are 0.4 and 0.0034 km^3 respectively (these estimates are provided by centres of hydrometeorology and environmental monitoring in St. Petersburg and Tiksi). Therefore, the water from Ebitiem River dominates the cold current formation. However, due to highly turbulent flow at Kusur GS, the temperature vertical distribution is almost uniform for the entire cross section (Reinberg, 1938). In the whole area of interest there are no other inflows, which could affect the temperature measurements.

A cold right bank current may distort the trend estimates at Kusur GS. However, due to a strong correlation of mean monthly surface temperature measured at Kusur GS with mean monthly air temperature (Fig. 6), based on a 10 year period from 2002 to 2011, we can assume that measured water temperature in the surface layer at Kusur GS reflects the thermal condition of the Lena River in general but differs from the true average temperature of the entire flow.

According to the results of temperature surveys in 1979 and 1985 provided by the hydrometeorology and environmental monitoring centre in Tiksi, the temperature measurements at Habarova GS are representative. The absolute differences between surface temperatures near the bank and midstream did not exceed 0.2°C (Fig. 3). Also, because of highly turbulent flows at Habarova GS, the vertical distribution is nearly uniform for the entire cross section, except for the skin surface layer (Fig. 7).

Figures 9a and 9b show that the correlation coefficient between water temperatures measured at Habarova GS and Kusur is almost as high as the correlation coefficient between water temperatures measured at Eremeyka GS and Kusur. The dynamics of fluctuations of monthly mean surface water temperatures measured at Eremeyka GS, Kusur and Habarova are almost completely determined by the heat exchange with the atmosphere. However, we cannot say that the influence of the atmosphere and heat accumulated upstream determines the daily or even monthly average temperature values at Habarova GS, as we mentioned before (Fig. 6 and 8).
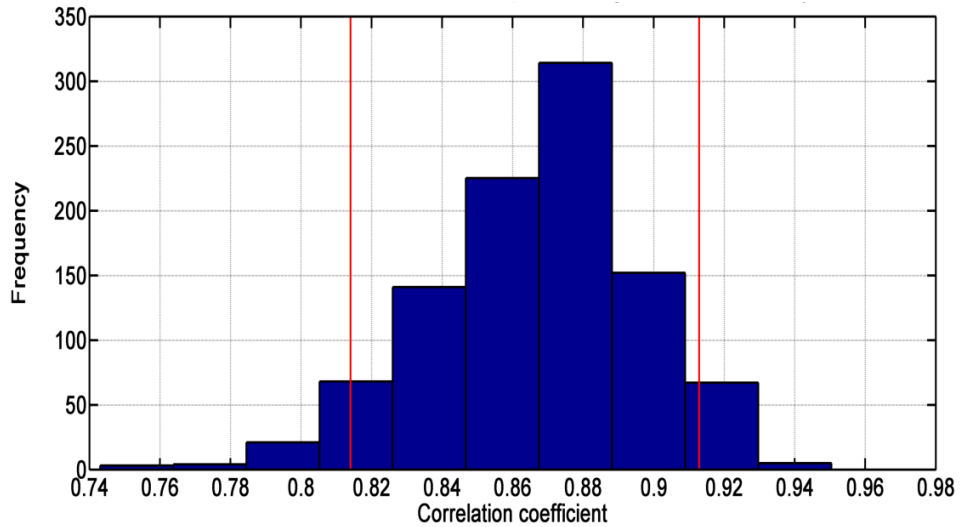
Fig. 9a. The correlation between mean monthly surface temperatures measured at GS Kusur and Eremeyka. The lines confine 95% confidence interval. Since the lower end of our confidence interval is above zero, we conclude that our correlation is significant at the $p<0.01$ level (two-tailed). The 148 data points (the data set contains monthly mean values for open water season from 1974 to 2010) are resampled to create 1000 different data sets, and the correlation between the two variables is computed for each data set. The histogram shows the variation of the correlation coefficient across all the bootstrap samples.
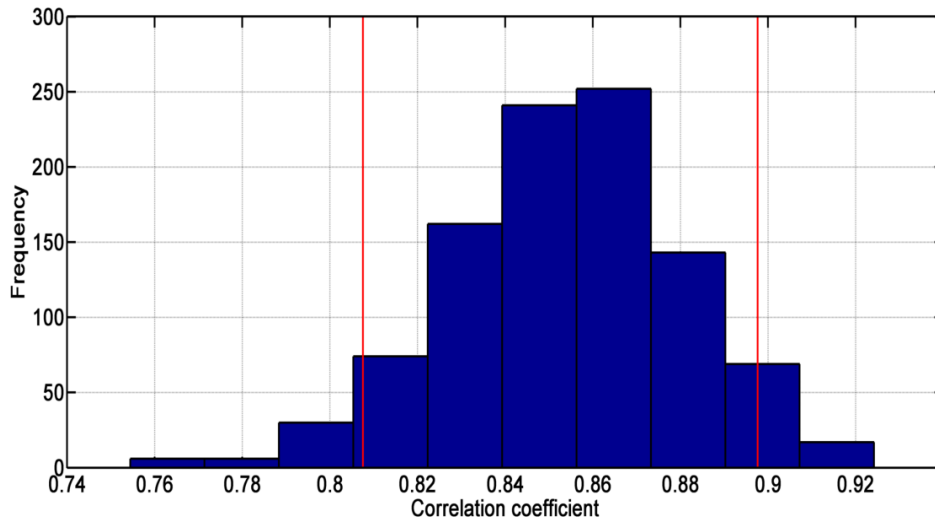
Fig. 9b. The correlation between surface temperatures measured at GS Habarova and Eremeyka. The 148 data points (the data set contains monthly mean values for open water season from 1974 to 2010) are resampled to create 1000 different data sets. The other details are the same as for Fig. 9a.

Unfortunately, we do not have temperature data for the Ebitiem River. Here, we assume that water temperatures at the lower reaches of the Eremeyka and Ebitiem rivers have similar dynamics and values. Thus, the influences of cold water from the Eremeyka and Ebitiem are considered simultaneously.

To find out the influence of water from the Eremeyka and Ebitiem rivers on water temperature measurements at Kusur GS, and, thus, the amplitude of the anomaly, we did additional computations. We calculated correlation coefficient using bootstrap analysis between times when the surface water temperature at Kusur GS and Habarova reaches the maximum (Fig. 10) and correlation coefficient between:

$$x_1 = \frac{Tw_{Erem}}{Tw_{Hab}}, \quad \text{and}$$

$$x_2 = -(Tw_{Hab} - Tw_{Kus})/Tw_{Hab},$$

where Tw_{Erem} is the water temperature measured at Eremeyka GS (the estuary zone of the Eremeyka River), Tw_{Hab} is the water temperature measured at Habarova GS (which is representative) and Tw_{Kus} is the water temperature measured at Kusur GS.
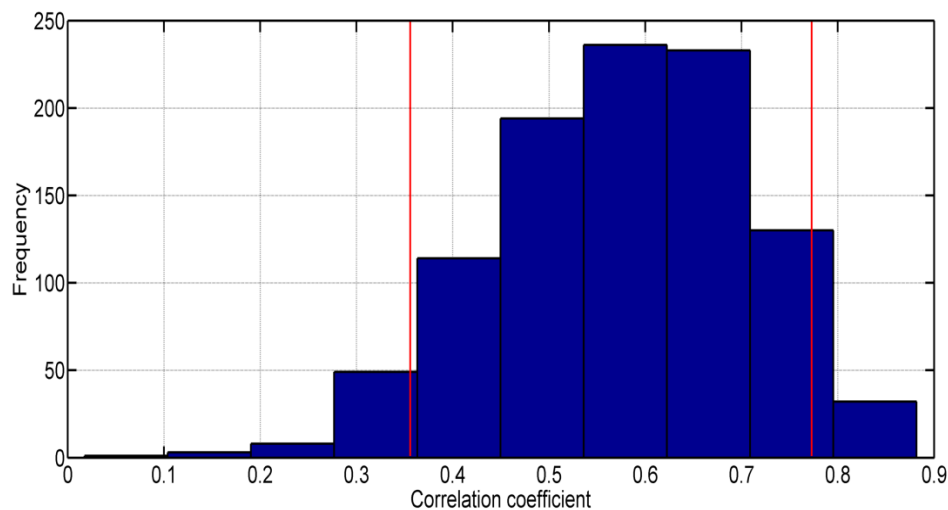
Fig. 10. The correlation between times at GS Kusur and Habarova when the surface water temperature reaches the maximum. 60 data points (the data set contains times for each year from 1951 to 2010) are resampled to create 1000 different data sets. The other details are the same as for Fig. 9a.

In both cases, sample minimums are positive, indicating that the relationships are not accidental (Fig. 10 and 11). The correlation coefficient between the times when the surface water at Kusur GS and Habarova reaches the maximum temperature has nearly the same value as the correlation coefficient between the surface water temperature at Eremeyka GS and the amplitude of the anomaly (Fig. 10 and 11). *This means that the anomaly can be explained by the 60% non-representativeness of measurements at Kusur GS due to the cold right bank current formed from Ebitiem and Eremeyka inflows. However, a clear answer as to whether this anomaly is fully explained by the non-representativeness of measurements at Kusur GS cannot be given without additional data.*
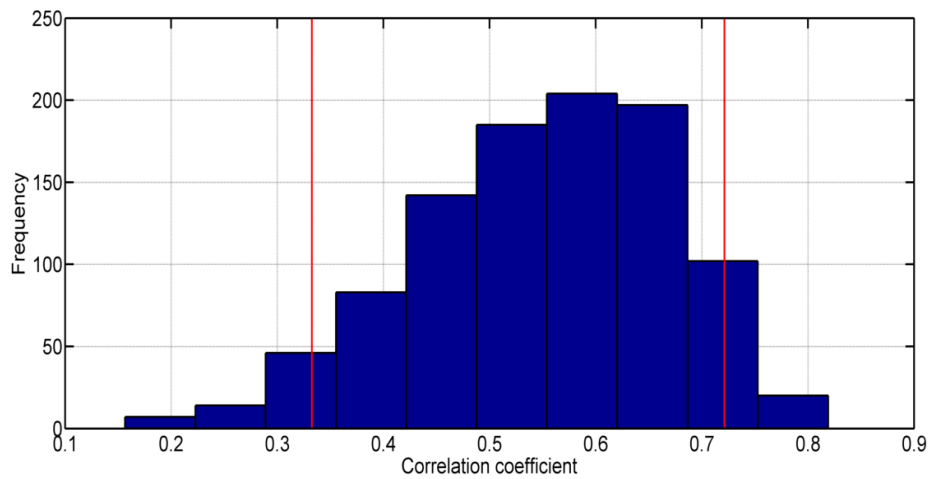
Fig. 11. The correlation between the normalized surface water temperature at GS Eremeyka (x1) and amplitude of anomaly (x2). The 148 data points (the data set uses monthly mean values for open water season from 1974 to 2010) are resampled to create 1000 different data sets. The other details are the same as for Fig. 9a.

Figure 7 and Figs. 10 and 11 indicate the possible existence of other important factors influencing and determining the anomaly. Below, we present these additional facts, which also confirm that the anomaly is *not fully explained* by the non-representativeness of measurements at Kusur GS:

a) Tit-Ari GS (Fig. 1), located between Kusur GS and Habarova, operated from 1976 to 1990. Table 2 and Fig. 4 show that the anomaly also exists between Tit-Ary GS and Habarova GS, a segment of the river with a length of about 50 km (Fig. 1), assuming the representativeness of measurements at Tit-Ary GS.

The dynamics of surface water measured at Tit-Ary GS are almost identical to the dynamics of surface water temperature measured at Kusur GS and Habarova. According to the temperature data from Tit-Ary GS, the anomaly can vary during the season from between a fraction of a degree to three degrees (Fig. 4. and Tab. 2).

Table 2. The mean surface water temperature measured at different gauging stations.

Station	Mean temperature for June – September from 1981 to 1990			
	06	07	08	09
Eremeyka	4.41	8.41	6.39	2.2
Kusur	5.49	14	12.25	6.11
Tit-Ary	5.27	13.19	11.63	5.36
Habarova	6.48	14.56	13.24	7.62

b) The short series of observations in the framework of Russian-German cooperation near the recently opened Samoylovskiy station at Stolb GS main channel and at Habarova GS also supports the idea that the anomaly cannot be explained only by the non-representativeness of measurements at Kusur GS (Fig. 7). Also, during the period of observations, the temperature of the stream at the beginning of the Bykovskaya channel (Habarova GS) is higher on average than in the main channel under similar air temperatures.

c) The beginning of ice conditions at Habarova GS is observed on average four days later than at Kusur GS based on available observations from 1986 to 1990 and from 1999 to 2007 (Table 3). Ice formation is a complex process, but it largely depends on heat exchange with the atmosphere and heat stored in a river (Antonov, 1961). A decrease in the flow velocity caused by an increase in the water mirror could also be responsible for cooling at Habarova GS in autumn. However, given that the air temperatures are nearly equal at Kusur and Habarova stations for the first decade of October, we conclude that the shift in the beginning of ice conditions is mostly explained by the impact of heat stored in the stream.

Table 3. The date of the first ice appearance in the fall.

Year	1986	1987	1988	1989	1990	1999	2000	2001	2002	2003	2004	2005	2006	2007
Station	Date													
Kusur	6.10	5.10	11.10	7.10	9.10	2.10	6.10	5.10	7.10	30.09	9.10	6.10	7.10	7.10
Habarova	10.10	8.10	18.10	9.10	12.10	5.10	8.10	13.10	11.10	9.10	13.10	8.10	13.10	14.10

The date of fall ice appearance is taken as the date of formation of stable grease, landfast ice, slush ice run (shuga-drift) and drift ice. Despite the difficulty in determining this date, Kusur GS is considered to be one of the most representative for surveillance regarding ice phenomena (Antonov, 1961).

d) The anomaly has a tendency to develop from June to September (Figs. 6 and 8). In general, the difference between the surface temperatures measured at Kusur GS and Eremeyka in September is less than in August, when it reaches maximum, and July (Fig. 8). The behaviour of the

anomaly can also be influenced by changes in the mixing process of Lena water with Ebitiem and Eremeyka water due to the decrease in runoff volume. However, the mean discharge rates (water levels) for the whole period of observation measured at Kusur GS for August and September are close to each other (Tab. 4).

Table 4. The mean discharge rate for the Lena River for the period from 1935 to 2011, measured at mainstream Kusur Station, [m³/sec], and mean water level for the period from 2002 to 2011 (zero level corresponds to station level mark), [mm].

Month	June	July	August	September
Mean discharge rate	74003	39578	27356	24926
Mean water level	1446.633	999.7667	780.4667	822.1

e) The differences between the mean water temperature extremes during the warm season (June–September) measured at Habarova GS are higher than at Kusur GS, which is not true for the mean air temperature extremes (see, e. g., Fig. 8). We have concluded above that the water temperature measurements at Kusur GS reflect thermal conditions of the Lena River in general. If we assume that the anomaly is explained solely by the non-representativeness of measurements at Kusur GS, we cannot explain the behaviour of mean water temperature extremes.

8.4. Discussion

Considering the behaviour of the anomaly and its analysis, we can assume that the Lena River heat content during the summer period is partly stored in the alluvial strata of the river bed and sediments at the delta head area, from Tit-Ary GS to the beginning of the Bykovskaya and Trofimovskaya channels (Fig. 1), and, with strong air cooling trends, the heat stored in the underlying layers is released back to the water. This guess was also expressed by Burdikina (1961) who compared the surface water temperatures at Tit-Ary GS and Kusur without regard to non-representativeness of the latter. However, this assumption requires a more detailed analysis of riverbed characteristics, sediment fluxes and hyporheic zones and a more complete database of observations for assessing the heat balance. Nevertheless, some details concerning this hypothesis are given below.

8.4.1. Sediment fluxes

Total (suspended load and bedload) annual sediment flux at the Lena Delta head is the largest of all Russian arctic rivers. According to numerous recent estimates, the Lena River supplies its delta with 20.7 to 21.4 million tones (mln t) of suspended material, as measured at Kusur GS (Holmes et al., 2002; Hasholt et al., 2005). Following the inter-annual variability of the river flow, the annual suspended sediment load (SSL) varies from 16.6 to 26.2 mln t (Korotaev, 2012). The vast majority of SSL passes by the Kusur cross-section in early summer (June to early July) when snowmelt events provide around 85% of the total water discharge. Suspended sediment concentrations, on average, peak later than does the discharge, reflecting the dominant role of more distant material sources and the erosion-limiting setting of the Lena lower reaches, which are dominated by permafrost (Tananaev, 2013). Sediment peaks on the falling limb of the hydrograph enhance accumulation within the lower floodplain levels and large alluvial bedforms.

Bedload transport estimates are not obtainable due to the lack of a reliable methodology to base such estimates on. Tananaev and Anisimova (2013) employed an empirical calculation procedure, described in Simons et al. (1965) and further developed by Alekseevskiy (2004), in the assessment of the bedload flux by computing the volumetric unit bedload transport rate. According to their results, annual bedload flux at Kusur GS is 14.9 mln t, which comprises nearly 42% of the total sediment delivery to the delta head. Bed material transport occurs mostly during snowmelt floods (78.5%). This is followed by rain-induced events (19.5%) and the summer low flow period (2%) (Tananaev and Anisimova, 2013).

The accumulative environment of the Lena Delta significantly limits sediment delivery to the marine zone. Presumably, the whole volume of bedload material is retained within the delta in large bedforms (point and side bars), especially in the delta head area. Only 10 to 17% (2.1 to 3.5 mln t) of the total suspended material is delivered to the Laptev Sea margin (Peregovich et al., 1999; Rachold et al., 1996). Most of the material takes part in floodplain construction. The vast majority of sediment material is retained within the riverine part of the delta. Sediment-associated heat flux is expected to have higher impact within the deposition area. The timing of this effect occurs towards late summer as the suspended sediment wave arrives at the considered area towards the end of the annual flood. Water depth decrease and active movement of smaller bedforms (ripples) can potentially promote energy dissipation and heat release from the moving upper layer of deposited material.

8.4.2. Alluvial composition and structure

The upper part of the 'Lena Pile', a narrow river section extending some 165 km from the Kusur settlement to the head of Tas-Ary Island, almost lacks a fine alluvial cover. Fluvial deposits are predominantly composed of very coarse sand and pebble fractions (0φ to -6φ), with medium sands only found along the shore in numerous side bars, along with local boulder inclusions. Both descriptive models and field measurements provide evidence of active convective heat release from the river flow towards the alluvial strata within the hyporheic zone underflow in areas with coarser alluvial composition (Mikhaylov, 2003; Wankievicz, 1984). Below Tas-Ary Island, channel widening promotes sediment deposition in large accumulative forms (Sobol and Billyakh sands) and alluvial islands, which contribute to higher thermal conductivity. An example of the latter is Tit-Ary Island, which is a remnant of the high floodplain probably dating back to the latest stage of the Flandrian transgression and which preserves a northernmost larch forest colony in the region. Pebbles also constitute a significant part of the bedload material below Stolb Island in the Bykovskaya deltaic branch – up to 60% of the channel area. Sands, medium to coarse, are rarely found there, except in secondary branches, but are widely presented in the major Trofimovskaya channel (Korotaev, 2012). The heat capacity and water content of different alluvial compositions require detailed analysis.

There is evidence for the presence of a variety of cavities and probably channel underflows (Fig. 12), which also probably contribute to losing a certain amount of the total runoff measured at Kusur GS. This fact also supports the possibility of a deeper penetration of heat waves to the alluvial strata compared to the prediction based on solving diffusion equations for temperature waves.
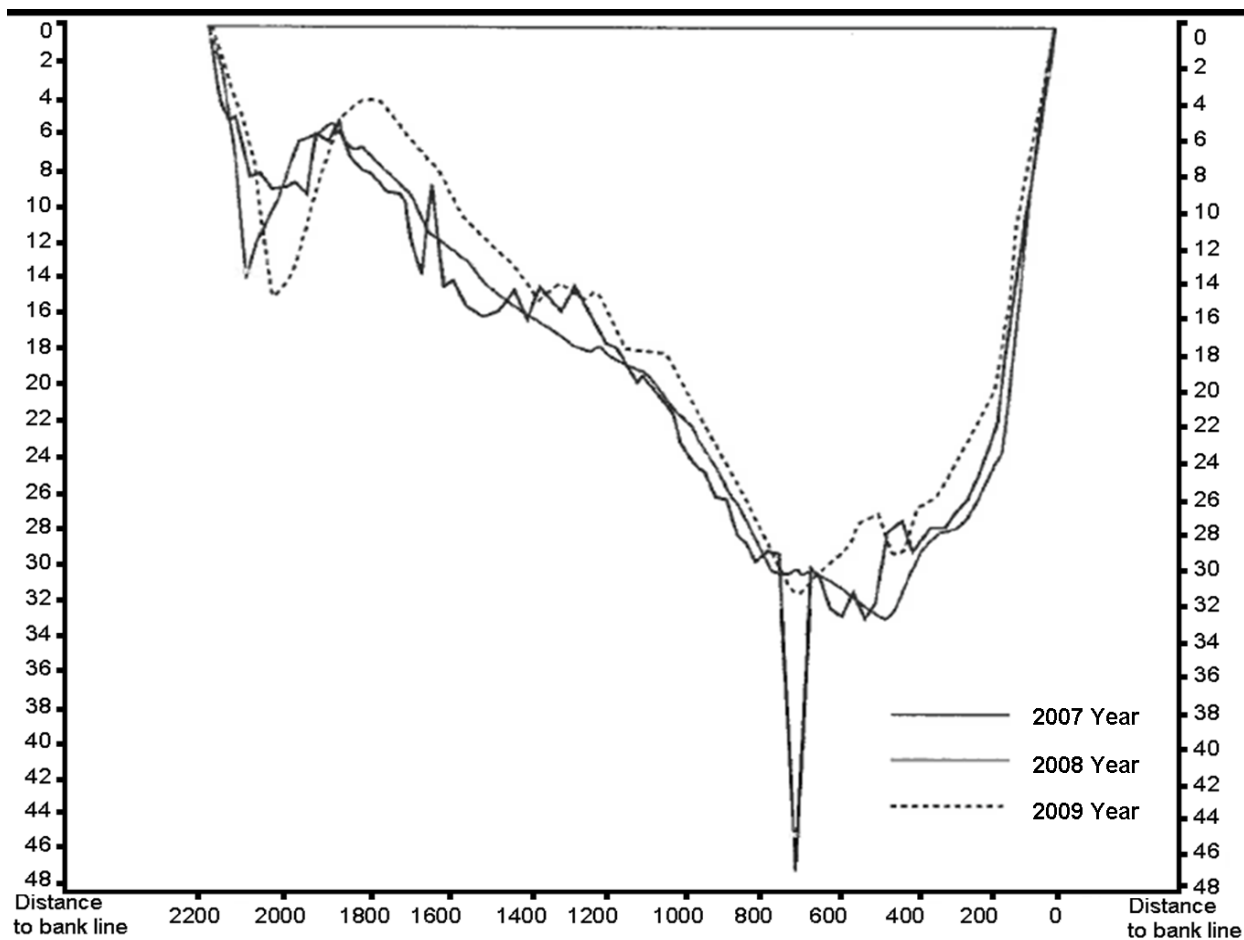
Fig. 12. The Lena River bed profile, area of GS Stolb, main channel, August [m]. The picture is taken from Bolshiyanov et al., 2013.

8.4.3. Geocryology

The high-arctic location of the Lena Delta secures its position within the continuous permafrost. Frozen ground thickness in the region can reach 600 m (Grigoriev, 1966) with temperatures at zero annual amplitude depth around -9 to -11°C, and a shallow, seasonally thawed layer, rarely exceeding 0.8 to 1.2 m in depth. Taliks usually occur below the large water bodies, such as lakes and river channels; talik zones are mostly 'open' beneath the major channels and largest lakes, while remaining 'closed' under the secondary branches and smaller water bodies (Grigoriev, 1993). Channel alluvium, though, is also subject to deep seasonal freezing where it is either exposed or directly contacts the ice bottom during the winter low flow and freeze-up period. The climate of central Yakutia allows around 8.0 m of bed material (silty sands) to be frozen during the wintertime (Tananaev, 2013). Given estimates should be reduced to about 2.5 m for the Lena Delta region due

to generally coarser alluvium and higher winter temperatures. Also, the river does not freeze completely at Kusur and Habarova stations (Hydrological Yearbooks).

In high-energy environments, adjacent to the midstream, with normally coarser bed material grain sizes, the frozen state of the alluvium cannot be retained throughout the summer season due to lesser ice content and higher bed mobility. In contrast, aside from the midstream, a perennially frozen core can be retained in side bars subsequently merging with the floodplain or valley bottom permafrost (Tananaev, 2013). Albeit scarcely studied in nature due to technical limitations, frozen cores are believed to underlie the majority of bedforms within the Lena Delta region (Korotaev, 2012). In this case, seasonal freeze is replaced by seasonal thaw, which penetrates the bedforms to a depth of 1.6 to 2 m. Relevant to the aims of our study may be the permafrost-induced limitation of bedform mobility, constraining the channel deformations only to the freshly deposited sediment within areas of higher heat content, which are non-frozen and readily available for transportation by the stream. The thermal impact of such alluvial forms on the stream is unstudied to date. However, based on the results of the expedition in August 1955 in the Bykovskaya channel, no frozen soils in the furrows have been found (Ivanov, 1967). In this case, no frozen alluvium thaw is occurring, and the channel areas store the largest portion of incoming solar radiation, while being exposed to direct sunlight during the low-flow period. Heat release from the channel bars occurs mostly towards the end of summer when the bars are covered with water during level increase from major rain events. Large accumulative forms dominate the channel topography in the area of Habarova GS and can facilitate water temperature increase at this location.

8.4.4. Supporting considerations and summary

The measurements from 1947 to 2010 of the surface temperature at the lower reaches of the Olenek River at Taymylyr GS and Ust-Olenek do not detect the presence of a temperature anomaly. Ust-Olenek GS is situated at the beginning of the Olenek Delta and Taymylyr is 95 km upstream. However, on average, the positive gap between temperatures measured above and downstream, at the beginning of the delta, is reduced to zero by the end of September. The lower reaches of the Olenek and Lena rivers are in close proximity and in the same climate zone. Both rivers are meridional, elongated from north to south. But, the contribution of these rivers is very different; the mean total annual discharge volume for Olenek River is approximately 14 times less that of Lena River (http://www.r-arcticnet.sr.unh.edu).

Investigation of heat accumulation by the river bed combined with a complex dynamic structure in the area of the delta head is a difficult, but reasonable, question for the future when a sufficient observational database is formed. However, if the water temperature measurements at Tit-Ary GS truly reflect the midstream water temperature for this cross-section, or, in other words, there is no large impact of coastal effects due to the heat capacity of Tit-Ary Island itself or for another reason, the explanation of the anomaly solely as being due to heat accumulation is highly unconvincing without additional sources of endogenous heat (Table 2). In case of the representativeness of measurements at Tit-Ary GS, it is hard to explain the presence of the anomaly in June and July (Table 2). To clarify this issue, a large number of additional measurements is required, including bottom water temperature measurements in the area of the delta head (from Tit-Ary GS to the beginning of the Bykovskaya and Trofimovskaya channels). Appropriate consideration of possible sources of endogenous heat is probably also necessary. The measurements of water surface temperatures in July 2006 from the beginning of the delta to the mouth area along the central channels (Tumatskaya - Osohtoh) showed a regular drop in the temperature of the river water by 1 degree for every 30 km (Bolshiyanov et al., 2013). Fresh water from the Bykovskaya and Trofimovskaya channels enters into Tiksi Bay (Fig. 1), so that the water in the bay is almost fresh. Observations in Tiksi Bay in August 2011 showed that flow cools naturally in the mouth area due to the direct influence of the sea.

Thus, the main point to study for the first step is the heat transfer between the river water and the riverbed in terms of the complex dynamic structure in the area from Tit-Ary GS to the beginning of the Bykovskaya and Trofimovskaya channels and an analysis of other possible sources of endogenous heat.

8.5.   Conclusions

This paper analyses water temperature characteristics in the outlet area of the Lena River during the summer season (June–September). Based on our analysis, we conclude that the measured water temperature in the surface layer at Kusur GS reflects the dynamics of the mean stream temperature in general but incorrectly characterizes the value of the mean stream temperature, highly underestimating it due to the non-representativeness of the measurements at the right bank.

The anomaly in water temperature between Kusur GS and Habarova considered in this paper (the differences between stream surface temperatures measured at Kusur GS and Habarova are almost always negative for the period from July to September since the beginning of observations)

can be explained by the 60% non-representativeness of measurements at Kusur GS due to the influence of water from small inflows of the Eremeyka and Ebitiem close upstream that are shaped into a cold right bank current. However, a clear answer on whether or not this anomaly is fully explained by the non-representativeness of measurements at Kusur GS cannot be given without additional data.

The anomaly does not have a significant trend towards increasing from year to year. However, the anomaly develops from June to September every year.

At present, there is no significant trend for the mean stream temperature for the summer season (June–September) in the Lena River basin outlet area based on the data from Kusur GS and Habarova. Since the beginning of observations till 2011 at Kusur GS and Habarova, the temperature increases by ~0.25 °C for the whole summer season. The trends exists with more than 90% probability only for August at Kusur GS and for June at Habarova GS, indicating a temperature increase of ~1.3 °C for both stations since the beginning of observations. However, due to the high amplitude of mean stream temperature fluctuations from year to year, there is no guarantee that these trends are reliable. Also, we would like to stress that water temperature measurements at Kusur GS cannot be taken directly for analysis of the water temperature changes in the mouth area.

When considering the heat balance for the lower reaches of the Lena River, it is important, especially in the delta head area, to take into account the characteristics of the riverbed, such as the thickness of the active layer and its geomorphologic characteristics. One of the most difficult issues is the morphological structure of the underflow, which can be responsible for releasing heat stored earlier in the season.

There are indications in favour of an unaccounted source of heat from the riverbed in the area of the delta head from Tit-Ary GS to the beginning of the Bykovskaya and Trofimovskaya channels. More analysis and observations are required to make further statements in this direction.

Acknowledgments

9. Materials in preparation for submission

9.1. Multidimensional scaling projection method and its application to current study

V. Fofonova[1], A. Fofonov[2], K.H. Wiltshire[1]

[1]Alfred Wegener Institute, Helmholtz Centre for Polar and Marine Research; Kurpromenade, D-27498 Helgoland, Germany;
[2] Jacobs University; Campus Ring 1, D-28759 Bremen, Germany;

The modern numerical models with large numbers of nodes, vertical layers and simulated variables require new techniques for data analysis and visualization. In our study we face a problem of estimation of the different factors impacting on the Lena River freshwater plume propagation in the Laptev Sea. We solved this problem in two ways. One has been already described above. It represents the analysis of some variables in different cross-sections in a series of experiments. In our study we analyzed Brunt–Väisälä frequency and salinity. However, this method has some obvious weaknesses; the main one is a limitation of analysis in the whole domain to analysis in cross sections. In our case it was not crucial, but we would like to present an alternative way.

In the model we have M vertical layers and N nodes for each of them. In order to get an opportunity to proceed with such data, a representative description of a field distribution in the domain is required. For each geographical point of the domain a vertical profile of Brunt–Väisälä frequency was assigned; for every depth layer we have N values of Brunt–Väisälä frequency. Due to the complexity of the bottom profile, we put zeros to the values which refer to the ground. First, we should decide how each vertical profile of Brunt–Väisälä frequency should be compared with others. In other words, we tried to find the proper metric. Probably, it is the hardest and most important step. For comparison of N vectors (with dimension M), we chose the maximum metric (Chebyshev distance).

After a proper distance function is defined, we can build a corresponding distance matrix (or dissimilarity matrix) $\mathbf{D} = [d_{i,j}]$. Basing on this matrix, a dimensionality reduction technique can be applied to map the high-dimensional vectors to a 2D or 3D visual space. For this purpose, we chose the multidimensional scaling projection approach (MDS) described by Wickelmaier (2003). The projection algorithm can be summarized as follows:

$\ll$ 1. Set up the matrix of squared distances $\mathbf{P} = [d_{i,j}^2]$.

2. Apply double centering: $\mathbf{B} = -\frac{1}{2} \cdot \mathbf{J} \cdot \mathbf{P} \cdot \mathbf{J}$, where $\mathbf{J} = \mathbf{I} - n^{-1} \cdot \mathbf{E}$, $\mathbf{I}$ is the identity matrix, $\mathbf{E}$ is the matrix with all entries being 1, and n is the number of samples.

3. Extract the m largest positive eigenvalues $\lambda_1, \dots, \lambda_m$ of $\mathbf{B}$ and the corresponding m eigenvectors $v_1, \dots, v_m$.

4. An m-dimensional spatial configuration of the n objects is derived from the coordinate matrix $\mathbf{X} = \mathbf{V}_m \cdot \mathbf{\Lambda}_m^{1/2}$, where $\mathbf{V}_m$ is the matrix of the m eigenvectors and $\mathbf{\Lambda}_m^{1/2}$, is the diagonal matrix of the m eigenvalues of $\mathbf{B}$.   >>

As a result, the MDS projection shows a distribution of the domain points taking into account their difference or similarity in terms of the chosen descriptor. It means that similar points (points with a low distance) will be placed closely, while very different ones (points with a high distance) would be far from each other. It is very important that the positions of the points on the projection depend on all involved points.

For an additional analysis we created a tool, which allows interactive selection of the points on the projection space and further displaying the corresponding points on the domain (Fig. 1). Depending on the input data, the resulting projection has a different structure. It is possible to distinguish some groups and formations on the projections, which link to certain areas on the domain. Thus, we can easily understand to which regions we can pay attention and find out important features in the field distribution.

The described method is a flexible instrument for data analysis and visualization. In our test cases we can clearly follow, for example, that only wind forcing significantly changes the plume propagation extent north and west of the Lena Delta.
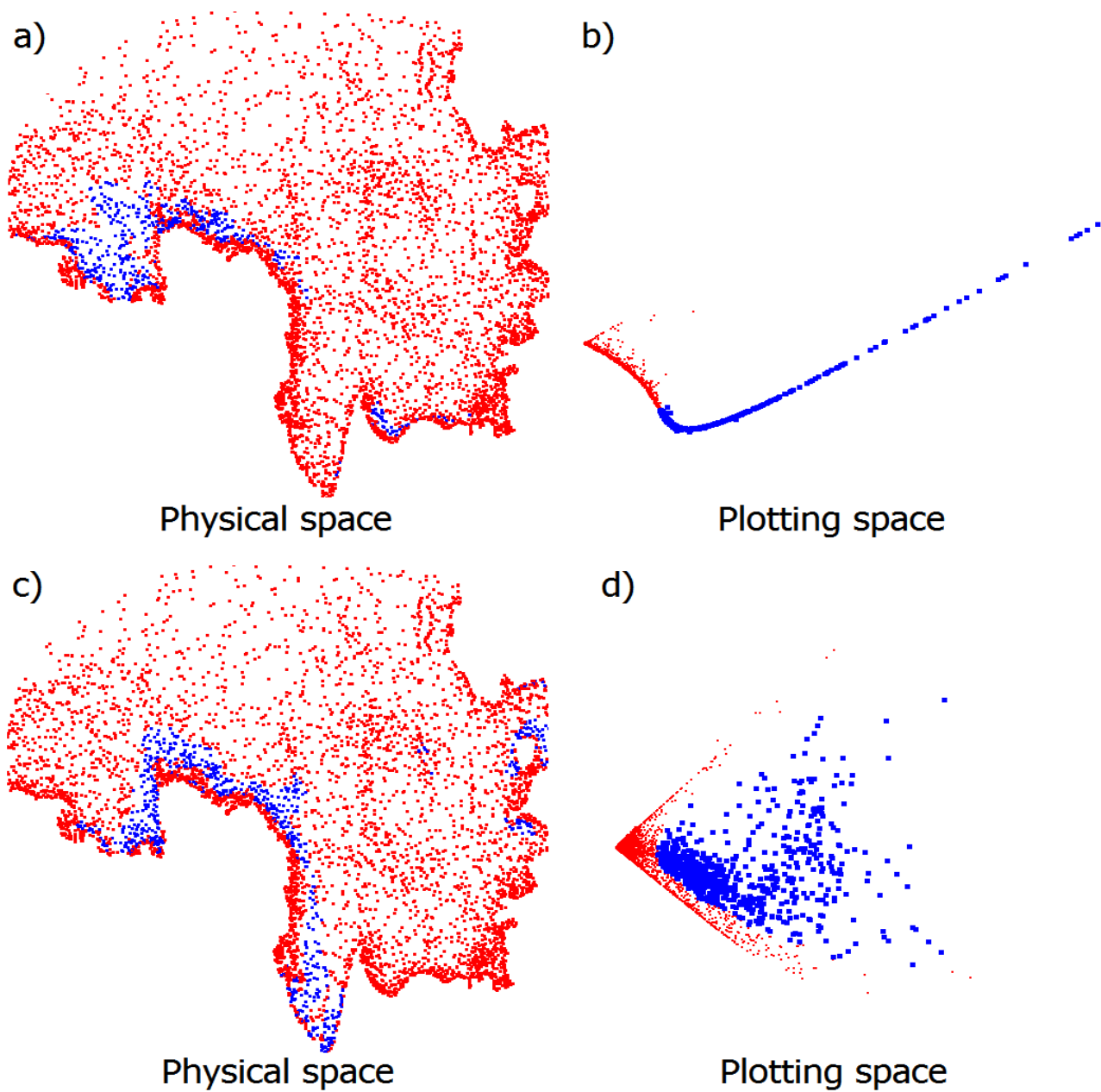
Fig. 1. MDS projections (b, d) and the considered domain (a, c). Selected points on the projections and corresponding points on the domain are highlighted by a blue colour. Two test cases: without tides (a, b) and without wind forcing (c, d).

## 9.2. Modeling of the Lena River stream temperature using nonlinear regression

V. Fofonova[1], A. Kraberg[1], M. Krayneva[2], K.H. Wiltshire[1]

[1]Alfred Wegener Institute, Helmholtz Centre for Polar and Marine Research; Kurpromenade, D-27498 Helgoland, Germany;
[2]Institut of Computational Mathematics and Mathematical Geophysics, Siberian Branch of the Russian Academy of Sciences (SBRAS); 6, Lavrentiev avenue, Novosibirsk 630090, Russia;

In this section we describe briefly how we can predict daily Lena River temperature in the mouth area based on known water temperature at the Delta head and meteorological conditions in the area in the summer season. The modern research station on the Samoilovsky Island (Delta head) has been operating since 2003. It provides hourly and daily meteorological and hydrological data. However, for this moment the available observational database in frame of morphology, hydrology and meteorology for the Lena Delta head is still insufficient to provide the base for deterministic modeling approach. Thus, we decided to choose a statistical approach, which requires relatively small amounts of observational data.

For the first step we analyzed available temperature profiles for the main Lena River channels based on the expedition's data for August, 2010 (Fig. 2). Since the mean difference is less than 1 degree (Fig. 2, bottom picture), we assumed that the temperature profiles are uniform. Of course, this approximation can be lifted in the future.
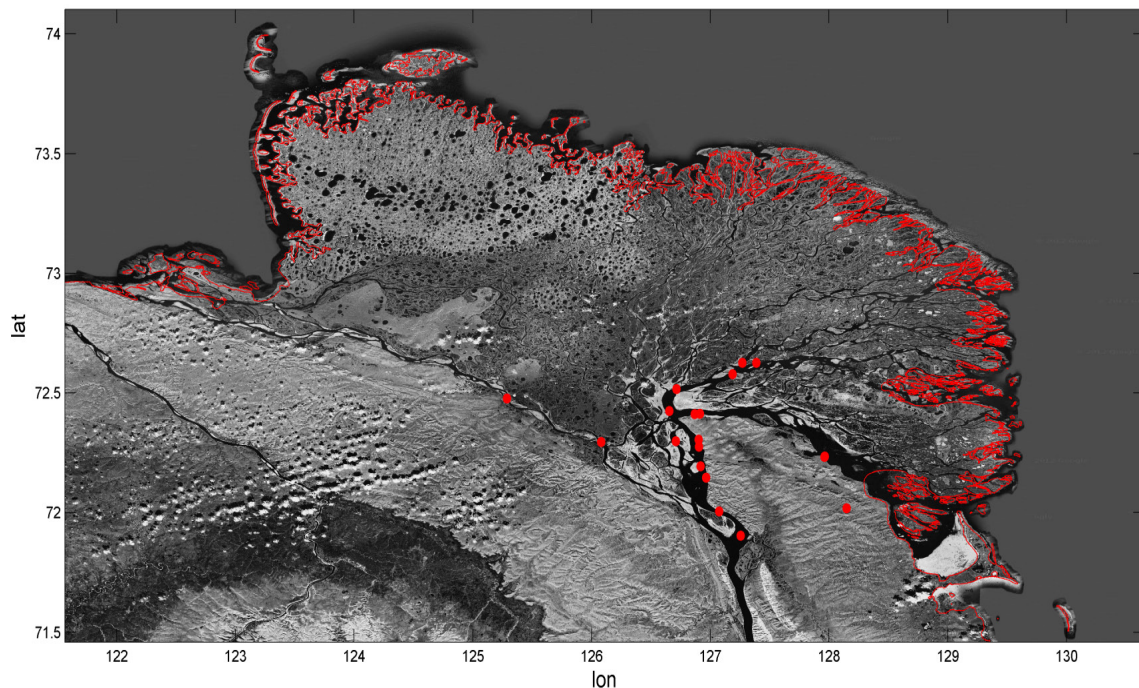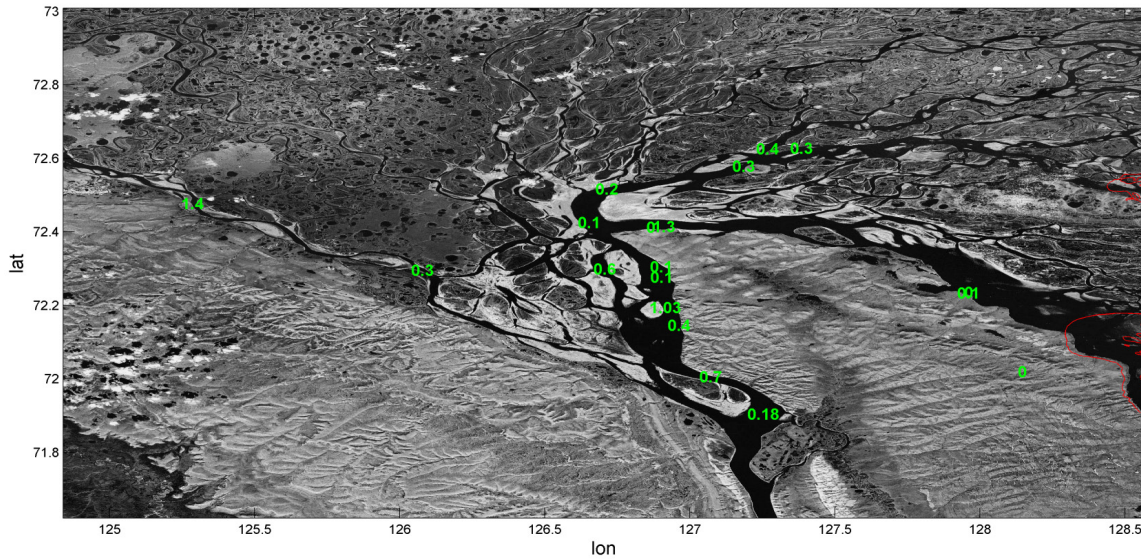
Fig. 2. Upper picture shows the positions of CTD measurements in August, 2010 in the Lena Delta. The bottom picture presents the difference between measured maximum and minimum temperatures at the positions, which are marked on the upper picture.

The second step was to choose a statistical approach. For 2011 we have had the observational data both in the Lena Delta and mouth areas. It was our base for verification. We should mention here that the distance between the Samoilovsky Island and mouth area is an average of 150 km. Therefore, we cannot assume the uniformity of meteorological condition of the whole Lena Delta. It requires additional data from the models. As a source of meteorological data the ECMWF modeling results can be used (Fig. 3). As mentioned before, it has a 40 km horizontal resolution and can provide information at several points in the considered region. The daily surface air temperature data from ECMWF and observations at Samoilovsky Island highly correlate with each other. However, the values of air temperatures can differ from each other significantly.
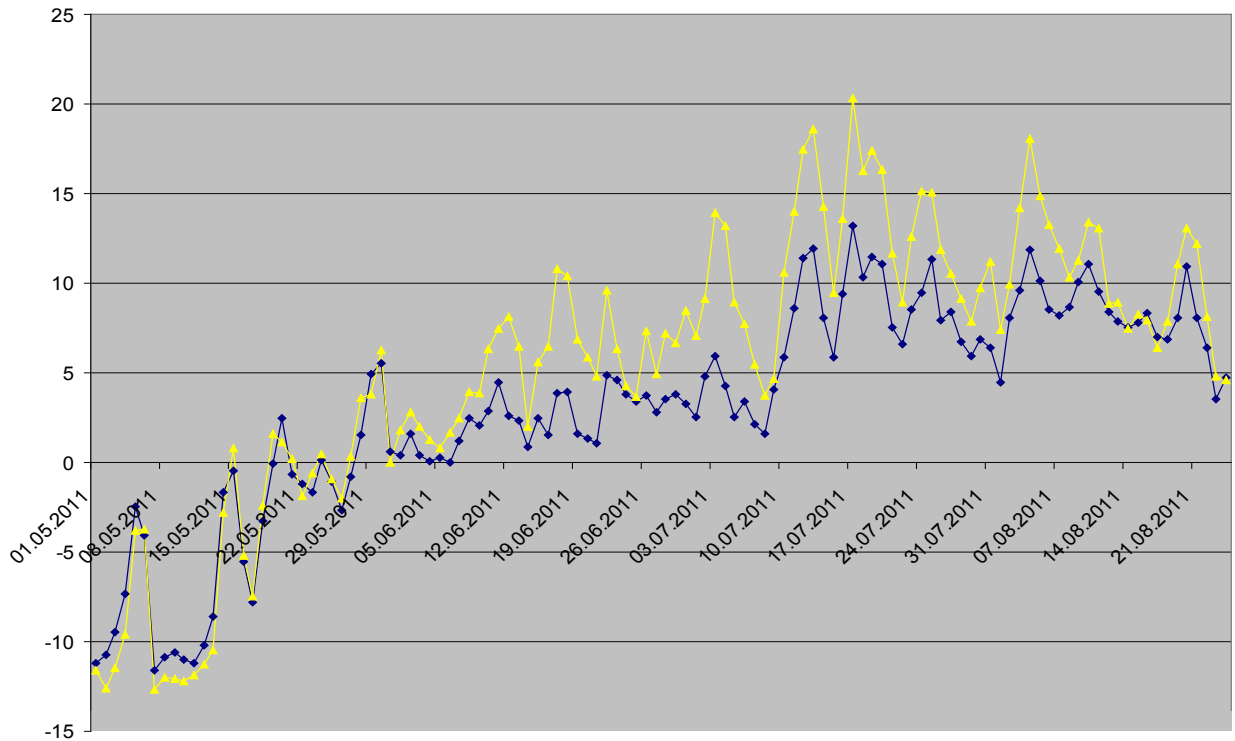
109

Fig. 3. The daily surface air temperature at Samoylovskay Island based on observations (blue line) and ECMWF modeling results (yellow line).

We decided to restrict usage of meteorological data to surface air temperature. We have already indicated that the Lena Delta area is a complex region with only partly known permofrost conditions, complex morphology and temperature anomalies. Despite the low air temperatures in the region, the air-water temperature interaction has a pronounced non-linear component, especially within a short time period. To obtain the daily mouth temperatures in some channels, we had two input data sets. The first is the daily temperature at Samoylovsky Island the day before (or even two days before depending of the distance between the Lena Delta head and the channel mouth). The second is averaged over space (channel area) and time (estimated time lag of water from the Lena Delta head to the channel mouth) surface air temperature. We noted that the non-linear regression approach, described in Mohseni et al. 1999, with four parameters can be successfully applied for the prediction of daily water temperature. It is a quite flexible approach, which allows to take into account the difference in behaviour from channel to channel, to adapt the modeling approach to the source of meteorological data and to work with different time periods. The non-linear function, which connects the air and water temperatures and also takes into account the upstream information via parameters, is presented below:

110

$$T_w = \mu + \frac{\alpha - \mu}{1 + e^{\gamma(\beta - T_\alpha)}},$$

where $\gamma = \frac{4\tan\theta}{\alpha-\mu}$, T_w – Water temperature, T_a – Air temperature, μ – Lowest water temperature, α – Highest water temperature, γ – function of the steepest slope (inflexion point) of the T_w function (when plotted against T_a) and β – Air temperature at the inflection point.

We successfully validated this technique for the daily prediction of water temperature on weekly and monthly scales. Nash-Sutcliffe coefficient of efficiency equals to 0.73 for weekly scale and on average 0.3 (varies from 0.6 to 0.1 from June to August) for monthly scales. But we still need make improvements, and they should be discussed in a future work.

10. Synthesis

10.1. Summary

This PhD thesis presents the analysis of the Laptev Sea shelf dynamics with focus on the Lena Delta region, the description of the numerical ocean circulation model set up to carry out the simulations, the model evaluation against available observational data and the analysis of data on the Lena River temperature. The analysis of the dynamics in the Lena Delta vicinity is based on a new setup developed as a part of this work. This development required special attention to barotropic tidal dynamics and to Lena River discharge characteristics at the basin outlet, which were explored in detail. The skill of the model in simulating the circulation on the Laptev Sea shelf allows one to consider the model as the basis for the ecosystem modeling in the Lena Delta region. The series of manuscripts was written to report about the progress.

Manuscript 1 focuses on the barotropic dynamics induced by semidiurnal tides, which are dominant in the region under consideration. The analysis of the model skill in representing tides in the Lena Delta region of the Laptev Sea, presented in this manuscript, served as a first necessary step for further circulation modeling. Two main issues were solved in the framework of barotropic tidal simulations. First, the open boundary conditions were designed which allow reaching the best accuracy among existing models in simulated tidal maps. Second, a triangular unstructured grid was constructed, which accurately resolves the irregular coastal topography with a large number of small islands and narrow channels and also bathymetry features in the domain, which is the basis of accurate model performance. Studying barotropic tides allowed us to analyze the residual circulation, sensitivity to variable bathymetry and energy balance and to trace in detail the energy flux pattern.

The results described in **Manuscript 1** made possible a step toward higher model complexity. The open boundary conditions and mesh were further used in the full setup. **Manuscripts 2 and 3** focus on the full baroclinic dynamics in the region. Their main goal is an analysis of the Lena River freshwater plume propagation under the influence of different factors, such as tides, wind forcing and heat exchange with the atmosphere during the warm season. The different atmospheric forcing provided by the local high-resolution model (COSMO), regional (ECMWF) and global (NCEP) products were compared and used. It was shown that the simulated and observed Lena River plume dynamics compare very reasonably, indicating that the full models can be used further for the ecosystem modeling. Full simulations used the best available information on the Lena River

discharge properties, including its temperature. Compiling this information led to a separate in-depth study presented in **Manuscript 4**.

Manuscript 4 contains description of the Lena water temperature characteristic at the basin outlet area during the summer season (June-September). Due to the limited information about the Lena River discharge characteristics at the basin outlet, they are usually taken from the Kusur Station. However, the surface water temperature anomaly was found to exist between the Kusur Station and the beginning of the Bykovskaya Channel (delta head zone) during the open water season from July to September; the differences between the stream surface temperature at the Kusur Station and temperature 200 km downstream to the north were almost always negative for the considered period since the beginning of the observations. The description of this anomaly and its basic analysis were presented. It was shown that the measured water temperature in the surface layer at the Kusur Station reflects the dynamics of the mean stream temperature in general, but significantly underestimates its value, due to non-representativeness of the measurements at the right bank. **Manuscript 4** provided the necessary base for the correct input of the Lena River discharge characteristics in to the model.

Unpublished results include a technique for the results visualization and deal with the development of a statistical module which would predict the Lena water temperature at the mouth area in function of atmospheric conditions in the region. These results are intertwined with the published material, and they all will assist future work in all planned directions.

10.2. Conclusions

The main result of this thesis is the model setup, which is capable of simulating the Lena freshwater plume dynamics, which agrees favourably with observational data, and a set of conclusions on the plume dynamics that can be deduced from various sensitivity experiments. Articles and manuscripts presented in the thesis contain conclusions on their particular questions, which are not repeated here in full. The main achievements of this thesis are the following:

1. Analysis of available data-based tidal solutions and observational data for dominant semidiurnal waves in the region and construction on their base of optimal open boundary conditions for the elevation is provided. These conditions warrant improved agreement with observations and are important components of the full model. Tidal ellipses of simulations with optimal boundary conditions agree well with observations and a full analysis of simulated tidal dynamics allows estimation of the magnitude of residual circulation, which affects sediment and nutrients transport.

Important information about evolution of energy fluxes in the region and zones of intensive mixing generated by tides is also provided.

2. There is also an analysis of the Lena River hydrology in the basin outlet area based on the information from several gauging stations, which are rarely used but extremely important for understanding the processes in the Lena River basin outlet area. A statistical approach to modeling the stream temperature in function of the regional atmospheric conditions is proposed.

This analysis allows assessing the changes in the Lena River hydrology regime and getting new insights in complex system dynamics in the basin outlet area. It also provides high quality input data on the Lena River inflow to the Laptev Sea shelf model.

3. The analysis of the Lena River freshwater plume dynamics in the Laptev Sea allows one to predict the plume propagation depending on atmospheric conditions and to understand the observed anomalies in temperature and salinity patterns. The immediate implication of this analysis is the need for high quality wind forcing data for the seamless plume spreading modeling. Although in the simulations a little sensitivity of plume dynamics to the plume temperature is detected, it could be of more significance in future studies involving biology.

4. The current work compiles most of available data that have been otherwise scattered and indicates important correlations in them.

There are several directions the modeling efforts described in this thesis can be further improved. First, it should be augmented with explicit sea-ice dynamics. This would allow exploring interannual variability and would presumably lead to reduced sensitivity to the initial temperature and salinity distributions. Second, special focus should be placed on the analysis of numerical mixing in the model. There are indications showing that a temperature signal gradually penetrates from the surface to the bottom over the summer season in model simulations, which does not necessarily find support in observations. These matters are the subject of future work.

10.3. Future perspectives

The future plans have been discussed already in the body of the articles and manuscripts. In this section other aspects of the future work will be highlighted.

Mostly all models which include the Laptev Sea shelf zone, do not resolve the Lena Delta and, as a consequence, lose information about changes in the Lena River stream using input data of insufficient quality. In the modeling solution for the Laptev Sea shelf region presented in this thesis the Lena River hydrology peculiarities were taken into account, however, the model still does not resolve the delta. It can be critical for further ecosystem modeling step. Modeling efforts of the Lena Delta are virtually absent. This is easily explained by the high complexity of the region which has a very considerable number of freshwater channels. More than thirty thousand lakes and a multitude of flat islands are also found in the Delta. One will never be able to develop predictive capabilities without resolving the Lena River interaction with the Laptev Sea and Arctic Ocean in necessary detail. More work is needed to understand this interaction, which calls for further research on modeling side. The other issue is the lack of data that would back such modeling.

To fill this important gap all available information about morphology, hydrodynamics features, temperature regime, permafrost conditions, chemical composition of water, concentration of organic material in different freshwater channels in the Lena Delta and the coastal areas, into which these channels discharge, should be accounted. As the lack of ecological data is particularly severe, considerable efforts should be devoted to collecting biological data. A BMBF grant proposal was submitted to organize a series of workshops on the Lena River contribution. The main goal of the proposal is to develop a complex set of numerical modules for the Lena Delta region, which will provide input information for the larger scale regional models of the Laptev Sea shelf including ecosystem models. These will include information about velocity structure, temperature profiles, concentration of nutrients and other transported materials – organic and inorganic, the freshwater spreading structure across the entire Lena Delta mouth. Based on it, the next important step of ecosystem modeling can be done.

The Lena River is one of the largest rivers in the Arctic, and permafrost underlies 78-93% of the watershed with continuous permafrost extending south to 50°N (Zhang et al., 1999). Thawing permafrost will cause a change in the carbon chemistry and probably also the inorganic nutrients and other chemical constituents discharged into the coastal Laptev Sea (Frey and McClelland, 2009; Schuur et al., 2008). One of the big tasks in framework of region study is to quantify the flux of permafrost organic matter into the Lena River and to assess its bioavailability. Considerable

progress in that area has already been made at AWI, Bremerhaven. Recent estimates of the total amount of dissolved organic carbon discharged by arctic rivers into the Arctic Ocean is 18-34*1012 g C year-1. The Lena River discharges 3.4-5.7 *1012 g C year-1 (Dittmar and Kattner, 2003; Holmes et al., 2012). Very little is known about the molecular composition of dissolved organic matter (DOM) and its role in biogeochemical processes of the Lena River and the Laptev Sea. This knowledge is essential for the assessment of sources and fluxes of DOM. Untargeted chemical analytics such as Fourier Transform Ion Cyclotron Resonance Mass Spectrometry allow a highly detailed view on the molecular complexity of DOM (e.g. Flerus et al., 2011; Koch et al., 2007). In combination with biomarker information (amino acids, lipid composition and lignin phenols; e.g. Amon et al. (2012); Lara et al. (1998)) and stable isotope analyses, DOM sources and fluxes can be determined (Dubinenkov et al., in prep). The combination of molecular chemical information with other bulk chemical and non- chemical parameters (pH, salinity, nutrients, water discharge) will support a better view on the response of DOM fluxes to changing environmental conditions in the Lena Delta. Using this information for setting up ecosystem models, and verifying these models would be the next important step in ability to assess and predict the unfolding processes in the Lena Delta.

Bibliography

1. Alekseevskiy, N. I., 2004. Movement of bed forms and sediment yield of rivers. Sediment Transfer through the Fluvial System, IAHS Publ. 288, pp. 395–403.

Balashov, K.N. and Tamarskiy, I.I., 1938. Hydrology of Ebitiem River. Hydrology of Soviet Arctic Rivers: Hydrology information about Lena, Ebitiem, Indigirka, Hatanga, Yenisei and Kolyma Rivers, Edited by Prof. Rodevich V.M., Trudy AARI (Proceedings of the Arctic and Antarctic Research Institute), Leningrad: Glavsevmorputi, 105(2), pp. 51-72 (in Russian).

2. Alexandrov, V.Y., Martin, T., Kolatschek, J., Eicken, H., Kreyscher, M., Makshtas, A.P., 2000. Sea ice circulation in the Laptev Sea and ice export to the Arctic Ocean: Results from satellite remote sensing and numerical modeling. Journal of Geophysical Research 105 (C5), 17143–17159. doi:10.1029/2000JC900029.

3. Amon, R.M.W., Rinehart, A.J., Duan, S., Louchouarn, P., Prokushkin, A., Guggenberger, G., Bauch, D., Stedmon, C., Raymond, P.A., Holmes, R.M., McClelland, J.W., Peterson, B.J., Walker, S.A., Zhulidov, A.V., 2012. Dissolved organic matter sources in large Arctic rivers. Geochimica Et Cosmochimica Acta 94, 217-237.

4. Androsov, A., Liberman, Y., Nekrasov, A., Romanenkov, D., Voltzinger, N., 1998. Numerical Study of the M_2 Tide on the North Siberian Shelf. Continental Shelf Research 18, pp. 715-738.

5. Androsov, A.A., Kagan, B.A, Romanenkov, D.A., Voltzinger, N.E., 2002. Numerical modelling of barotropic tidal dynamics in the strait of Messina. Advances in Water Resources 25(4), pp. 401–415.

6. Antonov, V.S., 1961. The influence of river runoff on freezing of estuaries and coastal zone of the Laptev Sea. Trudy AARI (Proceedings. of the Arctic and Antarctic Research Institute), 213(4), pp. 5-37 (in Russian).

7. Bauch, D., Dmitrenko, I., Kirillov, S., Wegner, C., Hölemann, J., Pivovarov, S., Timokhov, L., Kassens, H., 2009. Eurasian Arctic Shelf hydrography: Exchange and residence time of southern Laptev Sea waters. Continental Shelf Research 29 (15), pp. 1815-1820.

8. Bauch, D., Hölemann, J.A., Nikulina, A., Wegner, C., Janout, M., Timokhov, L.A., Kassens, H., 2013. Correlation of river water and local sea-ice melting on the Laptev Sea shelf (Siberian Arctic). J. Geophys. Res. Oceans 118, pp. 550–561.

9. Bolshiyanov, D., Makarov, A., Schneider, W., Stof, G., 2013. Origination and development of the Lena River Delta. AARI. St.Petersburg. 268 p. (in Russian).

10. Burdikina, A.P., 1961. The method for predicting the freezing of Lena River lower reaches. Hydrology of Soviet Arctic Rivers, Edited by Antonov V.S., Trudy AARI (Proceedings of the Arctic and Antarctic Research Institute), Leningrad: Morskoy transport, 213(4), pp. 38-111(in Russian).

11. Chen, C., Liu, H., Beardsley, R. C., 2003. An Unstructured Grid, Finite-Volume, Three-Dimensional, Primitive Equations Ocean Model: Application to Coastal Ocean and Estuaries. Journal of Atmospheric and Oceanic Technology 20(1).

12. Chen, C., Beardsley, R.C., Cowles, G., 2006. An Unstructured Grid, Finite-Volume Coastal Ocean Model. FVCOM User Manual, second ed. SMAST/UMASSD-06-0602.

13. Chen, C., Gao, G., Qi, J., Proshutinsky, A., Beardsley, R. C., Kowalik Z., Lin H., Cowles G., 2009. A new high-resolution unstructured grid finite volume Arctic Ocean model (AO-FVCOM): An application for tidal studies. J. Geophys. Res. 114, C08017.

14. Conlan, K., Lane, S., Ormerod, S., Wade, T., 2005. Preparing for Climate Change Impacts on Freshwater Ecosystems (PRINCE). Environment Agency Science Report: SC030300/SR, Published by: Environment Agency Rio House Waterside Drive, Aztec West Almondsbury, Bristol BS32 4UD, 101 pp.

15. Costard, F., Gautier, E., Brunstein, D., Hammadi, J., Fedorov, A., Yang, D., Dupeyrat, L., 2007. Impact of the global warming on the fluvial thermal erosion over the Lena River in Central Siberia. Geophys. Res. Lett. 34, L14501.

16. Crawford, W. R., 1984. Energy flux and generation of diurnal shelf waves along Vancouver Island. J. Phys. Oceanogr. 14, pp. 1600 – 1607.

17. Dittmar, T., Kattner, G., 2003. The biogeochemistry of the river and shelf ecosystem of the Arctic Ocean: a review. Marine Chemistry 83, 103-120.

18. Dmitrenko, I., Kirillov, S., Eicken, H., Markova, N., 2005. Wind-driven summer surface hydrography of the eastern Siberian shelf. Geophysical ReSearch Letters 32, L14613.

19. Dmitrenko, I. A., S. A. Kirillov, and L. B. Tremblay, 2008a. The long-term and interannual variability of summer fresh water storage over the eastern Siberian shelf: Implication for climatic change. J. Geophys. Res. 113, C03007, doi:10.1029/2007JC004304.

20. Dmitrenko, I. A., Kirillov, S. A., Ivanov, V. V., Woodgate, R. A., 2008b. Mesoscale Atlantic water eddy off the Laptev Sea continental slope carries the signature of upstream interaction. J. Geophys. Res. 113, C07005, doi:10.1029/2007JC004491.

21. Dmitrenko, I. A., Kirillov, S. A., Krumpen, T., Makhotin, M., Abrahamsen, E. P., Willmes, S., Bloshkina, E., Hölemann, J. A., Kassens, H., Wegner, C., 2010a. Wind-driven diversion of summer river runoff preconditions the Laptev Sea coastal polynya hydrography: Evidence from summer-to-winter hydrographic records of 2007–2009. Continental Shelf Research 30(15), 1656-1664.

22. Dmitrenko, I. A. , Kiriilov, S. A. , Tremblay, L. B. , Bauch, D., Hölemann, J. , Krumpen, T. , Kassens, H. , Wegener, C. , Heinemann, G., Schröder, D., 2010b. Impact of the Arctic Ocean Atlantic water layer on Siberian shelf hydrography. Journal of Geophysical Research 115, C08010, doi: 10.1029/2009JC006020.

23. Dmitrenko, I. A., Kirillov, S. A., Bloshkina, E., Lenn, Y.D., 2012. Tide-induced vertical mixing in the Laptev Sea coastal polynya, J. Geophys. Res. 117, doi:10.1029/2011JC006966.

24. Dobrovolsky, A. D. and Zalogin, B. S., 1982. The Seas of the U.S.S.R. Lomonosov Moscow State University Press (in Russian).

25. Dvorkin, E.N., 1970. Tides. In: Gakkel, Ya.Ya., Govorukha, L.S. (Eds.), Soviet Arctic. Nauka, Moscow, pp. 191–197 (in Russian).

26. Dvorkin, E.N., Kagan, B.A., Cleshyova, G.P., 1972. The calculation of the tide motions in Arctic Seas. Izvestiya Akademii Nauk SSSR Fiziko Atmosf. Okeana 8, pp. 298-306 (in Russian).

27. Dubinenkov, I., Kattner, G., Schmitt-Kopplin, P., Flerus, R., Koch, B.P., in prep. Origin-specific molecular signatures of dissolved organic matter in the Arctic Lena River Delta. Marine Chemistry.

28. Ebner, L., Schröder, D., Heinemann, G., 2011. Impact of Laptev Sea flaw polynyas on the atmospheric boundary layer and ice production using idealized mesoscale simulations. Polar Research 30, 7210, doi:10.3402/polar.v30i0.7210.

29. Egbert, G.D, Bennett A.F., Foreman, M. G., 1994. TOPEX/Poseidon tides estimated using a global inverse model. J. Geophys. Res. 99, C12, pp. 24821–24852.

30. Ernsdorf, T., Schröder, D., Adams, S., Heinemann, G., Timmermann, R., Danilov, S., 2011. Impact of atmospheric forcing data on simulations of the Laptev Sea polynya dynamics using the Sea-ice ocean model FESOM. J. Geophys. Res., 116, C12038, doi:10.1029/2010JC006725.

31. Flerus, R., Koch, B.P., Lechtenfeld, O.J., McCallister, S.L., Schmitt-Kopplin, P., Kaiser, K., Kattner, G., 2011. A molecular perspective on the ageing of marine dissolved organic matter. Biogeosciences Discussions 8, 11453-11488.

32. Fofonova, V., Danilov, S., Androsov, A., Zhukov, M., Semenova, O., Overduin, P., Wiltshire, K.H., 2013. Simulation of shelf circulation dynamics in the Laptev Sea. Geo-Siberia-

2013, Remote sensing and photogrammetry methods, environmental monitoring, geoecology, Novosibirsk 2013, Siberian State Geodesic Academy, v. 2, pp. 8-18.

33. Fofonova, V., Androsov, A., Danilov, S., Janout, M., Sofina, E., Wiltshire, K.H., 2014. Semidiurnal tides in the Laptev Sea Shelf zone in the summer season. Continental Shelf Research, 73, pp. 119-132.

34. Frey, K.E. and McClelland, J.W., 2009. Impacts of permafrost degradation on arctic river biogeochemistry. Hydrological Processes 23, 169-182.

35. Grigoriev, N.F., 1966. Perennially frozen grounds of the coastal zone of Yakutia. Moscow, Science Publ., 177 pp. (in Russian).

36. Grigoriev, M.N., 1993. Cryomorphogenesis of the Lena River mouth area. Yakutsk, Permafrost Institute, 176 pp. (in Russian).

37. Hammond, D. and Pryce, A.R. Climate change impacts and water temperature, 2007. Environment Agency Science Report: SC060017/SR, Published by: Environment Agency Rio House Waterside Drive, Aztec West Almondsbury, Bristol BS32 4UD, 91 pp.

38. Hasholt, B., Bobrovitskaya, N. N., Bogen, J., McNamara, J., Mernild, S., Milburn, D., Walling, D. E., 2005. Sediment transport to the Arctic Ocean and adjoining cold oceans // 15th International Northern Research Basins Symposium and Workshop. Luleå to Kvikkjokk, Sweden, pp. 41–67.

39. Hölemann, J., Kirillov, S., Klagge, T., Novikhin, A., Kassens, H., Timokhov, L., 2011. Near-bottom water warming in the Laptev Sea in response to atmospheric and sea ice conditions in 2007. Polar Research 30.

40. Holmes, R.M., McClelland, J.W., Peterson, B.J., Shiklomanov, I.A., Shiklomanov, A.I., Zhulidov, A.V., Gordeev, V.V., Bobrovitskaya, N.N., 2002. A circumpolar perspective on fluvial sediment flux to the Arctic Ocean. Global Biogeochem. Cycl., 16(4), 1098, doi:10.1029/2001GB001849.

41. Holmes, R.M., McClelland, J.W., Peterson, B.J., Tank, S.E., Bulygina, E., Eglinton, T.I., Gordeev, V.V., Gurtovaya, T.Y., Raymond, P.A., Repeta, D.J., Staples, R., Striegl, R.G., Zhulidov, A.V., Zimov, S.A., 2012. Seasonal and Annual Fluxes of Nutrients and Organic Matter from Large Rivers to the Arctic Ocean and Surrounding Seas. Estuaries and Coasts 35, 369-382.

42. Hydrological Yearbooks (State water cadastre), 1936-2010.The basins of the Lena-Indigirka Rivers. Yakutsk (in Russian).

43. Ivanov, 1967. The bedload sediments and variability of riverbed topography in the Bykovskaya Channel. Hydrological regime of the Arctic zone Rivers, Edited by Antonov V.S., Trudy AARI

(Proceedings of the Arctic and Antarctic Research Institute), Leningrad: Hydrometeorological publishing house, 278, pp. 126-141 (in Russian).

44. Jakobsson, M., Macnab, R., Mayer, L., Anderson, R., Edwards, M., Hatzky, J., Schenke, H.W., Johnson, P., 2008. An improved bathymetric portrayal of the Arctic Ocean: Implications for ocean modeling and geological, geophysical and oceanographic analyses. Geophys. Res. Lett. 35, L07602.

45. Jakobsson, M., Mayer, L., Coakley, B., Dowdeswell, J. A., Forbes, S., Fridman, B., Hodnesdal, H., Noormets, R., Pedersen, R., Rebesco, M., Schenke, H. W., Zarayskaya, Y., Accettella,D., Armstrong, A., Anderson, R. M., Bienhoff, P., Camerlenghi, A., Church, I., Edwards, M., Gardner, J. V., Hall, J. K., Hell, B., Hestvik, O.,Kristoffersen, Y., Marcussen, C., Mohammad, R., Mosher, D., Nghiem, S. V., Pedrosa, M. T., Travaglini, P. G., and Weatherall, P., 2012, The International Bathymetric Chart of the Arctic Ocean (IBCAO) Version 3.0. Geophys. Res. Lett. v. 39, no. 12, p. L12609.

46. Janout, M. A. and Lenn Y.D., 2013. Semidiurnal tides on the Laptev Sea Shelf based on oceanographic moorings with implications for shear and vertical mixing. Journal of Physical Oceanography (accepted).

47. Johnson, M.A. and Polyakov, I., 2001. The Laptev Sea as a source for recent Arctic Ocean salinity change. Geophysical ReSearch Letters 28 (10), 2017–2020.

48. Johnson, S.L., 2003. Stream temperature: scaling of observations and issues for modelling. Hydrological Processes 17, pp. 497-499.

49. Kagan, B.A., Romanenkov, D.A., Sofina, E.V., 2008a. Tidal ice drift and ice-generated changes in the tidal dynamics/energetics on the Siberian Continental Shelf. Continental Shelf Research 28 (3), pp. 351–368.

50. Kagan, B.A., Romanenkov, D.A., Sofina, E.V., 2008b. Combined Tidal Ice Drift and Ice-Induced Changes in the Dynamics and Energy of the Combined Tide on the Siberian Continental Shelf. Oceanology 48(3), pp. 317–326.

51. Kagan, B.A. and Sofina E.V., 2010. Ice-induced seasonal variability of tidal constants in the Arctic Ocean. Continental Shelf Research 30(6), pp. 643-647.

52. Kattner, G., Lobbes, J.M., Fitznar, H.P., Engbrod, R., Nötthig, E.-M., and Lara, R.J., 1999. Tracing dissolved organic substances and nutrients from the Lena River through Laptewsee (Arctic). Marine Chemistry 65, pp. 25–39.

53. Koch, B.P., Dittmar, T., Witt, M., Kattner, G., 2007. Fundamentals of Molecular Formula Assignment to Ultrahigh Resolution Mass Data of Natural Organic Matter. Analytical Chemistry 79, 1758-1763.

54. Kotyukh, A.A., Kluyev, Ye.V., Morozov, B.N., 1990. Repeated depth measurements - main source to find out the change of the bottom topography of the Laptev Sea in the current epoch. Vestnik of the Leningrad University, ser. geology and geography, ser.7 (3), pp.53060.

55. Korotaev V.N., 2012. Essays on the geomorphology of estuarine and coastline systems. Moscow, Moscow State University Publ., 540 pp. (in Russian).

56. Kowalik, Z. and Proshutinsky A.Yu., 1993. Diurnal tides in the Arctic Ocean. J. Geophys. Res. 98, C9, pp. 449–468.

57. Kowalik, Z. and Proshutinsky, A.Yu., 1994. The Arctic Ocean tides. In: Johannessen, O., Muench, R.D., Overland, J.E., (Eds.), The Polar Oceans and Their Role in Shaping the Global Environment. The Nansen Centenia Volume. Geophysical Monogrophy Series, 85. AGU, Washington, DC, pp. 137-158.

58. Kowalik, Z. and Proshutinsky, A.Yu., 1995. Topographic enhancement of tidal motion in the western Barents Sea. J. Geophys. Res. 100, C2, pp. 2613-2637.

59. Kraberg, A., Druzhkova, E., Heim, B., Loeder, M.J. and WiltshireK.H., 2013. Phytoplankton community structure in the Lena Delta (Siberia, Russia) in relation to hydrography. Biogeosciences Discuss. 10, 2305-2344.

60. Krumpen, T., Janout, M., Hodges, K. I., Gerdes, R., Girard-Ardhuin, F., Hölemann, J. A., and Willmes, S., 2012. Variability and trends in Laptev Sea ice outflow between 1992–2011, The Cryosphere Discuss., 6, pp. 2891-2930, doi:10.5194/tcd-6-2891-2012, 2012.

61. Lara, R.J., Rachold, V., Kattner, G., Hubberten, H.W., Guggenberger, G., Skoog, A., Thomas, D.N., 1998. Dissolved organic matter and nutrients in the Lena River, Siberian Arctic: Characteristics and distribution. Mar. Chem. 59, 301-305.

62. Lenn, Y. D., Rippeth, T. P., Old, C. P., Bacon, S., Polyakov, I., Ivanov, V., Hölemann, J., 2011. Intermittent Intense Turbulent Mixed under Ice in the Laptev Sea Continental Shelf. Journal of Physical Oceanography 41 (3), pp. 531-547.

63. Liu, B., Yang, D., Ye, B. and Berezovskaya, S., 2005. Long-term openwater season stream temperature variations and changes over Lena River Basin in Siberia. Global Planet. Change 48, pp. 96 – 111.

64. Lu, X. and Zhang, J., 2006. Numerical study on spatially varying bottom friction coefficient of a 2D tidal model with adjoint method. Continental Shelf Research 26(16), pp. 1905-1923.

65. Lyard, F.H., 1997. The tides in the Arctic Ocean from a finite-element model . J. Geophys. Res. 102, C7, pp. 15611–15638.

66. Magritsky, D. V., 2001. The natural and anthropogenic changes in the hydrological regime of the lower reaches and estuaries of major rivers of Eastern Siberia. Dissertation, Lomonosov Moscow State University (in Russian).

67. McClelland, J.W., Déry, S.J., Peterson, B.J., Holmes, R.M., and Wood, E.F., 2006. A pan-arctic evaluation of changes in river discharge during the latter half of the 20th century. Geophysical Research Letters 33, L06715.

68. Mikhaylov, V.M., 2003. Hydrothermal regime of watercourses as an indicator of the existence of ground-filtration taliks (from the results of field research). Earth Cryosphere 7 (2), pp. 57-66.

69. Morison J., Kwok, R., Peralta, F.C., Alkire, M., Rigor, I., Andersen, R., and Steele, M., 2012. Changing Arctic Ocean freshwater pathways, Nature, 481, 66–70.

70. Müller, L., 2008. Sauerstoffdynamik der Nordsee, Untersuchungen mit einem drei-dimensionalen Ökosystemmodell. Berichte des BSH 43. Bundesamt für Seeschiffahrt und Hydrographie (in German).

71. Munk, W. H. and C. Wunsch, 1998. Abyssal recipes II: Energetics of tidal and wind mixing, Deep Sea Res., Part I, 45, pp. 1977– 2010.

72. Nekrasov, A.V., 1990. Energy of the Ocean Tides. Gidrometeoizdat Publishers, Leningrad, pp. 290 (in Russian).

73. Nicholls, R.J., Wong, P.P., Burkett, V.R., Codignotto, J.O., Hay, J.E., McLean, R.F., Ragoonaden, S. and Woodroffe, C.D., 2007. Coastal systems and low-lying areas.Climate Change 2007: Impacts, Adaptation and Vulnerability. Contribution of Working Group II to the Fourth Assessment Report of the Intergovernmental Panel on Climate Change, M.L. Parry, O.F. Canziani, J.P. Palutikof, P.J. van der Linden and C.E. Hanson, Eds., Cambridge University Press, Cambridge, UK, 315-356.

74. Örek, H., Doerffer, R., Röttgers, R., Boersma, M. and Wiltshire, K.H., 2013. A Bio-optical model for remote sensing of Lena water. Biogeosciences Discuss. 10, pp. 4887-4925.

75. Padman, L. and Erofeeva, S., 2004. A barotropic inverse tidal model for the Arctic Ocean. Geophys. Res. Lett. 31.

76. Peregovich, B., Hoops, E., Rachold, V., 1999. Sediment transport to the Laptev Sea (Siberian Arctic) during the Holocene – evidence from the heavy mineral composition of fluvial and marine sediments. Boreas 28, pp. 205-214.

77. Persson, P.O. and Strang, G., 2004. A simple mesh generator in MATLAB. SIAM Review 46 (2), pp. 329-345.

78. Peterson, B. J., Holmes, R. M., McClelland, J. W., Vörösmarty, C. J., Lammers, R. B., Shiklomanov, A. I., Shiklomanov, I. A. and S. Rahmstorf, 2002. Increasing river discharge to the Arctic Ocean, Science, 298, pp. 2171– 2173.

79. Polyakov, I.V., 1994. The M_2 tide in Arctic Ocean. The structure of barotropic tide. Meteorology and Hydrology №1, pp.56-68 (in Russian).

80. Polyakov, I.V., 1995. Maintenance of the Arctic Ocean large-scale baroclinic structure by the M2 tide. Polar Res. 13, 219–232.

81. Polyakov, I.V., Alexeev, V.A., Belchansky, G.I., Dmitrenko, I.A., Ivanov, V.V., Kirillov, S.A., Korablev, A.A., Steele, M., Timokhov, L.A., Yashayaev, I., 2008. Arctic Ocean freshwater changes over the past 100 years and their causes. Journal of Climate 21 (2), 364–384.

82. Rachold, V., Alabyan, A. M., Hubberten, H. W., Korotaev, V. N., Zaitsev, A. A., 1996. Sediment transport to the Laptev Sea – hydrology and geochemistry of the Lena River. Polar Res. 15, pp. 183–196.

83. Reinberg, A.M., 1938. Hydrology of Lena River lower reaches. Hydrology of Soviet Arctic Rivers: Hydrology information about Lena, Ebitiem, Indigirka, Hatanga, Yenisei and Kolyma Rivers, Edited by Prof. Rodevich V.M., Trudy AARI (Proceedings of the Arctic and Antarctic Research Institute), Leningrad: Glavsevmorputi, 105(2), pp. 51-72 (in Russian).

84. Rigor, I. G., Colony, R. L., 1997. Sea-ice production and transport of pollutants in the Laptev Sea, 1997–1993. Sci. Total Environ. 202, 89–110.

85. Rozman, P., Hölemann, J. A., Krumpen, T., Gerdes, R., Köberle, C., Lavergne, T., Adams, S., Girard-Ardhuin, F., 2011. Validating satellite derived and modelled Sea-ice drift in the Laptev Sea with in situ measurements from the winter of 2007/08. Polar ReSearch 30, 7218, doi:10.3402/polar.v30i0.7218Schättler et al. A Description of the Nonhydrostatic Regional COSMO-Model, Part VII: User's Guide [Book Section]. - 2008 : [s.n.].

86. Schröder, D., Heinemann, G., Willmes, S., 2011. The impact of a thermodynamic Sea-ice module in the COSMO numerical weather prediction model on simulations for the Laptev Sea, Siberian Arctic. Polar Res. 30, 6334, doi:10.3402/polar.v30i0.6334.

87. Schuur, E.A.G., Bockheim, J., Canadell, J.G., Euskirchen, E., 2008. Vulnerability of Permafrost Carbon to Climate Change: Implications for the Global Carbon Cycle. BioScience 58, 701-715.

88. Simons, D.B., Richardson, E.B., Nordin, C.F. Jr., 1965. Bedload equations for ripples and dunes, USGS Prof. Paper 462-H.

89. Simpson, J.H., Crawford, W.R., Rippeth, T.P., Campbell, A.R., Choak, J.V.S. , 1996. Vertical Structure of turbulent dissipation in shelf seas. Journal of Physical Oceanography 26(8), 1580-1590.

90. Sofina, E.V., 2008. The simulation of tidal ice drift and ice-related changes in tidal dynamics and energy in Siberian Continental Shelf. Dissertation, Russian State Hydrometeorological University (in Russian).

91. Sorokin, Y.I. and Sorokin, P.Y., 1996. Plankton and Primary Production in the Lena River Estuary and in the South-eastern Laptev Sea. Estuarine, Coastal and Shelf Science 43(4), pp. 399-418(20).

92. State Hydrologic Institute, 1961. Recommendation on Methods of Compiling Data on Water Resources, vol. 9, Thermal and Ice Conditions on Rivers, 207 pp., St. Petersburg (in Russian).

93. Steppeler, J., Doms, G., Schättler, U., Bitzer, H.W., Cassmann, A., Damrath, U., Gregoric, G., 2003. Meso-gamma scale forecasts using the nonhydrostatic model LM.s.l. Meteorol. Atmos. Phys. 82, 75–96, doi:10.1007/s00703-001-0592-9.

94. Tananaev, N.I., 2013. Hydrological and geocryological controls on fluvial activity of rivers in cold environments. Cold and Mountain Region Hydrological Systems Under Climate Change: Towards Improved Projections, IAHS Publ. 360, 161-167.

95. Tananaev, N.I., 2013. Hysteresis effects of suspended sediment transport in relation to geomorphic conditions and dominant sediment sources in medium and large rivers of Russian Arctic. Hydrol. Res., in press, doi: 10.2166/nh.2018.099.

96. Tananaev, N.I. and Anisimova, L.A., 2013. Evaluating the annual runoff of traction load on the rivers in the north of Siberia and the Far East. Geogr. and Nat. Resour., 34(1), pp. 79-87.

97. Timokhov, L. A., 1994. Regional characteristics of the Laptev and the East Siberian seas: climate, topography, ice phases, thermohaline regime, circulation. Ber. Polarforsch. 114, L04501, doi:10.1029/2004GL021810.

98. Valentim, J.M., Vaz, L., Vaz, N., Silva, H., Duarte, B., Caçador, I. and Dias, J.M., 2013. Sea level rise impact in residual circulation in Tagus estuary and Ria de Aveiro lagoon. Proceedings 12th International Coastal Symposium (Plymouth, England), Journal of Coastal Research, Special Issue 65, pp. 1981-1986.

99. Voinov, G., 2002. Tide and tidal streams, in Polar Seas Oceanography: An Integrated Case Study of the Kara Sea. Springer, pp. 147 – 214.

100. Wankievicz , A., 1984. Hydrothermal processes beneath Arctic river channels. Water Resources Research 20 (10), pp. 1417-1426.

101. Willmes, S., Adams, S., Schroeder, D., Heinemann, G, 2011. Spatio-temporal variability of polynya dynamics and ice production in the Laptev Sea between the winters of 1979/80 and 2007/08. Polar Research 30 (5971), doi:10.3402/polar.v30i0.5971.

102. Yang, D., Liu, B., Ye, B., 2005. Stream temperature changes over Lena River Basin in Siberia. Geophys. Res. Lett. 32, L05401, doi:10.1029/2004GL021568.

103. Yang, D., Kane, D. L., Hinzman, L., Zhang, X., Zhang, T., Ye, H., 2002. Siberian Lena River hydrologic regime and recent change. J. Geophys. Res. 107(D23), 4694, doi:10.1029/2002JD002542.

104. Zhang, T., Barry, R.G., Knowles, K., Heginbottom, J.A., Brown, J., 1999. Statistics and characteristics of permafrost and ground ice distribution in the Northern Hemisphere. Polar Geography 23, pp. 147-169.

105. Zhao, L., Chen, C., Cowles, G., 2006. Tidal flushing and eddy shedding in Mount Hope Bay and Narragansett Bay: An application of FVCOM. J. Geophys. Res. 111, C10015.

106. Zotin, M.I., 1947. Fluid and thermal runoff in the Laptev Sea, Edited by Lopatin G.V., Trudy AARI (Proceedings of the Arctic and Antarctic Research Institute), Leningrad: Glavsevmorputi, 198, 67 pp (in Russian).